GLOBAL EVOLUTION OF SPIRAL GALAXIES BY MEANS OF CUMULATIVE OXYGEN ABUNDANCES

Stuart Dack

A thesis submitted to the Faculty of Graduate Studies in partial fulfillment of the requirements for the degree of

MASTER OF SCIENCE

Graduate Program in Physics and Astronomy

York University

Toronto, Ontario, Canada

August 2011

Abstract

Studying the global evolution of spiral galaxies requires determining their overall chemical compositions. However, since spirals tend to possess gradients in their chemical compositions, determining their overall chemical abundances poses a challenge. In this study, the framework for a newly proposed method for determining the overall oxygen abundance of a disk is established. By separately integrating the absolute amounts of hydrogen and oxygen out to large radii, the overall oxygen abundance is shown to reach an asymptotic value. In this manner, a reliable account of the overall chemical state is revealed. Knowing the chemical state of spirals then allows for their study alongside other galaxies, such as dwarf irregulars, whose chemical states are better understood. The relationship between the gas fraction and the overall oxygen abundance is established, and a comparison is made to the corresponding relationship for dwarf irregular galaxies. It is concluded that the effective oxygen yield for spirals is consistent with recent closed-box model estimates of yields for dwarf irregulars. Thus, it appears that the galaxy type does not have an effect on the formation of stars or the enrichment process associated with them, and no relation between yield and metallicity exists.

Acknowledgments

It was not a simple decision for me to leave my job and go back to school. However, with all the love and support I received from family and friends, my transition was made easy and I haven't looked back.

First of all, I would like to give a sincere thanks to my amazing supervisor, Dr. Marshall McCall, who took a leap of faith and accepted a bright-eyed and enthusiastic Electrical Engineer with minimal background in astronomy to a Master's program at York. This thesis would not have been possible without his ongoing guidance and support. His patience and direction helped me every step of the way. He is everything anyone could ever hope for in a teacher and mentor, and I can never thank him enough.

To my amazing family who has always supported me in my decisions, and specifically in the decision to leave my job in order to pursue a Master's degree, I am eternally grateful. Without the love and support I knew they would provide, I do not know if I would have had the courage to embark on this journey. A very special thanks must be given to my parents, Nancy and Joseph Dack, who have always been there for me.

To my friends and colleagues at York, without whose support I don't know where I would be. To George Conidis with whom I slaved away for many hours working on homework assignments and studying for exams. He has always been there to lend a helping hand or to answer any questions I may have had. To Robin Fingerhut who was one of the first people I met at York. Listening to her speak during our weekly

meetings gave me my first introduction to real astronomy talk and although I often didn't understand a lot of what was being said, her knowledge and vigor inspired me to work hard and learn all I could in my short time at York.

To the rest of the astronomy faculty and grad students at York, the enthusiasm and passion I have witnessed over the past two years have motivated me to discover more outside of the classroom, and I always looked forward to our Wednesday Astronomy Journal Clubs.

Last but not least, I will forever be indebted to Vanessa Martin, who not only spent hours proof-reading this thesis, but who has also brightened my days over the past two years. Vanessa would have been totally justified in complaining about my working late into the night, spending too much time in front of my computer, or not giving her all the attention that she deserves. But she never complained once, and she has been my biggest supporter since the day we met.

This thesis is dedicated to my Grandpa Davy, an intelligent, loving, and wonderful man who had an insatiable thirst for knowledge and always had a smile on his face.

Contents

1 Background **1**

1.1 Introduction 1

1.2 Chemical Compositions 2

1.3 HII Regions and Oxygen Abundances 4

1.4 Planetary Nebulae 5

1.5 Dwarf Irregular Galaxies 6

1.6 Chemical Evolution of Galaxies 7

1.7 Spiral Galaxies and Cumulative Abundances 9

1.8 Purpose of this Study 15

1.9 Thesis Outline 15

2 Analysis of Nebular Spectra **17**

2.1 Direct and Indirect Methods for Calculating Oxygen Abundances . . 17

2.2 SNAP 20

2.3 Correcting for Reddening 21

2.4 Atomic Data 22
2.5 Reddening Law and Extinction 22
2.6 Temperature and Density Determinations 24
2.7 Ionic Abundances and Total Oxygen Abundances 26

3 Calculation of Oxygen Abundances 28

3.1 The Double-Valued Nature of R_{23} 28
3.2 Ionization Hardening 30
3.3 Options for Calibration Choices 31
3.4 Theoretical Justification for Calibration 33
3.5 Empirical Comparison of Direct and Indirect Abundances 34
3.6 Verification of R_{23} Calibration with Planetary Nebulae 37

4 Selection of Galaxies 40

4.1 Selection Criteria for Galaxies 40
4.2 Published Information 41
4.3 Attributes of Sample Galaxies 41

5 Measurements of Oxygen Abundances in Galaxies 45

5.1 Gradients 45
5.2 Deviations in O/H Between Individual HII Regions and the Gradient 53

6 Overall Quantities of Hydrogen and Oxygen 82

6.1 Motivation 82

6.2 Calculating the Quantity of Neutral Hydrogen 83

6.3 Calculating the Absolute Amounts of Molecular Hydrogen, H_2 84

7 Cumulative Oxygen Abundances **88**

7.1 Method of Calculation 88

7.2 The Asymptotic Value of O/H 91

7.3 Contribution of Molecular Hydrogen 104

7.4 Uncertainties in Asymptotes 105

7.5 Cumulative Abundance of NGC 2403 107

7.6 Oxygen Abundance at $0.4R_o$ 108

8 Gas Fractions **113**

8.1 Background 113

8.2 Gas Masses 113

8.3 Light Profiles 114

8.4 Calculating Absolute Magnitudes 118

8.5 Stellar Masses 122

8.6 Gas Fractions 123

9 Evolution **126**

9.1 Review of Past Work 126

9.2 Mass-to-Light Ratio 127

9.3 A Comparison of Oxygen Abundances and Gas Fractions for Spirals . 128

9.4 Do Spiral Galaxies Follow the Closed-Box Model? 130

10 Conclusions and Future Directions **133**

10.1 Asymptotic Abundances 133

10.2 Future Directions 137

Appendix A: Glossary of Names and Terms **139**

References **143**

List of Tables

3.1 Comparison of various O/H calibration methods 37

4.1 List of published sources 43

4.2 Physical attributes of galaxies in the study 44

5.1 Oxygen abundance data for all HII regions 54

7.1 Parameters of the oxygen abundance plots 111

7.2 Comparison of asymptotic abundances vs $0.4R_o$ 112

8.1 Parameters for fits to the K_s-band light profile 119

8.2 Apparent magnitudes, flux ratios, and absolute magnitudes 124

8.3 Luminosities, masses and gas fractions 125

List of Figures

1.1 Oxygen abundance vs. gas fraction for dwarf irregulars 10

1.2 Representation of O/H distribution of a typical spiral galaxy 12

1.3 Oxygen abundances for NGC 5457 14

2.1 Forbidden line energy level diagram for [OIII] 18

2.2 The Fitzpatrick reddening law 24

3.1 O/H vs. R_{23} 29

3.2 Oxygen abundances for NGC 300 and NGC 5457 36

3.3 Oxygen abundances of PNe and HII regions for NGC 3031 39

5.1 O/H versus deprojected radius for all sample galaxies 48

6.1 HI column density across NGC 1232 85

6.2 HI and H_2 column densities across NGC 5457 87

7.1 HI column density of NGC 4258 92

7.2 Cumulative oxygen abundance versus radius 93

7.3 Cumulative O/H for NGC 628 with and without H_2 105

7.4 Comparison of asymptotic abundances vs $0.4R_o$ 110

8.1 K_s-band light profile of NGC 1232 117

9.1 Comparison of mass-to-light ratios 129

9.2 Oxygen abundance vs. gas fraction for dwarfs and spirals 131

Chapter 1

Background

1.1 Introduction

In order to fully understand the history of the universe, it is essential to understand the history of the individual galaxies within it. To understand the history of galaxies, it is necessary to learn about the types and amounts of elements of which they consist. Many factors contribute to the evolution of galaxies, including initial conditions (Güsten & Mezger 1982), mass accretion (Chiosi 1980; Lacey & Fall 1985; Tsujimoto et al. 1995), star formation (Wyse & Silk 1989; Phillipps & Edmunds 1991), interactions of galaxies (Barnes & Hernquist 1991; Stewart et al. 2008), and the outflow of gas (Dahlem et al. 1998; Pettini et al. 2000). These factors may affect evolution locally or globally.

Determining the types and amounts of elements that make up a galaxy grants

insight into its evolution because the elemental composition is directly related to star formation. As stars are born and live out their lives, they create heavier elements through nuclear fusion. In certain instances, as they die out, their mass, now enriched with elements heavier than helium, is ejected into the interstellar medium of the galaxy via supernova explosions. Thus, the cumulative effect of all star formation during the history of the galaxy is seen in the total enrichment of heavy elements. Within each galaxy, local variations of the mix and amounts of elements may occur.

1.2 Chemical Compositions

The chemical composition of a galaxy is the mixture of atoms that make up that galaxy. In this study, the term "chemical" will be used to refer to any element. This definition differs from that in chemistry, where "chemical" usually refers to compound molecules that are used in reactant processes. The term "metal" will be used to refer to all elements other than hydrogen and helium. The "metallicity" of a galaxy refers to the concentration of heavy elements (i.e., elements other than hydrogen and helium) within it. Generally, metallicity is presented in terms of a "chemical abundance" (or simply "abundance"), which is the ratio of the number density of a particular metal to that of hydrogen.

The metallicity of a galaxy provides clues to its global evolution. Material ejected from dying stars mixes in with the interstellar medium, and ultimately new, more metal-rich stars are created. Therefore, younger stars have a higher metallicity than

do older stars.

The metallicity of a galaxy can be measured in a variety of ways. Historically, the most common way of calculating chemical abundances was by analyzing absorption lines of iron in the integrated spectra from starlight of the central parts of galaxies. The iron abundance of a gas is given by equation 1.1, where (Fe/H) represents the iron abundance of the medium, and $(\mathrm{Fe/H})_\odot$ represents the iron abundance of the Sun:

$$[\mathrm{Fe/H}] = \log\left[\frac{(\mathrm{Fe/H})}{(\mathrm{Fe/H})_\odot}\right] = \log(\mathrm{Fe/H}) - \log(\mathrm{Fe/H})_\odot \tag{1.1}$$

Most of the observed iron in galaxies comes from binary systems in which an intermediate-mass star has evolved to a white dwarf. Once the white dwarf has accreted enough matter from the companion to reach the Chandrasekhar limit of about 1.38 solar masses, a type Ia supernova occurs (Mazzali et al. 2007). Since the stars from which the iron was produced are relatively small, they lived long lives, and thus reflect the primordial interstellar medium from which they were created long ago. Therefore, the iron abundance in stars cannot be said to trace the current metallicity of the interstellar medium, and knowledge of the detailed history of star formation is required to understand how the iron abundance came to be.

1.3 HII Regions and Oxygen Abundances

A better way to evaluate metallicity is by analyzing large clouds of mainly ionized gas where star formation has recently taken place. These areas are called HII regions, and they are named for the large amount of ionized hydrogen contained within them (HII refers to ionized hydrogen, whereas HI refers to neutral hydrogen). Observing these regions to determine metallicity has its advantages. First, because of the young, hot, luminous stars within them, they are visible out to very large distances and their spectra can be easily obtained. Second, since HII regions contain many stars (typically tens to hundreds), they are good indicators of metallicity at a given radius (Vila-Costas & Edmunds 1992; Zaritsky et al. 1994). The stars within HII regions contribute to ionizing flux, so the radiation field from the gas is tied to the metallicity in the stars. At any given distance from the centre of a galaxy, the metallicity as judged from different HII regions is usually relatively homogeneous (Kobulnicky & Skillman 1997). With respect to metallicity, though, what is important are the differences between HII regions at different radii. Many galaxies tend to possess a downward-trending gradient, with metallicity falling as distance from the centre increases, while others tend to be relatively homogeneous, with no large-scale observable trend in metallicity with radius.

A readily observable gauge of metallicity in HII regions is the oxygen abundance (Searle 1971; Shields 1974). The oxygen abundance of an object can be described as the ratio of the number density of oxygen atoms, n(O), to the number density of hy-

drogen atoms, n(H). This ratio can simply be written as O/H, and is usually conveyed via the logarithm with an offset of 12. The way to represent oxygen abundances by number thus becomes 12+log(O/H).

Oxygen is a useful probe of metallicity. Oxygen is created almost entirely through stellar processes, and most of it is created inside short-lived massive stars. These stars end their lives as type II supernovae, which eject oxygen and other products of nucleosynthesis into the interstellar medium. Since the lifetimes of these stars are negligible on a cosmic timescale, the creation of oxygen can be said to occur at a rate proportional to that of star formation. Moreover, oxygen lines are among the most prominent within spectra of HII regions, and techniques for analyzing them are well-developed (Edmunds & Pagel 1984; Vílchez & Pagel 1988; McCall et al. 1985).

1.4 Planetary Nebulae

Another possible approach to finding chemical abundances is by observing planetary nebulae (PNe). Planetary nebulae consist of a glowing shell of ionized gas ejected during the asymptotic giant branch phase of stars with masses below eight solar masses. They offer the advantage of being hot compared to giant extragalactic HII regions, making their spectra easier to analyze. However, they are very faint.

Planetary nebulae result from the death of long-lived stars, so they have oxygen abundances approximately equal to that of their progenitors (with little or no self-enrichment). Thus, depending on the star formation rate since the birth of the

progenitors, planetary nebulae may undervalue the oxygen abundance in the interstellar medium (McCall & Richer 2003). HII regions are thought to have chemical compositions closest to that of the interstellar medium (McCall & Richer 2003).

With enough statistics, planetary nebulae may still be used to gauge oxygen abundances. Richer et al. (1997) showed that there is a relationship between planetary nebulae and HII region abundances at a given radius. Gradients of the oxygen abundance found for HII regions and planetary nebulae for the same galaxy have the same slope, but the trends can be offset from each other by a small amount, with HII regions displaying higher abundance values at all radii. The offset amounts to less than 0.15 dex, so it is possible to use planetary nebulae to check HII region determinations. This is particularly valuable where the oxygen abundance is high; HII regions are so cool that abundances cannot be determined without the aid of models. This study focuses mainly on HII regions, and uses planetary nebulae where available simply to check the calibrations of empirical abundance indicators.

1.5 Dwarf Irregular Galaxies

Dwarf irregular galaxies are small galaxies that typically contain between a million and a billion stars. These galaxies generally have a diameter of less than a few kiloparsecs (kpc). Because of the small size of dwarf irregulars, type II supernovae that occur within them tend to spread their ejected elements throughout large portions of the galaxies in a short time. Consequently, dwarf galaxies possess a relatively con-

stant chemical abundance throughout their bulk. Much research has been done on the two dwarf irregular galaxies known as the Magellanic Clouds, with most works concluding that there is no significant gradient in the metallicity of the Small Magellanic Cloud (SMC) (Parisi et al. 2009; Cioni 2009) or of the Large Magellanic Cloud (LMC) (Olszewski et al. 1991; Bica et al. 1998), although the conclusion for the latter has recently come into question. A very slight metallicity gradient may in fact be present in the LMC (Alves 2004; Cioni 2009). Nevertheless, these conclusions mean that for dwarf irregulars, analysis of a single HII region is sufficient to fully characterize the chemical makeup of the ISM in the entire galaxy.

1.6 Chemical Evolution of Galaxies

The "closed-box model" guides thinking about chemical evolution (Searle & Sargent 1972; Pagel 1997). This model suggests that galaxies start off with an un-enriched collection of gas (i.e., without metals). This gas is then continuously processed into stars that have various lifespans, depending on their masses. Stars with masses above approximately eight solar masses blow up as supernovae after a time on the order of a few million years, a relatively short amount of time on a cosmic timescale. In the closed-box model, the lifetime of massive stars is thus approximated to be zero years. Their gas, enriched by a lifetime of fusion, is instantly sent back into the galaxy and mixes with the interstellar medium on a short timescale, also approximated to be zero years. This assumption has been shown to be accurate by Kobulnicky & Skillman

(1997). Other, less massive stars are formed simultaneously and continue to burn for times large compared to the age of the universe. In the model, lifetimes of low-mass stars are approximated to be infinite. Births and deaths continue, and the abundance of metals within a galaxy increases as the fraction of gaseous matter declines.

In the closed-box model, it is also assumed that the initial mass function (IMF), which represents the distribution of stellar masses immediately after stars have formed, remains constant with time.

The closed-box model predicts that the relationship between metallicity, Z, and gas fraction, μ, take on the following form (Searle & Sargent 1972; Lee et al. 2003a):

$$Z = y \ln(1/\mu) \tag{1.2}$$

The constant, y, called the yield of oxygen, is the ratio of the mass of newly formed oxygen to the mass of gas locked permanently in stars for each star formation event. This equation translates to:

$$\mathrm{O/H} = y_o \ln(1/\mu) \tag{1.3}$$

where y_o is the *number* yield of oxygen. Equation 1.3 can be rewritten as:

$$\log(\mathrm{O/H}) = \log(y_o) + \log(\ln(1/\mu))$$

$$12 + \log(\mathrm{O/H}) = 12 + \log\left(2.303 y_o\right) + \log(\log(1/\mu)) \tag{1.4}$$

The factor of 2.303 comes from the conversion from ln to log (base 10). Thus, for a closed system, the plot of 12+log(O/H) versus log(log($1/\mu$)) will necessarily have a slope of 1.

For dwarf irregular galaxies, the closed box model holds up well (Lee et al. 2003a; Lee et al. 2003b; Vaduvescu et al. 2007). Figure 1.1 shows a plot of the oxygen abundances versus gas fractions for 22 dwarf irregular galaxies. Abundances were taken from a variety of published works, and the gas fractions were all calculated by McCall et al. (2011). The slope is consistent with the closed-box model.

1.7 Spiral Galaxies and Cumulative Abundances

Spiral galaxies are notable for a flat, rotating disk of stars, gas and dust. They are all relatively large, ranging in size from a few kiloparsecs to 250 kpc. They often contain a central bulge of luminosity, and are characterized by "arms" that spiral around the centre.

Spirals come in a variety of forms. They vary in the size of their bulges, tightness of their spiral arms, and the presence of a central bar. Moreover, spiral galaxies demonstrate evidence for a roughly spherical dark matter halo, as indicated by the shape of their rotation curves.

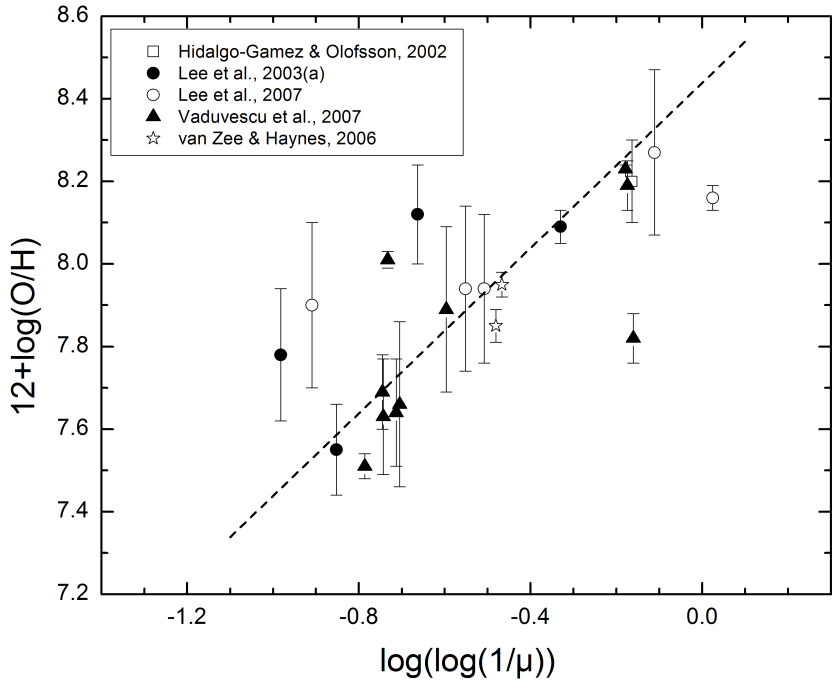

Figure 1.1: **Oxygen abundance vs. gas fraction for 22 dwarf irregular galaxies. Abundances from various sources are shown in the legend. Gas fractions were all calculated by McCall et al. (2011). The abundance increases upward and gas fraction increases to the left. The least squares best fit line with a slope of 1 is shown.**

In general, a spiral tends to possess a gradient in chemical composition, meaning that there is a higher metallicity closer to the centre (Searle 1971; Smith 1975). This gradient has been shown to be fit very well by an exponential profile (Vila-Costas & Edmunds 1992; Zaritsky et al. 1994; Pilyugin 2002). Since oxygen abundances are most often plotted on a logarithmic scale, the gradient of the logarithm of the oxygen abundance versus radius forms a straight line sloping downward as radius increases. Moreover, oxygen abundances are known to be azimuthally homogeneous.

A problem exists in determining oxygen abundances in spiral galaxies. In a galaxy possessing a gradient in their chemical composition, the oxygen abundance at any given radius can not generally be said to represent the overall oxygen abundance of the galaxy. A simple method that is sometimes adopted is to merely choose a particular radius to characterize the entire galaxy. Such a method was introduced by Zaritsky et al. (1994). Different galaxies can then be compared via chemical compositions at this chosen radius. This method, however, is not without its limitations. Without any further knowledge of the composition of the entire galaxy, the radius chosen is necessarily arbitrary and may not truly represent the actual composition of the galaxy as a whole. Since the overall abundance in each galaxy is unknown, comparisons among galaxies are fraught with danger.

A method of measuring global oxygen abundances in spirals in a methodical way has recently been proposed by Sadavoy and McCall (2006). They calculated the total number of oxygen atoms out to a certain distance from the centre and divided it by the

total number of hydrogen atoms within that distance. They observed that the ratio of the total number of oxygen atoms to the total number of hydrogen atoms approached a constant at large radii. The reason why the oxygen abundance approaches an asymptote is as follows. In the inner parts of a galaxy, n(O)/n(H) is high. However, oxygen is spread over a small volume. The outer parts of a galaxy have less oxygen, but it is spread over a larger volume. A representation of the oxygen abundance distribution for a typical spiral galaxy is illustrated in Figure 1.2. As it turns out, the rate of decline of O/H with radius wins out over the rate of increase in surface area of the disk, with the result that O/H within some radius approaches an asymptote as the radius becomes large.

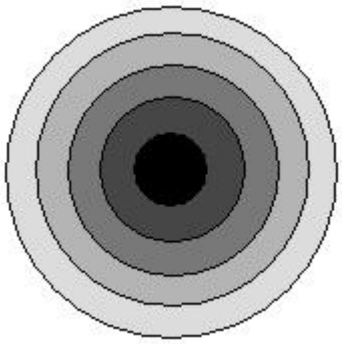

Figure 1.2: **Representation of the oxygen abundance distribution of a typical spiral galaxy. The inner regions of the galaxy (dark) contain the highest abundance of oxygen. The outer regions (light) contain less oxygen, but the oxygen is spread over a larger volume.**

Sadavoy and McCall (2006) were the first to introduce the idea that the ratio of the total abundance of oxygen relative to hydrogen within a spiral galaxy might

be determinable. They calculated the amounts of oxygen and hydrogen at various radii, and then summed each over the entire disk of the galaxy. This was done for two spirals, NGC 5457 and NGC 6946. Figure 1.3(a) shows the oxygen abundance gradient for NGC 5457, while Figure 1.3(b) shows the *cumulative* abundances (i.e., the ratio of the total number of oxygen atoms to that of hydrogen atoms) as a function of radius. In each plot, there are three sets of data points representing different methods for calculating oxygen abundances. These methods are be discussed in §3.3. In the second plot, each point represents the cumulative oxygen abundance of the entire galaxy out to that radius. As can be seen, the points at the greatest radii appear to reach an asymptote. This asymptote is interpreted as representing the overall oxygen abundance of the galaxy.

Although the method of Sadavoy and McCall shows promise, the work they did suffered from several deficiencies. Only two galaxies were studied. Although the cumulative oxygen abundance plots for these galaxies seem to trend toward an asymptotic value, two galaxies are not enough to make any concrete conclusions. A larger sample is therefore necessary to prove the concept. Moreover, errors were made in the determination of oxygen abundances of various HII regions. These deficiencies are discussed further in §3.3.

Quantification of global chemical abundances for spiral galaxies would permit comparisons with dwarfs. For example, it would be possible to compare spirals to dwarfs by plotting them on the same graph of oxygen abundance versus gas fraction.

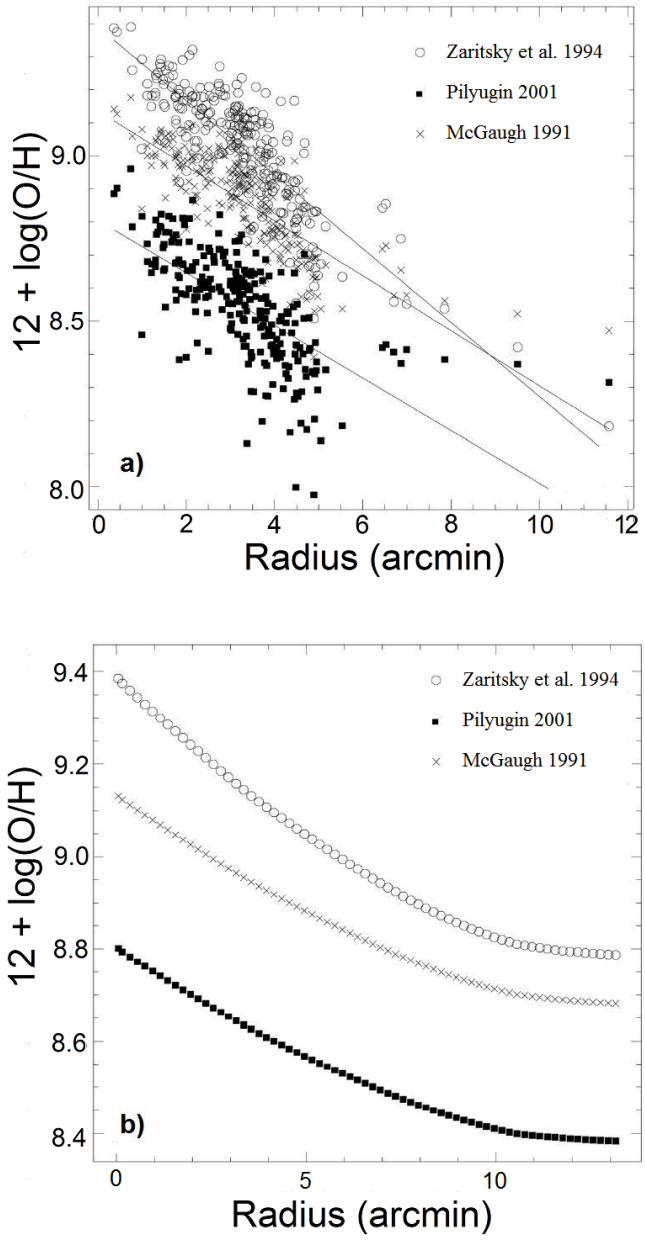

Figure 1.3: **Oxygen abundance versus radius for NGC 5457, from Sadavoy and McCall (2006). The top panel (a) shows the oxygen abundances estimated by three different methods for various HII regions within the galaxy, with least squares fits superimposed. Oxygen abundance errors are ±0.1 dex. The bottom panel (b) is a graph of *cumulative* oxygen abundances as a function of radius.**

Doing so would indicate if spirals globally follow an evolutionary path similar to dwarfs (i.e., a clear relation between metallicity and gas fraction).

1.8 Purpose of this Study

The goals of the research presented in this study are as follows:

1. To test whether the cumulative abundances for a large sample of spirals systematically approach asymptotes at large radii.

2. To analyze and understand the shape of the cumulative oxygen abundance curves, and thereby develop a way of quantifying the asymptotic abundances.

3. To compare the spirals from the sample to dwarf irregular galaxies by examining how the oxygen abundances correlate with gas fractions, and to demonstrate whether or not dwarfs and spirals evolved globally in a similar manner.

1.9 Thesis Outline

This thesis is organized in the following manner. In §2, methods for measuring oxygen abundances are examined, and an indirect method for calculating oxygen abundances is established. In §3, the sample of galaxies for study is constructed. In §4, the methods of data reduction for oxygen abundance analyses are described. In §5, plots of oxygen abundances for HII regions are presented for all galaxies in the study, and

an analysis of these plots is performed. In §6, the oxygen abundance data is combined with measurements of hydrogen within each galaxy to compute amounts of hydrogen and oxygen as a function of radius. In §7, the cumulative oxygen abundance curves are plotted and asymptotes are established. In §8, gas fractions are determined for each galaxy, and in §9, the correlation with overall oxygen abundances is studied. Finally, in §10, the validity of the closed-box model for the evolution of spirals is discussed and some directions for further research are developed. A glossary of terms and symbols appearing throughout the text is given in Appendix A.

Chapter 2

Analysis of Nebular Spectra

2.1 Direct and Indirect Methods for Calculating Oxygen Abundances

Forbidden transitions arising from collisionally-excited metastable states give rise to emission lines from low-density ionized gases. Figure 2.1 shows the energy level diagram for forbidden lines of doubly ionized oxygen ([OIII]). One of these forbidden transitions produces the "auroral" line at 4363 Å (also represented as "[OIII]λ4363"), which provides the most direct method for obtaining oxygen abundances. By comparing the ratio of the emissivity of this line to that of the doublet [OIII]$\lambda\lambda$4959,5007 "nebular" lines, it is possible to obtain the electron temperature of the gas, T_e, wherever O^{++} is the predominant form of oxygen. This is possible because the relative strengths of the emissivities depend highly on the electron temperature.

Calculating the oxygen abundance of an HII region can be difficult because of

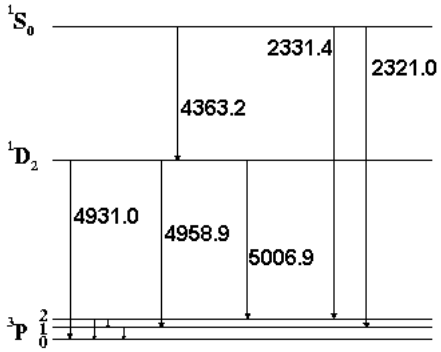

Figure 2.1: **Forbidden line energy level diagram for [OIII].**

ionic stratification and the concomitant changes in thermal equilibrium. HII regions are often modelled as two distinct zones of ionization, one of low-ionization for species such as O^+, and one of high-ionization for species such as O^{++}. An electron temperature is associated with each of these zones. The temperatures for the O^+ and O^{++} zones are referred to as T[OII] and T[OIII], respectively. Several models relating the temperatures in these zones to one another have been devised (Pagel et al. 1992; Izotov et al. 1997; Deharveng et al. 2000). One of the most popular is that of Garnett (1992), and it is this model that will be used in this study. It relates the two zones via the following equation:

$$\mathrm{T[OII]} = 0.7\mathrm{T[OIII]} + 3000\mathrm{K} \tag{2.1}$$

The most effective method of finding abundances is to first measure the temperature of the zones, specifically T[OIII] and T[OII]. Models of statistical equilibrium

can give a good estimate of electron temperatures from a comparison of the line flux at [OIII]λ4363 and one of the other doubly ionized oxygen ions, [OIII]λ4959 or [OIII]λ5007. The computer program used for the analysis will be introduced in §2.2. Knowing T[OIII], then T[OII] can be estimated from equation 2.1, and then the abundances of O^{+} and O^{++} can be estimated and summed to determine the oxygen abundance. This method of calculating oxygen abundances is most often referred to as the "direct" method, "electron temperature" method, or T_e method.

A challenge arises if the oxygen abundance of a region is larger than approximately 12+log(O/H)=8.5. An enhanced oxygen abundance allows for a greater cooling efficiency within the gas and a lower density of electrons capable of exciting ions into higher metastable states. The result is a weakening of collisionally excited lines in the optical part of the spectrum. Additionally, [OIII]λ4363 weakens with respect to [OIII]$\lambda\lambda$4959,5007. Thus, [OIII]λ4363 can become too faint to be observed.

Therefore, it is necessary to find another method for calculating oxygen abundances at high metallicities. Many techniques have been proposed, the most popular of which employs the combination of forbidden lines of oxygen in the R_{23} index (Pagel et al. 1979):

$$R_{23} = \frac{([\mathrm{OII}]\lambda 3727 + [\mathrm{OIII}]\lambda\lambda 4959, 5007)}{\mathrm{H}\beta} \tag{2.2}$$

Hβ refers to the hydrogen Balmer series line at 4861.32 Å. The forbidden line [OII]λ3727

is actually a combination of the close doublet [OII]$\lambda\lambda$3726,3729.

R_{23} has been shown to be a good index of temperature, because other factors that cause the density of O^{++} ions to decrease simultaneously cause the density of O^{+} ions to increase, and vice versa. Since there is a close connection between oxygen abundance and temperature, the R_{23} index allows for the estimation of an oxygen abundance without first obtaining a temperature (Pagel et al. 1979). In HII regions, most of the oxygen is in the form of O^{+} or O^{++} . Stars are not hot enough to ionize further than O^{++}, and O^{0} is confined to a narrow transition zone at the periphery. Therefore, it is reasonable to expect that a technique that predicts the overall oxygen abundance of HII regions would only require lines of O^{+} and O^{++} (i.e., [OII] and [OIII]). Some of the methods of arriving at a reliable value of O/H using the R_{23} index will be discussed in §3. All such methods are referred to as "indirect" methods.

2.2 SNAP

Fluxes arising from emission lines are directly related to the number of emitting ions. However, they may also be affected by other factors, such as the temperature of the gas, density of the gas, and dust in the interstellar medium.

SNAP stands for *Spreadsheet Nebular Analysis Package*. SNAP is a program that was developed by astronomers at York University in Toronto, Canada in order to address the needs of nebular spectroscopists. It is a tool for the analysis of nebular spectra. SNAP is an add-in to Microsoft Excel (version 2003 or earlier), and can be

used for several tasks, including the calculation of:

- the amount of extinction along any line of sight
- line intensities corrected for extinction
- temperatures and densities of the emitting gas
- individual ionic abundances and total elemental abundances

2.3 Correcting for Reddening

Dust can affect the view of luminous sources by absorbing them or acting like a screen and scattering photons out of the line of sight. The amount of absorption plus scattering, referred to as "extinction," depends on the wavelength of the photons. In general, emissions at longer wavelengths get extinguished less so than do emissions at shorter wavelengths. As a result, for gaseous nebulae, lines toward the blue end of the electromagnetic spectrum are suppressed with respect to lines toward the red end of the spectrum. The differential extinction between two wavelengths is referred to as "reddening."

Armed with knowledge of the relative strengths of certain spectral lines (e.g., from the Balmer series of hydrogen), a correction for the effects of dust can be made to obtain an estimation of the unfiltered spectrum. This correction is made possible by measuring two lines from a single ion whose ratio is not particularly sensitive to either density or temperature. With this ratio, a quantitative measurement of the amount of

dust that exists along the line of sight can be inferred for the entire electromagnetic spectrum. In order to obtain an accurate estimate of the reddening, lines chosen should be spaced widely apart in the spectrum.

2.4 Atomic Data

Atomic data include spontaneous emission coefficients and collision strengths for each transition. SNAP uses known values of atomic data to perform various analyses, such as correcting for reddening. Atomic data were updated in SNAP using the most recent data available from the MCHF/MCDHF Collection at Vanderbilt University (Fischer & Tachiev 2010).

2.5 Reddening Law and Extinction

The light of an HII region in another galaxy is obscured by dust in its host and by dust in the Milky Way. How the interstellar dust extinguishes light as a function of wavelength is quantified by a "reddening law." The shape of the law depends on the environment, but for the diffuse interstellar medium it is known to be constant along different sight lines (Fitzpatrick 1999). The law for the diffuse interstellar medium is the appropriate one to use for sources beyond the Milky Way. Most constructions are based on studies of extinguished stars within the Milky Way. It is thus necessary to assume that dust in the galaxies being studied is similar to that in the Milky Way.

One way of quantifying extinction is via the optical depth of dust at a particular wavelength. The optical depth, denoted by τ_λ, can be used to estimate the likelihood a photon will be obscured by a layer of dust (McCall & Armour 2000). By convention, the reference wavelength is chosen to be 1 μm. The emerging flux, f_λ, at wavelength, λ, is given by:

$$f_\lambda = f_\lambda^{\,0}\, e^{-\tau_\lambda} \tag{2.3}$$

where f_λ^0 refers to the corresponding unextinguished flux. The combination of τ_λ at one wavelength and a reddening law allows estimation of τ_λ at any wavelength.

Data published in the literature often comes in an unreddened form only (i.e., corrected). However, when analyzing galaxies, researchers tend to pick different reddening laws. To obtain a homogenous data set it is important to 1) obtain the "raw" data by undoing any correction procedure, and 2) redo the correction using a self-consistent method. Where raw data is already available, step 1 is not required.

The reddening law adopted for this study was that of Fitzpatrick (1999). However, in five of the galaxies chosen for this study (NGC 224, NGC 1097, NGC 3198, NGC 4559, and NGC 5236), not enough information was provided in the literature to undo (and redo using the Fitzpatrick law) extinction corrections. Usually missing were raw strengths of spectral lines of hydrogen from which a ratio must be taken in order to correct for extinction. In these cases, the corrected data from the original source were

adopted.

Figure 2.2 shows the Fitzpatrick reddening law. In this diagram, the quantities employed in characterizing the effects of reddening are extinction colour excess ratios, $\mathrm{E}(\lambda - V)/\mathrm{E}(B - V)$, where B and V refer to the B-band and V-band of the UBV - *Johnson and Morgan* system.

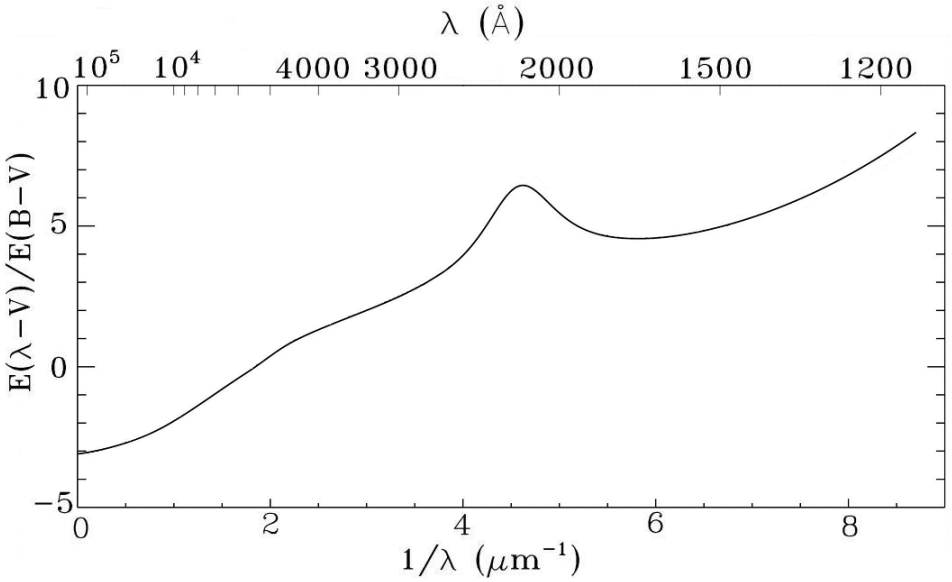

Figure 2.2: **The Fitzpatrick (1999) reddening law.**

2.6 Temperature and Density Determinations

In order to determine oxygen abundances via the direct T_e method, it is necessary to first determine temperatures and densities of the HII regions. One of the features of SNAP is the ability to estimate temperatures and densities from particular line

ratios.

Normally, a temperature is estimated from the ratio of intensities of two collisionally excited lines from a single ion which originate from upper levels which are separated significantly in energy. Because lines from the same ion are used, sensitivities of individual intensities to the number density of ions cancel out so that the differential dependence of the emissivities upon temperature can be gauged. It is also important to make use of a line ratio that is not strongly dependent on density. Here, the ratio of [OIII]λ5007 to [OIII]λ4363 was employed.

Density, on the other hand, is normally estimated from the ratio of intensities of two collisionally exited lines with different critical densities. "Critical density" refers to the density of a nebula at which collisionally excited line radiation starts to be suppressed by collisional de-excitations. This occurs because at high densities, collisional de-excitations have the effect of reducing the equilibrium population of the upper level, thereby reducing the emissivity. As with temperature, by taking a ratio of intensities of two lines from the same ion, the sensitivity of individual intensities to the number density of ions cancels out so that the differential dependence of the emissivities upon density can be gauged. In general, HII regions contain relatively low electron densities. Typically, densities range from 10 cm^{-3} to 250 cm^{-3}. Within this range, density variations barely affect statistical equilibrium. Over the range from 10 cm^{-3} to 250 cm^{-3} oxygen abundances change by less than 0.01 dex. This variation is more than an order of magnitude smaller than typical errors of measurement. In this

study, all densities are assumed to be 100 cm^{-3}.

2.7 Ionic Abundances and Total Oxygen Abundances

The intensity of a line is not only sensitive to temperature and density through the emissivity, but also to the total number of ions in a nebula contributing to the emission. Consequently, a ratio of intensities of lines from two different ions can be used to measure the relative number of ions. Normally, line intensities are referenced to Hβ, which in turn conveys the abundance of ions relative to H^+.

The "ionization correction factor" is a quantity used to convert ionic abundances of a given element to a total abundance. Typically, at a given location in a nebula, atoms of a particular element have been converted almost completely to a single stage of ionization, A, and nearly all hydrogen is in the form of H^+. That stage of ionization predominates over a well-defined volume of the nebula. The ionization correction factor for a single ion is determined simply by the fraction of the volume of the nebula occupied by the ion, i.e., $V(A)/V(H^+)$.

As discussed in §2.1, only two ions of oxygen predominate in HII regions, O^{++} and O^+. These ions are restricted to individual zones. Using the derived temperatures (see §2.6), ionic abundances can be calculated. Since

$$\frac{O^+}{H^+} \approx \left(\frac{O}{H}\right) \frac{V(O^+)}{V(H^+)}$$

and

$$\frac{O^{++}}{H^{+}} \approx \left(\frac{O}{H}\right) \frac{V(O^{++})}{V(H^{+})}$$

then summing these two ionic abundances gives the total oxygen abundance. In other words, the ionization correction factor for the sum can be adopted to be unity.

Chapter 3

Calculation of Oxygen Abundances

3.1 The Double-Valued Nature of R_{23}

One problem of employing a calculation of oxygen abundance that is based on the R_{23} index is that O/H is double-valued. From Figure 3.1, it can be seen that the graph of R_{23} versus oxygen abundance can be separated, though somewhat arbitrarily, into three separate sections (Pilyugin 2000; Pilyugin 2001). The "upper branch" refers to the part of the graph with 12+log(O/H) higher than 8.20, whereas the "lower branch" refers to the part with 12+log(O/H) lower than 7.95. The "transition zone" (i.e., values of 12+log(O/H) between 7.95 and 8.20) refers to the section where there is no significant correlation between the value of R_{23} and O/H. The HII regions in Figure 3.1 come from measurements of temperature, derived from temperature-sensitive [OIII]λ4363 line. At high abundances, temperatures become difficult to

measure since a higher metallicity leads to lower temperatures.

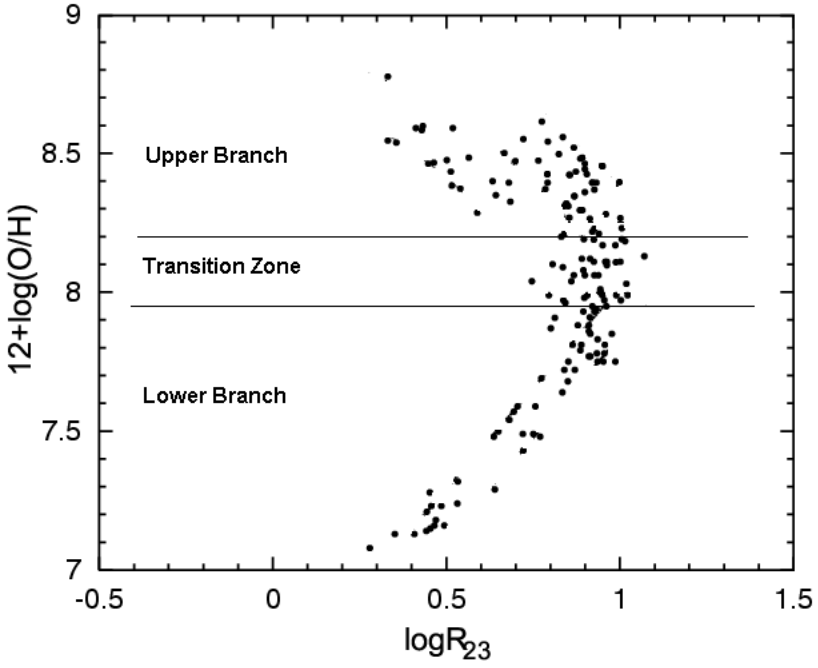

Figure 3.1: **O/H vs. R_{23} for HII regions from Pilyugin (2000) (low-metallicity) and Pilyugin (2001) (high-metallicity). Horizontal lines show the boundaries, as defined by Pilyugin, between the lower branch and the transition zone, and between the upper branch and the transition zone. Note that measurements on the upper branch are least certain because of the low temperatures of the gas.**

In order to make use of the R_{23} index, galaxies must possess HII regions that fall outside of the transition zone. HII regions within large spiral galaxies do not typically have oxygen abundances that fall on the lower branch of the R_{23} curve. However, they may have an abundance that lies in the bend of the curve. When analyzing galaxies using a calibration of the R_{23} index, it is necessary to restrict the sample of

HII regions to those with oxygen abundances higher than 12+log(O/H)=8.20.

3.2 Ionization Hardening

Oxygen abundances cannot be derived from R_{23} alone. An examination of the upper branch of the O/H versus R_{23} curve in Figure 3.1 shows a scatter of up to 0.5 dex (Pilyugin & Thuan 2005). Although there is a good deal of scatter arising from uncertain temperatures, it is also believed that there is not a simple one-to-one correlation between oxygen abundance and R_{23}. The intensities of oxygen emission lines in the spectra of HII regions depend on more than just the abundance. They also depend on physical conditions of the region such as the density, the geometry, and the quantity and quality of the ionizing radiation, all of which affect ionization equilibrium.

For example, consider an HII region for which the ionizing radiation field is unusually hard due to an anomalous mix of hot stars. Because the fraction of photons with an energy greater than 1.8 Rydbergs is higher, more of the singly ionized oxygen loses an electron and turns into doubly ionized oxygen. Even though the O^+ abundance declines, the harder radiation field leads to more heating which strengthens [OII] to partially compensate. Since [OIII] is also enhanced by the higher temperature, R_{23} may increase, mimicking a decline in O/H. The signature of the effect lies in [OIII]/[OII], which has increased (Shields & Searle 1978).

The ratio of O^{++} to O^+ must therefore be incorporated into any calibration of the oxygen abundance. Otherwise, it is possible to misinterpret a spectral differ-

ence arising from a deviation in physical conditions as a consequence of a difference in chemical composition. The idea that the strong lines of oxygen, [OII]λ3727 and [OIII]$\lambda\lambda$4959,5007, include all the necessary information to correctly determine oxygen abundances in HII regions was put forth by McGaugh (1991). Both the ratio of [OIII] to [OII] (McGaugh 1991) and that of [OIII] to ([OII]+[OIII]) (Pilyugin 2001) have been used in combination with R_{23} to calibrate oxygen abundances.

3.3 Options for Calibration Choices

Many different strong line calibration techniques have been proposed since the original R_{23} index was introduced by Pagel et al. (1979). The most popular of these methods were put forward by Pagel et al. (1980), Edmunds & Pagel (1984), McCall et al. (1985), Dopita & Evans (1986), Torres-Peimbert et al. (1989), Skillman et al. (1989), McGaugh (1991), Zaritsky et al. (1994), and Pilyugin (2001).

Three of the most widely used calibration methods, McGaugh (1991), Zaritsky (1994), and Pilyugin (2001), were used in the study by Sadavoy and McCall (2006) (described in §1.7). The McGaugh (1991), Zaritsky et al. (1994) and Pilyigin (2001) calibrations for calculating oxygen abundances are, respectively, as follows:

$$12 + \log(\mathrm{O/H}) = 12 - 2.939 - 0.2x - 0.237x^2 - 0.305x^3 - 0.0283x^4 - y(0.0042 - 0.0221x - 0.102x^2 - 0.0817x^3 - 0.00717x^4) \quad (3.1)$$

where $x = \log(\mathrm{R_{23}})$ and $y = \log\left([\mathrm{OIII}]\lambda\lambda 4959, 5007/[\mathrm{OII}]\lambda 3727\right)$

$$12 + \log(\mathrm{O/H}) = 9.265 - 0.33x - 0.202x^2 - 0.207x^3 - 0.333x^4 \quad (3.2)$$

where $x = \log(\mathrm{R_{23}})$

$$12 + \log(\mathrm{O/H}) = \frac{\mathrm{R_{23}} + 54.2 + 59.45P + 7.31P^2}{6.07 + 6.71P + 0.37P^2 + 0.243\mathrm{R_{23}}} \quad (3.3)$$

where $P = \left([\mathrm{OIII}]\lambda\lambda 4959, 5007/\left([\mathrm{OII}]\lambda 3727 + [\mathrm{OIII}]\lambda\lambda 4959, 5007\right)\right)$

In Sadavoy and McCall's research, all three methods were used for the analysis of oxygen abundances without discrimination or proper justification. Each of these methods leads to a different oxygen abundance with a different least squares best fit line (see Figure 1.3). The differences in these fits are as much as 0.6 dex. Clearly, further analysis that would lead to the best choice for a sensible $\mathrm{R_{23}}$ calibration would be beneficial.

Moreover, Sadavoy and McCall made mistakes in the usage of the indirect $\mathrm{R_{23}}$ method of calibration, specifically when employing the Pilyugin (2001) calibration. As noted in §3.1, HII regions with oxygen abundance below 12+log(O/H)=8.20 fall

into the "transition zone" (see Figure 3.1). Thus their oxygen abundances cannot be determined from the R_{23} index. From Figure 1.3(a), it is clear that many of the points exhibit oxygen abundances below this 8.20 mark. Not only that, the best fit line through the points from the Pilyugin calibration crosses over the "transition zone" boundary at $r = 7'.5$. At radii beyond this point, there is an increasing likelihood that HII regions truly possess oxygen abundances below the 8.20 mark. Therefore, all points beyond $r = 7'.5$ should be excluded. After excluding the points already below 8.2 and those outside $r = 7'.5$ (even those that appear to be above 12+log(O/H)=8.20), a new least squares fit is necessary.

3.4 Theoretical Justification for Calibration

McGaugh's calibration, first proposed in 1991 (McGaugh 1991), was derived by obtaining oxygen abundances from HII regions in several galaxies for which the [OIII] λ4363 auroral line was available via the direct T_e method. Then, using R_{23}, an equation for a best fit line to the data was conceived.

The main problem with this empirical method of calibration is that the objects used for the direct measurements were from a variety of sources, the majority of which yield oxygen abundances that lay in or very near to the transition zone in the O/H versus R_{23} graph. Furthermore, since the publication of the McGaugh calibration, much better and more accurate measurements of the [OIII]λ4363 auroral line have become available.

The Zaritsky calibration (Zaritsky et al. 1994) suffers from similar problems. It was not created empirically from calculations of oxygen abundance obtained via the direct T_e method, but rather by averaging other calibrations, namely those of Edmunds & Pagel (1984), McCall et al. (1985), and Dopita & Evans (1986). Those calibrations themselves suffer from the same problems plaguing that of McGaugh. Moreover, the Zaritsky calibration does not take into account factors affecting the ionization state of the gas, for example, by accounting for the ratio of O^{++} to O^{+} as discussed in §3.2.

Of the three calibrations tested, the Pilyugin calibration (Pilyugin 2001) was the one published most recently. It was derived using 38 HII regions in spirals. The oxygen abundances from these regions were in the "upper branch" of the O/H versus R_{23} graph. Moreover, the Pilyugin calibration takes into account the state of ionization by accommodating the ratio [OIII]/([OIII]+[OII]), termed P, in equation 3.3.

3.5 Empirical Comparison of Direct and Indirect Abundances

Determining a proper calibration of oxygen abundances using indirect methods is done by comparing the results of the various calibrations to those obtained by the direct T_e method. For HII regions whose oxygen abundance levels are below 12+log(O/H)=8.20, this approach is not possible because of the double-valued nature of the R_{23} method. At high metallicities, there is a challenge, too. The [OIII]λ4363 auroral line becomes

too faint to detect, so comparisons of indirect methods of calibrating abundances can only be made with abundances determined from Planetary Nebulae in the vicinity of the HII regions. Verification of indirect methods of calibration via use of Planetary Nebulae will be explored in §3.6.

In this study, entire galaxies were chosen to anchor calibrations as opposed to individual HII regions from a large variety of galaxies. This was because abundance gradients will be used to guide the connection of R_{23} and direct abundances.

Figure 3.2 shows abundances as a function of radius for two different galaxies, NGC 300 and NGC 5457, for which both the direct T_e method and various indirect methods using R_{23} have been applied. In these plots, the slopes of the gradients from the various calibration methods have been constrained to match the slope of the gradient of the direct method. In this way, it is possible to get an overall picture of the systematic difference in gradients from different calibrations. The difference in O/H between the various methods of calibration and the direct method are listed in Table 3.1. It is evident that, of the three methods of calculating oxygen abundances, the closest approximation is that of Pilyugin (2001).

In table 3.1, it is clear that although the Pilyugin equation delivers abundances closest to the true values, there is still a small difference between the two. Nonetheless, the Pilyugin calibration was adopted in its original form (i.e., without modification) for several reasons. First, only two galaxies contained enough HII regions within them that a comparison of direct versus indirect methods of obtaining oxygen abundances

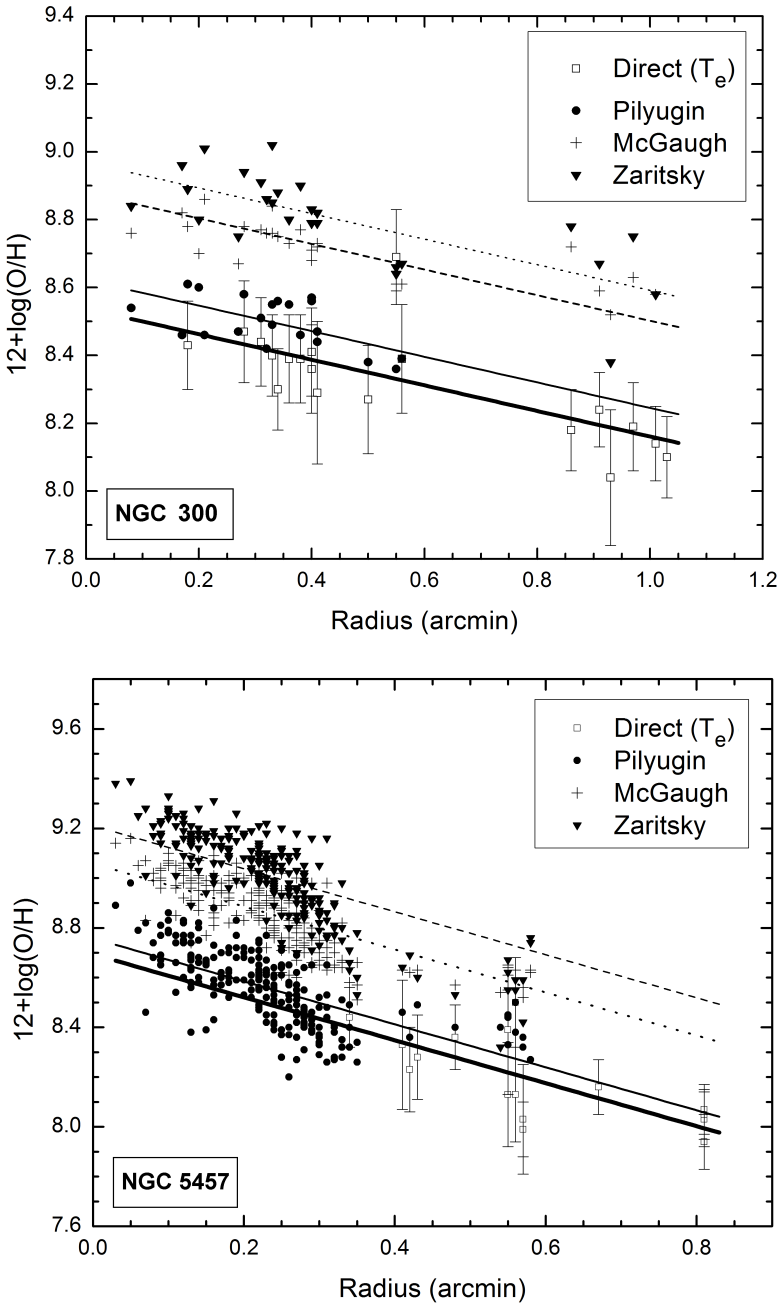

Figure 3.2: **Oxygen abundance versus deprojected radius for NGC 300 (top) and NGC 5457 (bottom). In each graph, the thick solid line represents the best fit line using the direct T_e method. The thin solid line, the thick dotted line, and the thin dotted line represent the best fit lines for the data using the calibrations from Pilyugin (2001), McGaugh (1991), and Zaritsky et al. (1994), respectively.**

Table 3.1: **Comparison of various calibration methods for determining oxygen abundances.**

Calibration		**NGC 300**	**NGC 5457**
	Number of HII regions with [OIII] λ4363	18	17
Direct (T_e)	Slope (dex/arcmin)	-0.38	-0.86
	Intercept (O/H at r =0)	8.54	8.69
Pilyugin	Intercept (O/H at r =0)	8.62	8.76
	Difference	**0.08**	**0.07**
McGaugh	Intercept (O/H at r =0)	8.88	9.06
	Difference	**0.34**	**0.37**
Zaritsky	Intercept (O/H at r =0)	8.97	9.21
	Difference	**0.43**	**0.52**

could be made. Second, the Pilyugin calibration (as well as others such as that of McGaugh) is used widely in the literature. Third, the average differences between the intercepts from the direct method versus the Pilyugin calibration are 0.08 dex for NGC 300 and 0.07 dex for NGC 5457. The differences in the intercepts can be interpreted as the uncertainty in the calibration methods.

3.6 Verification of R_{23} Calibration with Planetary Nebulae

Richer et al. (1997) showed that planetary nebulae may be used to gauge oxygen

abundances. Gradients of the oxygen abundance found for HII regions and planetary nebulae for the same galaxy have similar slopes, but the abundances for HII regions are systematically higher. Figure 3.3 shows a comparison of the abundances of planetary nebulae and HII regions in NGC 3031. The solid line represents the best fit for the HII regions, while the dotted line is the trend for planetary nebulae. Note that the slopes of the best fit lines (-0.052 and -0.065, respectively) are the same within the errors (0.008 and 0.015, respectively). With the slope for HII regions fixed at the value for planetary nebulae, the trends are separated by only 0.10 dex. This fact is important, because it gives confidence to the high oxygen abundance end of the Pilyugin calibration, where HII regions are too cool to detect, preventing the measurement of temperatures and the direct determination of abundances. The offset of HII region abundances from those for planetary nebulae is consistent with the abundance gap predicted for those metallicities by Richer et al. (1997).

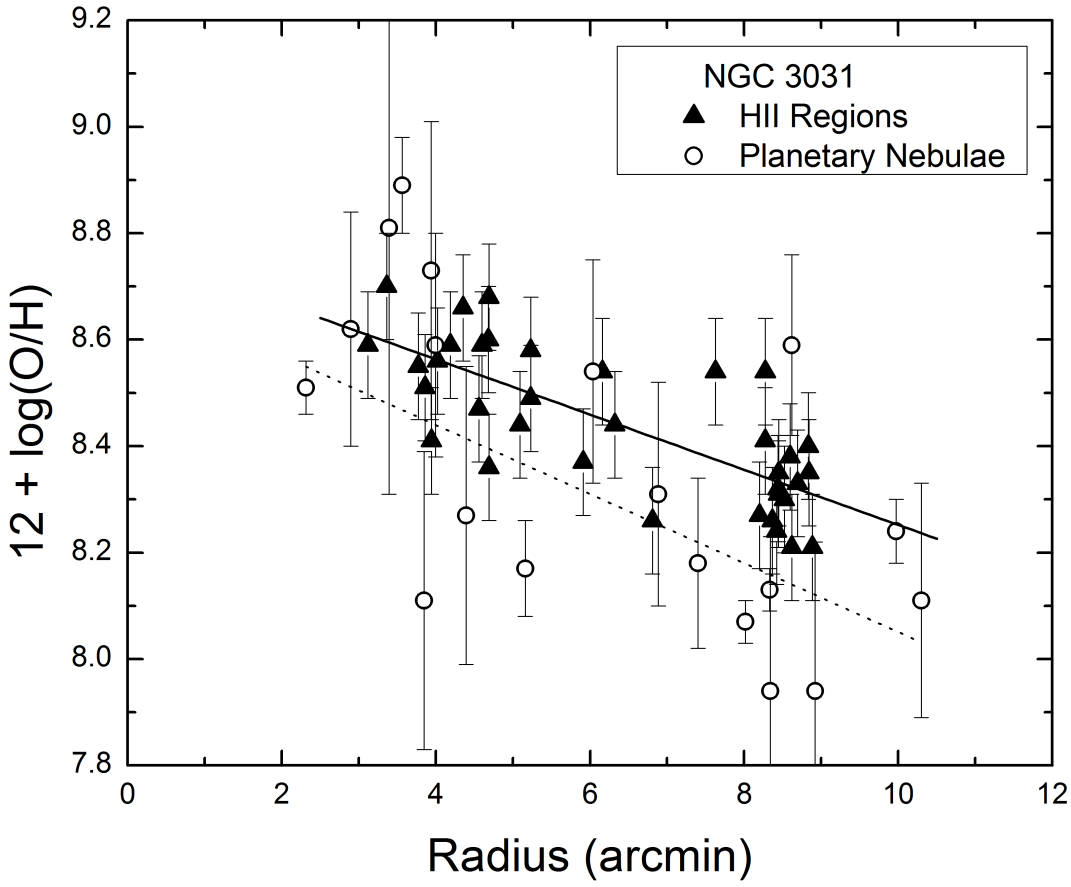

Figure 3.3: **Oxygen abundance versus deprojected radius for HII regions (closed triangles) and planetary nebulae (open circles) in NGC 3031. Abundances in HII regions were derived using the Pilyugin (2001) calibration. The solid and dotted lines represent, resepectively, the best fit trends for HII regions and planetary nebulae.**

Chapter 4

Selection of Galaxies

4.1 Selection Criteria for Galaxies

Twenty galaxies were chosen for study. Galaxies at either extreme of the Hubble sequence were excluded. Elliptical galaxies have little gas and so do not contain HII regions. Also, their planetary nebulae are difficult to observe. Thus, their abundance gradients are not well known. Irregular galaxies, such as dwarfs, were excluded since their chemical compositions are homogeneous (see §1.5) and they therefore do not generally possess a gradient in their oxygen abundance. The galaxies chosen in this sample range from 2.4 to 7.4 on the Hubble stage T scale (de Vaucouleurs et al. 1991).

The two galaxies studied by Sadavoy and McCall (2006) were included in order to compare and evaluate their findings. All analyses involving these two galaxies were re-done using self-consistent methods for data reduction and computations (see §3).

4.2 Published Information

For this study it was important to select galaxies for which there was published information on many HII regions located at a wide range of radii across each. Specifically, measurements of the emission lines of oxygen and hydrogen in HII regions and maps of 21.1 cm radiation from HI (which traces neutral hydrogen) were needed. In addition, galaxies with data relating to their molecular hydrogen content were favoured. Such information comes in the form of carbon monoxide maps, since CO traces molecular hydrogen (Dickman 1978).

All data used in this analysis were collected from published works. Table 4.1 lists the sample galaxies and shows the sources from which the data for each galaxy were taken.

4.3 Attributes of Sample Galaxies

The galaxies in this study and their physical attributes are listed in Table 4.2. In Table 4.2, "Type" refers to the Revised Hubble Type (de Vaucouleurs et al. 1991). "R_o," measured in arcminutes, refers to the corrected isophotal radius, i.e., the radius of the galaxy to the isophote at which the surface brightness is 25 mag/arcsec^2 in B. The parameters, "i," and "PA," refer to the inclination and the position angle, respectively, and they are measured in degrees. The inclination is the observed tilt of the galaxy (e.g., a galaxy with an inclination of 0° would appear face-on, while a

galaxy with an inclination of 90° would appear edge-on). The position angle is the angle between celestial north and the major axis of the elliptical projection of the galaxy on the sky, measured eastward from north.

Table 4.1: **Published sources from which data were obtained for this study.**

Galaxy	O/H	HI	CO
NGC 224	Blair et al. 1982	Chemin et al. 2009	Nieten et al. 2006
NGC 300	Bresolin et al. 2009 (b)	Westmeier 2011	
NGC 598	Bresolin 2011	Newton 1980	Corbelli 2003
NGC 628	McCall et al. 1985 Ferguson et al. 1998 van Zee et al. 1998 Bresolin et al. 1999	Wevers 1984	Leroy et al. 2009
NGC 925	Dors & Copetti 2005	Pisano et al. 1998	Leroy et al. 2009
NGC 1097	Storchi-Bergmann et al. 1996	Crosthwaite 2002	Gerin et al. 1988
NGC 1232	van Zee & Bryant 1999 Bresolin et al. 2005	van Zee & Bryant 1999	
NGC 1365	Bresolin et al. 2005	Holwerda et al. 2005	
NGC 2403	McCall et al. 1985 van Zee et al. 1998 Garnett et al. 1997 Bresolin et al. 1999	Leroy et al. 2008	Thornley & Wilson 1995
NGC 2903	van Zee et al. 1998 Bresolin et al. 2005	Wevers 1984	Young et al. 1995
NGC 3031	Garnett & Shields 1987 Bresolin et al. 1999 Stanghellini et al. 2010	Holwerda et al. 2005	Sage & Westpfahl 1991
NGC 3184	McCall et al. 1985 Zaritsky et al. 1994 van Zee et al. 1998	Leroy et al. 2008	Leroy et al. 2009
NGC 3198	Zaritsky et al. 1994	Begeman 1989	Leroy et al. 2009
NGC 4258	Bresolin 2011	Wevers 1984	Young et al. 1995
NGC 4559	Zaritsky et al. 1994	Barbieri et al. 2005	
NGC 5194	Bresolin et al. 1999 Bresolin et al. 2004	Schuster et al. 2007	Schuster et al. 2007
NGC 5236	Bresolin et al. 2005 Bresolin et al. 2009 (a)	Rogstad et al. 1974	Andersson 2002
NGC 5457	Kennicutt et al. 2003 Bresolin 2007 van Zee et al. 1998 Cedrés & Cepa 2002	Kenney et al. 1991	Kenney et al. 1991
NGC 6946	McCall et al. 1985 Ferguson et al. 1998	Tacconi & Young 1986	Leroy et al. 2009
NGC 7793	Webster & Smith 1983 McCall et al. 1985	Leroy et al. 2008	

Table 4.2: **Physical attributes of galaxies in the study.**

Galaxy name	Other names	Type	Distance Modulus	Dist. Mod. Error	R_o		i	PA
					(')	(kpc)	(^{o})	(^{o})
		(1)	(2)	(3)	(4)	(5)	(6)	(7)
NGC 224	M31, Andromeda	SA(s)b	24.34	0.09	102.09	722.9	78	38
NGC 300	Caldwell 70	SA(s)d	26.44	0.08	11.19	86.1	46	107
NGC 598	M33, Triangulum	SA(s)cd	24.62	0.08	37.07	265.5	54	23
NGC 628	M74	SA(s)c	29.64	0.07	5.36	46.2	9	48
NGC 925		SAB(s)d	29.78	0.05	5.48	47.5	61	109
NGC 1097		SB(s)b	31.11	0.20	4.77	43.2	31 [a]	141 [a]
NGC 1232		SAB(rs)c	31.34	0.20	3.71	33.8	30 [b]	108 [b]
NGC 1365	Great Barred Spiral	SB(s)b	31.25	0.06	5.61	51.0	40	32
NGC 2403	Caldwell 7	SAB(s)cd	27.50	0.05	11.45	91.6	60	125
NGC 2903		SAB(rs)bc	29.62	0.19	6.29	54.2	61	23
NGC 3031	M81	SA(s)ab	27.75	0.09	13.77	111.2	57	151
NGC 3184		SAB(rs)cd	30.22	0.20	3.71	32.6	16 [c]	179 [c]
NGC 3198		SB(rs)c	30.64	0.08	4.26	38.0	72	216
NGC 4258	M106	SAB(s)bc	29.29	0.09	9.31	79.3	67	150
NGC 4559		SAB(rs)cd	29.03	0.20	5.48	46.3	67 [d]	323 [d]
NGC 5194	M51, Whirlpool	SA(s)bc	29.41	0.11	5.61	48.0	20	166
NGC 5236	M83, Southern Pinwheel	SAB(s)c	28.35	0.10	6.59	54.3	25	66
NGC 5457	M101, Pinwheel	SAB(rs)cd	29.24	0.13	14.42	122.6	21	43
NGC 6946	Caldwell 12, Fireworks	SAB(rs)cd	28.83	0.22	8.30	69.6	33	66
NGC 7793		SA(s)d	27.78	0.24	4.77	38.5	52	105

Notes:

(1) Revised Hubble Type, from de Vaucouleurs et al. (1991)
(2) Distance modulus, in dex, from McCall (2011)
(3) Error in distance modulus, from McCall (2001)
(4) Isophotal radius, corrected to face-on and corrected for galactic extinction, in arcminutes, from de Vaucouleurs et al. (1991)
(5) Same as (4), but in kiloparsecs, from de Vaucouleurs et al. (1991)
(6) Inclination, from McCall (2011)
(7) Position angle, from McCall (2011)

[a] Ondrechen et al. 1989
[b] van Zee & Bryant 1999
[c] Begeman 1989
[d] Barbieri et al. 2005

Chapter 5

Measurements of Oxygen Abundances in Galaxies

5.1 Gradients

In order to calculate oxygen abundances for HII regions within the sample set of galaxies, both the indirect method and, where possible, the direct method were used. For HII regions where [OIII]λ4363 was available, only the direct method was applied so as not to double count the same region. It was possible to calculate oxygen abundances for NGC 300 solely using the direct T_e method. For the galaxies NGC 5236 and NGC 5457, a combination of direct and indirect methods was used to calculate oxygen abundances. Abundances for the remaining galaxies in this study were obtained strictly using the Pilyugin (2001) R_{23} method (see §3.3). All data were processed in a self-consistent manner as described in §3.

The two galaxies sampled by Sadavoy and McCall (2006), NGC 5457 and NGC 6496, were included in this study. However, compared to that study, the sample of

HII regions was enlarged and the analysis was improved. HII regions that lie within the "transition zone" (see §3.1) were eliminated. Moreover, only the best choice for indirect oxygen abundance calibrations was chosen, namely that of Pilyugin (2001).

Figure 5.1 shows plots of the oxygen abundance versus angular radius for all galaxies in this study. Radii are "deprojected," meaning they are evaluated as they would appear if the galaxy were face-on. In order to obtain a deprojection of a spiral galaxy, the disk of the galaxy is approximated to be planar with HII regions lying on the plane. This approximation is corroborated by studies of the Milky Way, which show that HII regions within 12 kpc from the galactic centre possess a dispersion (i.e., distance in the direction perpendicular to the disk) of less than 130 pc (Fich & Blitz 1984). Conversions to deprojected radii were performed using the inclination and position angles given in Table 4.2. Consider an HII region with coordinates r and θ in the plane of the sky, where, with respect to the centre of the galaxy, r is the distance and θ is the position angle measured east from north. If the host galaxy has a given inclination (i) and a major axis position angle (ϕ) measured east from north, then the deprojected radius, r', is given by equation 5.1.

$$r' = \sqrt{(r\cos(\theta - \phi))^2 + \left(\frac{r\sin(\theta - \phi)}{\cos(\mathrm{i})}\right)^2} \tag{5.1}$$

Sources of spectroscopy are listed in a legend within each graph. Since it is known that n(O)/n(H) decays exponentially with radius (Searle 1971; Zaritsky 1992), plots of 12+log(O/H) versus radius can justifiably be fitted with a line. Errors for

abundances derived from [OIII]λ4363 were propagated from uncertainties in line fluxes using SNAP. Errors for abundances derived from the R_{23} method are about 0.1 dex (Pilyugin 2001). In each plot, the thick solid line represents the oxygen abundance gradient, while the dashed lines represent the maximum and minimum gradients allowed by the data. These gradient limits were calculated by adding or subtracting the standard error of each slope to the slope itself, and then fitting the intercept.

All data relating to the oxygen abundance plots are listed in Table 5.1.

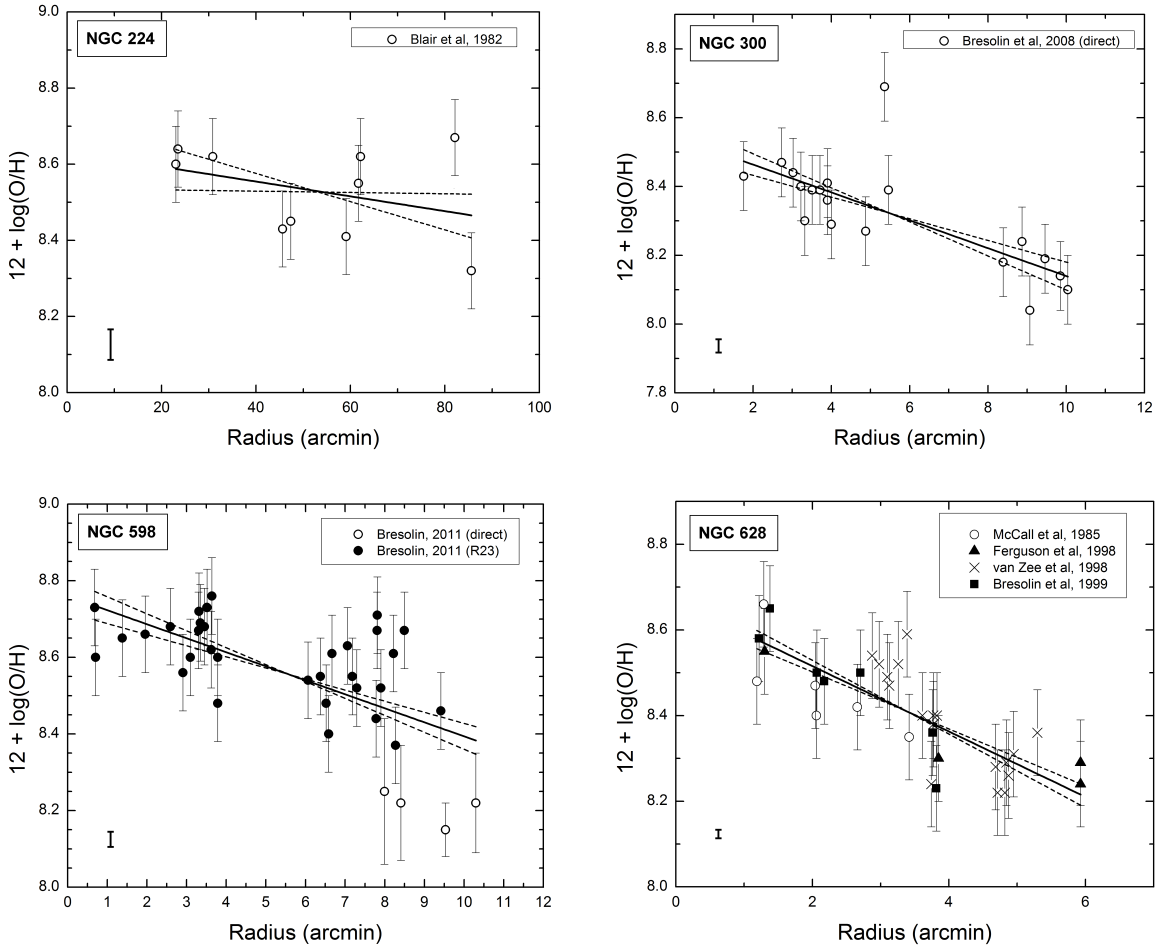

Figure 5.1: **Oxygen abundance versus deprojected radius for a) NGC 224, b) NGC 300, c) NGC 598, and d) NGC 628. In each plot, the source from which the spectroscopic data were obtained is listed in the legend. Data points obtained using the direct T_e method are indicated by the word "direct" next to the listed source. For sources from which points were obtained using the direct method as well as the R_{23} method, points obtained using the R_{23} method are indicated by "R23" next to the source. All other data points were obtained via the R_{23} method. The least squares best fit to the points is shown as a thick solid line. The dashed lines represent maximum and minimum fits calculated by adding or subtracting the standard error of each slope to the slope itself, and then fitting the intercept. The vertical error at the intersection is shown in the bottom-left corner.**

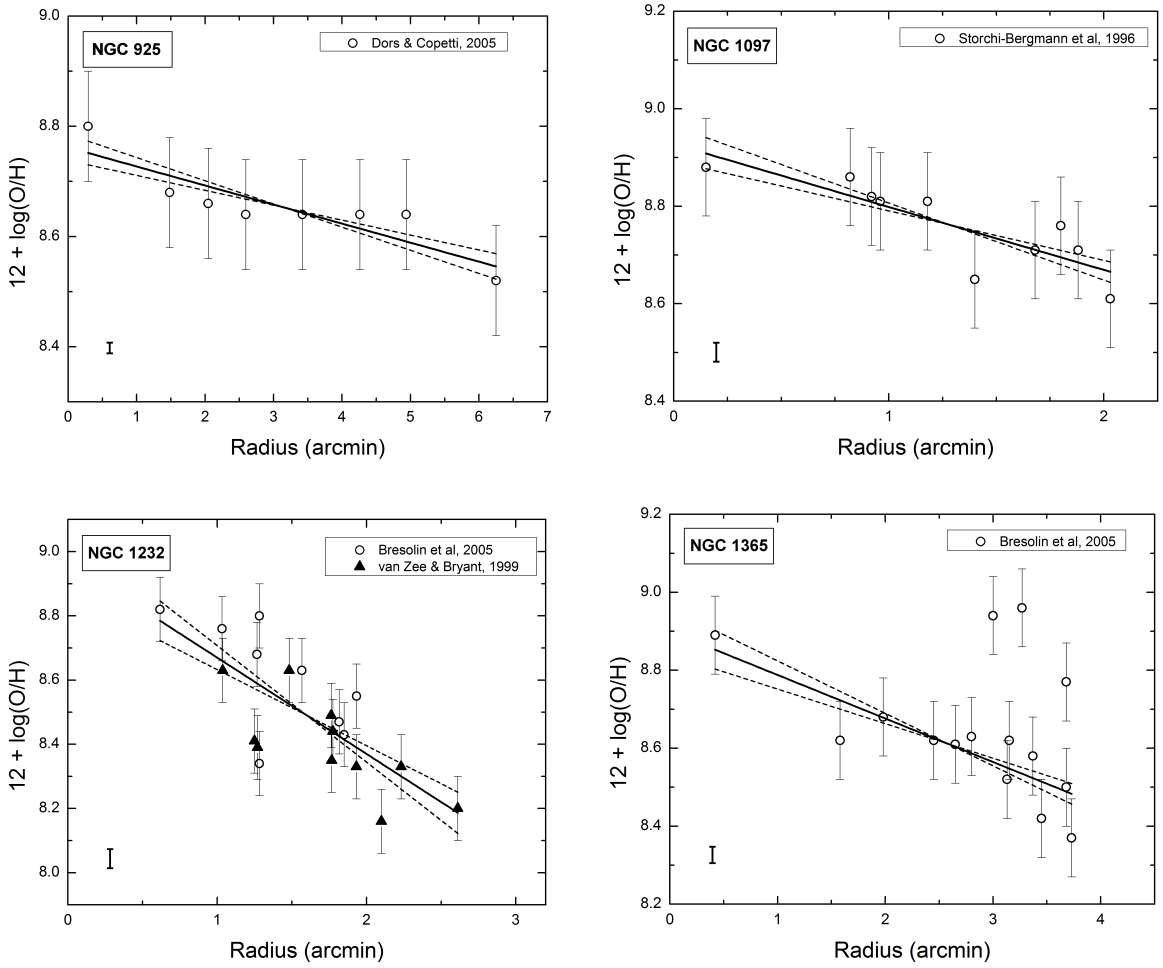

Figure 5.1 (cont'd): **Oxygen abundance versus radius for e) NGC 925, f) NGC 1097, g) NGC 1232, and h) NGC 1365**

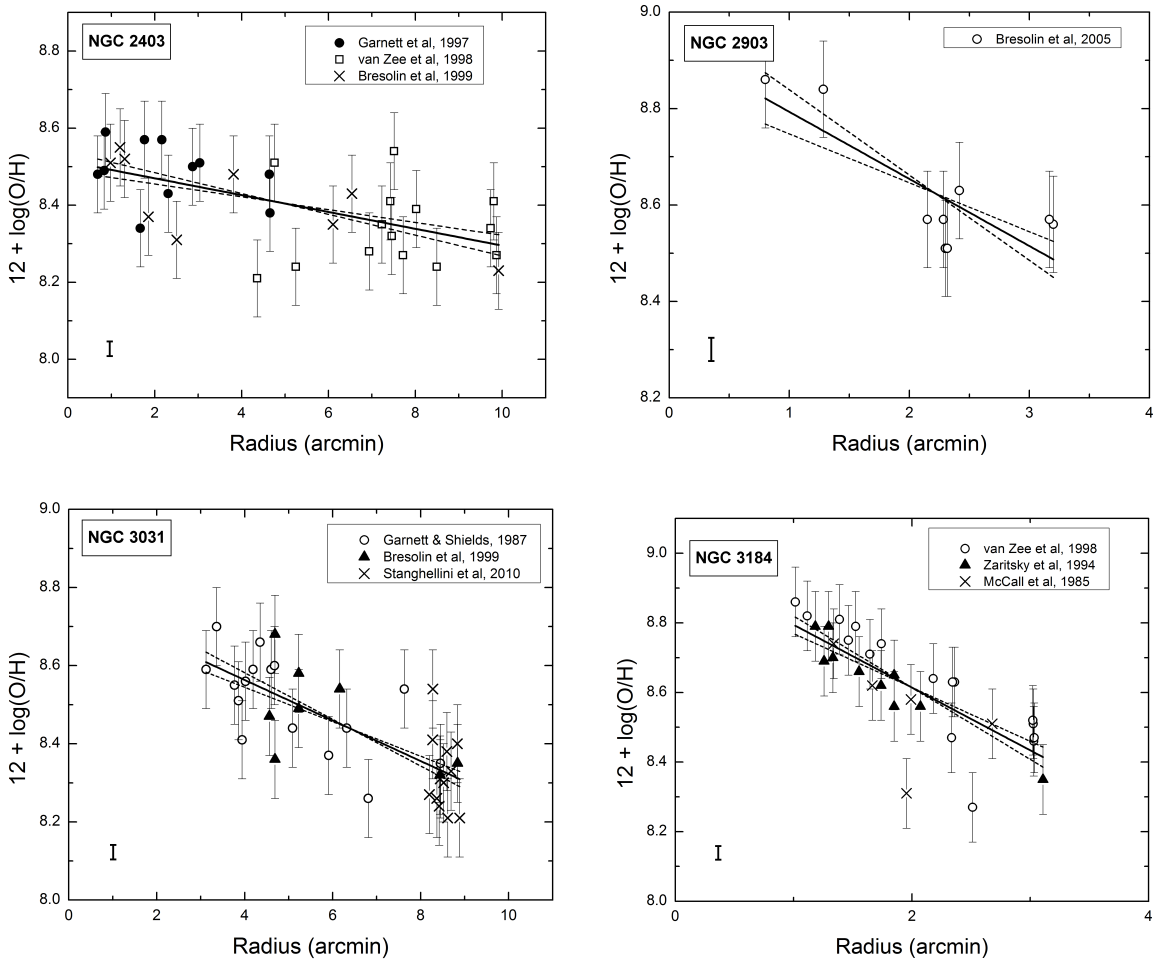

Figure 5.1 (cont'd): **Oxygen abundance versus radius for i) NGC 2403, j) NGC 2903, k) NGC 3031, and l) NGC 3184**

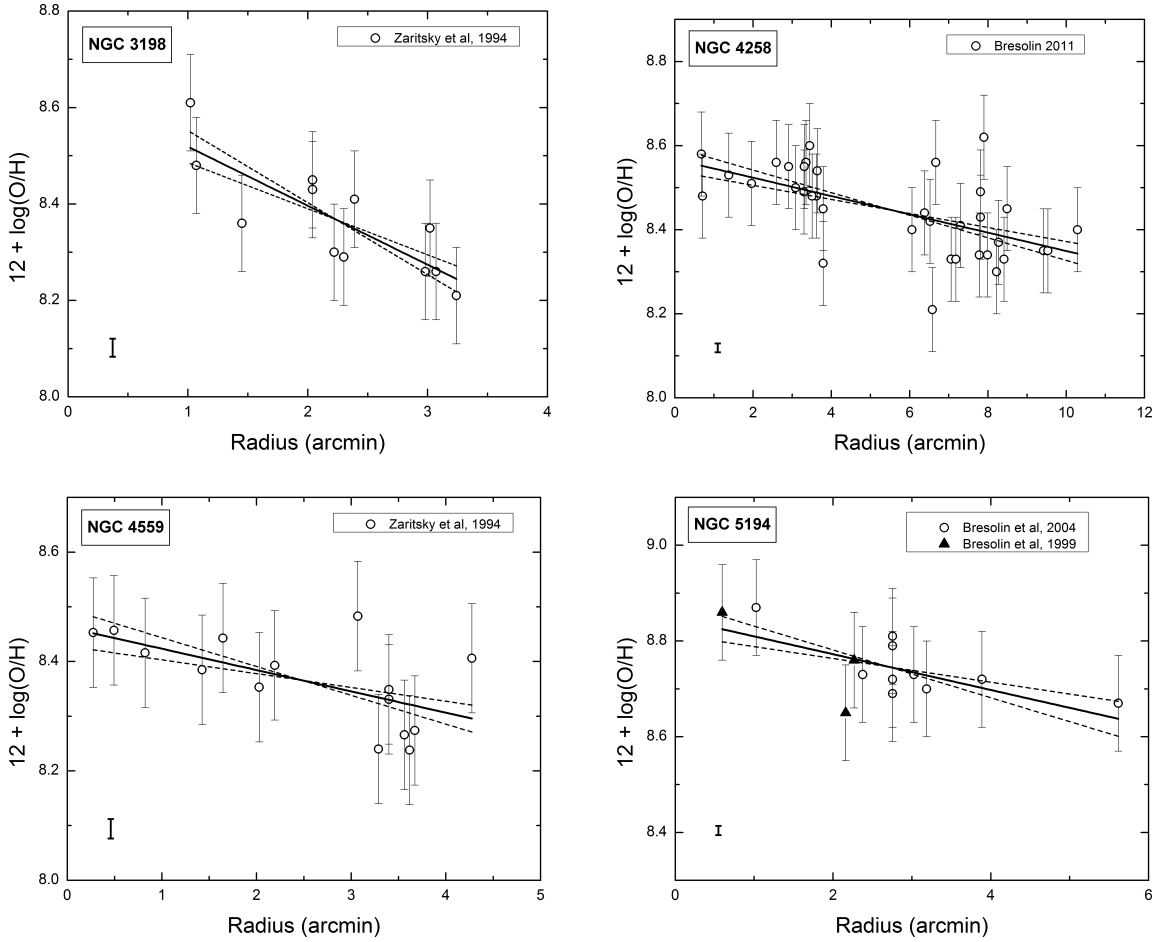

Figure 5.1 (cont'd): **Oxygen abundance versus radius for m) NGC 3198, n) NGC 4258, o) NGC 4559, and p) NGC 5194**

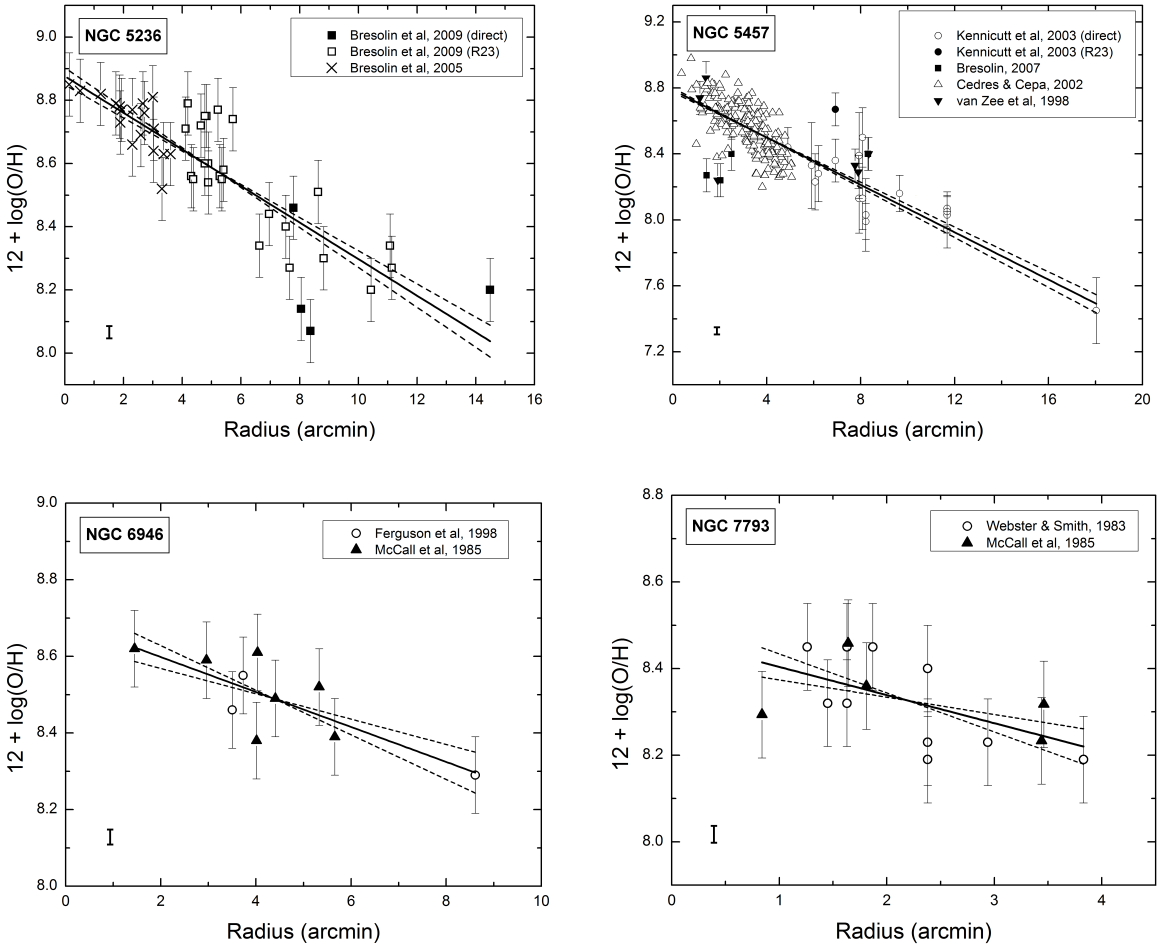

Figure 5.1 (cont'd): **Oxygen abundance versus radius for q) NGC 5236, r) NGC 5457, s) NGC 6946, and t) NGC 7793**

5.2 Deviations in O/H Between Individual HII Regions and the Gradient

In the plots of Figure 5.1, there are points which deviate significantly from overall trends. There are several factors that can explain this scatter. Points may suffer from observational errors. For HII regions with an available [OIII]λ4363 line, errors given in the raw data were propagated through the reduction and analysis processes.

Perhaps the main source of error in abundances calculated via the indirect R_{23} method is the calibration itself. Despite the inclusion of $\frac{[OIII]}{[OII]+[OIII]}$ in the Pilyugin calibration, the indirect method does not perfectly account for other properties of the HII regions, such as geometry and density. Abundances calculated via the indirect method were assigned an error of 0.1 dex, consistent with the typical error calculated by Pilyugin (2001) as well as this study (see §3.5). Errors in abscissae are negligible.

Finally, not all HII regions at a particular radius possess exactly the same oxygen abundance. This can be attributed to local variations in star formation rates and resulting inhomogeneities within each galaxy. However, Kobulnicky & Skillman (1997) showed that enrichment from massive OB stars or Wolf-Rayet stars does not significantly impact the local environment, and that oxygen abundance variations are constrained to less than 0.05 dex/kpc. It is the average of these HII regions that gives a decent picture of the overall oxygen abundance of the galaxy.

Table 5.1: **Oxygen abundance data for HII regions within all sample galaxies.**

NGC 224

HII Region	Deproj. radius (arcmin)	Oxygen Abundance (12 + log(O/H))	Method	Source
BA75	23.0	8.60	R_{23}	Blair et al., 1982
BA423	23.5	8.64	R_{23}	Blair et al., 1982
BA289	30.9	8.62	R_{23}	Blair et al., 1982
BA1/2	45.6	8.43	R_{23}	Blair et al., 1982
BA577	47.4	8.45	R_{23}	Blair et al., 1982
BA379	59.1	8.41	R_{23}	Blair et al., 1982
BA668	61.7	8.55	R_{23}	Blair et al., 1982
BA676	62.1	8.62	R_{23}	Blair et al., 1982
BA684	82.1	8.67	R_{23}	Blair et al., 1982
BA487/8	85.6	8.32	R_{23}	Blair et al., 1982

NGC 300

HII Region	Deproj. radius (arcmin)	Oxygen Abundance (12 + log(O/H))	Method	Source
1	10.04	8.10	Direct (T_e)	Bresolin et al., 2009
2	9.85	8.14	Direct (T_e)	Bresolin et al., 2009
3	9.07	8.04	Direct (T_e)	Bresolin et al., 2009
4	9.46	8.19	Direct (T_e)	Bresolin et al., 2009
5	5.36	8.69	Direct (T_e)	Bresolin et al., 2009
6	5.46	8.39	Direct (T_e)	Bresolin et al., 2009
8	4.88	8.27	Direct (T_e)	Bresolin et al., 2009
9	3.90	8.41	Direct (T_e)	Bresolin et al., 2009
10	3.51	8.39	Direct (T_e)	Bresolin et al., 2009
11	4.00	8.29	Direct (T_e)	Bresolin et al., 2009
14	3.71	8.39	Direct (T_e)	Bresolin et al., 2009
17	3.02	8.44	Direct (T_e)	Bresolin et al., 2009
19	3.32	8.30	Direct (T_e)	Bresolin et al., 2009
20	1.76	8.43	Direct (T_e)	Bresolin et al., 2009
23	2.73	8.47	Direct (T_e)	Bresolin et al., 2009
24	3.22	8.40	Direct (T_e)	Bresolin et al., 2009
26	3.90	8.36	Direct (T_e)	Bresolin et al., 2009
27	8.39	8.18	Direct (T_e)	Bresolin et al., 2009
28	8.87	8.24	Direct (T_e)	Bresolin et al., 2009

Table 5.1 (cont'd)

NGC 598

HII Region	Deproj. radius (arcmin)	Oxygen Abundance (12 + log(O/H))	Method	Source
24	7.99	8.25	Direct (T_e)	Bresolin, 2011
30	10.29	8.22	Direct (T_e)	Bresolin, 2011
34	8.41	8.22	Direct (T_e)	Bresolin, 2011
36	9.53	8.15	Direct (T_e)	Bresolin, 2011
1	6.52	8.48	R_{23}	Bresolin, 2011
2	6.38	8.55	R_{23}	Bresolin, 2011
3	6.06	8.54	R_{23}	Bresolin, 2011
4	3.62	8.62	R_{23}	Bresolin, 2011
5	3.30	8.67	R_{23}	Bresolin, 2011
6	3.09	8.60	R_{23}	Bresolin, 2011
7	3.64	8.76	R_{23}	Bresolin, 2011
8	3.51	8.73	R_{23}	Bresolin, 2011
9	3.45	8.68	R_{23}	Bresolin, 2011
10	3.35	8.69	R_{23}	Bresolin, 2011
11	3.31	8.72	R_{23}	Bresolin, 2011
12	2.91	8.56	R_{23}	Bresolin, 2011
13	2.59	8.68	R_{23}	Bresolin, 2011
14	1.96	8.66	R_{23}	Bresolin, 2011
15	0.68	8.73	R_{23}	Bresolin, 2011
16	0.71	8.60	R_{23}	Bresolin, 2011
17	1.38	8.65	R_{23}	Bresolin, 2011
18	7.81	8.67	R_{23}	Bresolin, 2011
19	3.79	8.60	R_{23}	Bresolin, 2011
20	3.79	8.48	R_{23}	Bresolin, 2011
21	6.67	8.61	R_{23}	Bresolin, 2011
22	8.49	8.67	R_{23}	Bresolin, 2011
23	6.58	8.40	R_{23}	Bresolin, 2011
25	7.90	8.52	R_{23}	Bresolin, 2011
26	8.22	8.61	R_{23}	Bresolin, 2011
27	7.06	8.63	R_{23}	Bresolin, 2011
28	7.30	8.52	R_{23}	Bresolin, 2011

29	7.18	8.55	R_{23}	Bresolin, 2011
31	7.78	8.44	R_{23}	Bresolin, 2011
32	7.81	8.71	R_{23}	Bresolin, 2011
33	8.27	8.37	R_{23}	Bresolin, 2011
35	9.42	8.46	R_{23}	Bresolin, 2011

Table 5.1 (cont'd)

NGC 628

HII Region	Deproj. radius (arcmin)	Oxygen Abundance (12 + log(O/H))	Method	Source
H292	1.22	8.58	R_{23}	Bresolin et al, 1999
H451	1.38	8.65	R_{23}	Bresolin et al, 1999
H572	2.07	8.50	R_{23}	Bresolin et al, 1999
H598	2.17	8.48	R_{23}	Bresolin et al, 1999
H627	2.70	8.50	R_{23}	Bresolin et al, 1999
H154-155	3.82	8.23	R_{23}	Bresolin et al, 1999
H13	3.76	8.36	R_{23}	Bresolin et al, 1999
628A	1.30	8.55	R_{23}	Ferguson et al., 1998
628B	3.85	8.30	R_{23}	Ferguson et al., 1998
628C	5.93	8.29	R_{23}	Ferguson et al., 1998
628D	5.93	8.24	R_{23}	Ferguson et al., 1998
+178-52	3.39	8.59	R_{23}	van Zee et al., 1998
+180-8	3.26	8.52	R_{23}	van Zee et al., 1998
+203-41	3.77	8.40	R_{23}	van Zee et al., 1998
+254-43	4.69	8.28	R_{23}	van Zee et al., 1998
+262-41	4.82	8.22	R_{23}	van Zee et al., 1998
+264-37	4.84	8.29	R_{23}	van Zee et al., 1998
+265-41	4.87	8.26	R_{23}	van Zee et al., 1998
+292-20	5.30	8.36	R_{23}	van Zee et al., 1998
+44-175	3.13	8.47	R_{23}	van Zee et al., 1998
+47-172	3.10	8.49	R_{23}	van Zee et al., 1998
+62-158	2.98	8.52	R_{23}	van Zee et al., 1998
+81-140	2.87	8.54	R_{23}	van Zee et al., 1998
-227+148	4.95	8.31	R_{23}	van Zee et al., 1998
-232+112	4.71	8.22	R_{23}	van Zee et al., 1998
-69+208	3.82	8.40	R_{23}	van Zee et al., 1998
-73+203	3.77	8.38	R_{23}	van Zee et al., 1998
-75+200	3.74	8.24	R_{23}	van Zee et al., 1998
-86+186	3.61	8.40	R_{23}	van Zee et al., 1998
+049+052	1.19	8.48	R_{23}	McCall et al., 1985
-074-022	1.29	8.66	R_{23}	McCall et al., 1985
-060-107	2.04	8.47	R_{23}	McCall et al., 1985
+042-116	2.06	8.40	R_{23}	McCall et al., 1985
-042-154	2.66	8.42	R_{23}	McCall et al., 1985
-186+086	3.42	8.35	R_{23}	McCall et al., 1985

Table 5.1 (cont'd)

NGC 925

HII Region	Deproj. radius (arcmin)	Oxygen Abundance (12 + log(O/H))	Method	Source
N925-01	0.29	8.80	R_{23}	Dors Jr. & Copetti, 2005
N925-02	1.48	8.68	R_{23}	Dors Jr. & Copetti, 2005
N925-03	2.05	8.66	R_{23}	Dors Jr. & Copetti, 2005
N925-04	2.59	8.64	R_{23}	Dors Jr. & Copetti, 2005
N925-05	3.42	8.64	R_{23}	Dors Jr. & Copetti, 2005
N925-06	4.26	8.64	R_{23}	Dors Jr. & Copetti, 2005
N925-07	4.94	8.64	R_{23}	Dors Jr. & Copetti, 2005
N925-08	6.25	8.52	R_{23}	Dors Jr. & Copetti, 2005

NGC 1097

HII Region	Deproj. radius (arcmin)	Oxygen Abundance (12 + log(O/H))	Method	Source
130-121.5	2.03	8.61	R_{23}	Storchi-Bergmann et al., 1996
139+49.2	0.82	8.86	R_{23}	Storchi-Bergmann et al., 1996
139+55.2	0.92	8.82	R_{23}	Storchi-Bergmann et al., 1996
139+107.9	1.80	8.76	R_{23}	Storchi-Bergmann et al., 1996
139-9	0.15	8.88	R_{23}	Storchi-Bergmann et al., 1996
139-57.8	0.96	8.81	R_{23}	Storchi-Bergmann et al., 1996
139-70.8	1.18	8.81	R_{23}	Storchi-Bergmann et al., 1996
139-100.8	1.68	8.71	R_{23}	Storchi-Bergmann et al., 1996
139-112.8	1.88	8.71	R_{23}	Storchi-Bergmann et al., 1996
170-83.7	1.40	8.65	R_{23}	Storchi-Bergmann et al., 1996

Table 5.1 (cont'd)

NGC 1232

HII Region	Deproj. radius (arcmin)	Oxygen Abundance (12 + log(O/H))	Method	Source
5	1.82	8.47	R_{23}	Bresolin et al., 2005
6	1.93	8.55	R_{23}	Bresolin et al., 2005
7	1.57	8.63	R_{23}	Bresolin et al., 2005
8	0.62	8.82	R_{23}	Bresolin et al., 2005
9	1.03	8.76	R_{23}	Bresolin et al., 2005
10	1.27	8.68	R_{23}	Bresolin et al., 2005
11	1.28	8.34	R_{23}	Bresolin et al., 2005
12	1.28	8.80	R_{23}	Bresolin et al., 2005
14	1.85	8.43	R_{23}	Bresolin et al., 2005
+21+91	1.78	8.44	R_{23}	van Zee & Bryant, 1999
+4-101	1.93	8.33	R_{23}	van Zee & Bryant, 1999
+56+106	2.23	8.33	R_{23}	van Zee & Bryant, 1999
+57+98	2.10	8.16	R_{23}	van Zee & Bryant, 1999
+59+58	1.48	8.63	R_{23}	van Zee & Bryant, 1999
+62+4	1.04	8.63	R_{23}	van Zee & Bryant, 1999
+75-1	1.25	8.41	R_{23}	van Zee & Bryant, 1999
+75-12	1.27	8.39	R_{23}	van Zee & Bryant, 1999
+93-110	2.61	8.20	R_{23}	van Zee & Bryant, 1999
-103+22	1.77	8.35	R_{23}	van Zee & Bryant, 1999
-103-21	1.76	8.49	R_{23}	van Zee & Bryant, 1999

Table 5.1 (cont'd)

NGC 1365

HII Region	Deproj. radius (arcmin)	Oxygen Abundance (12 + log(O/H))	Method	Source
3	3.68	8.50	R_{23}	Bresolin et al., 2005
4	3.37	8.58	R_{23}	Bresolin et al., 2005
5	3.15	8.62	R_{23}	Bresolin et al., 2005
6	2.80	8.63	R_{23}	Bresolin et al., 2005
7	3.73	8.37	R_{23}	Bresolin et al., 2005
8	1.58	8.62	R_{23}	Bresolin et al., 2005
9	0.42	8.89	R_{23}	Bresolin et al., 2005
10	1.98	8.68	R_{23}	Bresolin et al., 2005
11	2.45	8.62	R_{23}	Bresolin et al., 2005
12	2.65	8.61	R_{23}	Bresolin et al., 2005
13	3.00	8.94	R_{23}	Bresolin et al., 2005
14	3.27	8.96	R_{23}	Bresolin et al., 2005
15	3.13	8.52	R_{23}	Bresolin et al., 2005
16	3.45	8.42	R_{23}	Bresolin et al., 2005
17	3.68	8.77	R_{23}	Bresolin et al., 2005

Table 5.1 (cont'd)

NGC 2403

HII Region	Deproj. radius (arcmin)	Oxygen Abundance (12 + log(O/H))	Method	Source
VS35	0.08	8.48	R_{23}	Garnett et al., 1997
VS24	0.10	8.49	R_{23}	Garnett et al., 1997
VS38	0.10	8.59	R_{23}	Garnett et al., 1997
VS21	0.20	8.34	R_{23}	Garnett et al., 1997
VS28	0.21	8.57	R_{23}	Garnett et al., 1997
VS41	0.25	8.57	R_{23}	Garnett et al., 1997
VS44	0.27	8.43	R_{23}	Garnett et al., 1997
VS51	0.34	8.50	R_{23}	Garnett et al., 1997
VS3	0.36	8.51	R_{23}	Garnett et al., 1997
VS49	0.55	8.48	R_{23}	Garnett et al., 1997
VS48	0.55	8.38	R_{23}	Garnett et al., 1997
+166-229	0.48	8.24	R_{23}	van Zee et al., 1998
+178-203	0.44	8.51	R_{23}	van Zee et al., 1998
+186-177	0.40	8.21	R_{23}	van Zee et al., 1998
+360-190	0.64	8.28	R_{23}	van Zee et al., 1998
+376-106	0.68	8.41	R_{23}	van Zee et al., 1998
+377-163	0.66	8.35	R_{23}	van Zee et al., 1998
+383-56	0.74	8.39	R_{23}	van Zee et al., 1998
-104-256	0.78	8.24	R_{23}	van Zee et al., 1998
-105-218	0.69	8.54	R_{23}	van Zee et al., 1998
-377+104	0.68	8.32	R_{23}	van Zee et al., 1998
-381+82	0.71	8.27	R_{23}	van Zee et al., 1998
-421-17	0.91	8.27	R_{23}	van Zee et al., 1998
-423-10	0.90	8.41	R_{23}	van Zee et al., 1998
-425-2	0.89	8.34	R_{23}	van Zee et al., 1998
+010+032	0.09	8.48	R_{23}	McCall et al., 1985
+045+069	0.23	8.29	R_{23}	McCall et al., 1985
+063-049	0.12	8.45	R_{23}	McCall et al., 1985
+165+136	0.6	8.32	R_{23}	McCall et al., 1985
-133-146	0.56	8.46	R_{23}	McCall et al., 1985
-096+035	0.17	8.37	R_{23}	Bresolin et al., 1999

-045+055	0.11	8.55	R_{23}	Bresolin et al., 1999
-186+045	0.35	8.48	R_{23}	Bresolin et al., 1999
+010+032	0.09	8.51	R_{23}	Bresolin et al., 1999
-133-146	0.56	8.35	R_{23}	Bresolin et al., 1999
+063-049	0.12	8.52	R_{23}	Bresolin et al., 1999
+165+136	0.6	8.43	R_{23}	Bresolin et al., 1999
+045+069	0.23	8.31	R_{23}	Bresolin et al., 1999
-494+137	0.91	8.23	R_{23}	Bresolin et al., 1999

Table 5.1 (cont'd)

NGC 2903

HII Region	Deproj. radius (arcmin)	Oxygen Abundance (12 + log(O/H))	Method	Source
2	3.20	8.56	R_{23}	Bresolin et al., 2005
3	3.17	8.57	R_{23}	Bresolin et al., 2005
4	2.30	8.51	R_{23}	Bresolin et al., 2005
5	2.32	8.51	R_{23}	Bresolin et al., 2005
6	2.28	8.57	R_{23}	Bresolin et al., 2005
7	1.28	8.84	R_{23}	Bresolin et al., 2005
8	0.80	8.86	R_{23}	Bresolin et al., 2005
12	2.42	8.63	R_{23}	Bresolin et al., 2005
14	2.15	8.57	R_{23}	Bresolin et al., 2005
-60-100	2.13	8.29	R_{23}	van Zee et al., 1998
-62-85	2.05	8.37	R_{23}	van Zee et al., 1998
-65-73	2.06	8.28	R_{23}	van Zee et al., 1998
-67-61	2.08	8.35	R_{23}	van Zee et al., 1998

Table 5.1 (cont'd)

NGC 3031

HII Region	Deproj. radius (arcmin)	Oxygen Abundance (12 + log(O/H))	Method	Source
HK472	3.12	8.59	R_{23}	Garnett & Shields, 1987
13	3.36	8.70	R_{23}	Garnett & Shields, 1987
14	3.77	8.55	R_{23}	Garnett & Shields, 1987
2	3.86	8.51	R_{23}	Garnett & Shields, 1987
12	3.94	8.41	R_{23}	Garnett & Shields, 1987
3	4.02	8.56	R_{23}	Garnett & Shields, 1987
1	4.19	8.59	R_{23}	Garnett & Shields, 1987
11	4.35	8.66	R_{23}	Garnett & Shields, 1987
9	4.60	8.59	R_{23}	Garnett & Shields, 1987
5	4.68	8.60	R_{23}	Garnett & Shields, 1987
10	5.09	8.44	R_{23}	Garnett & Shields, 1987
4	5.91	8.37	R_{23}	Garnett & Shields, 1987
7	6.32	8.44	R_{23}	Garnett & Shields, 1987
17	6.81	8.26	R_{23}	Garnett & Shields, 1987
Munch18	7.63	8.54	R_{23}	Garnett & Shields, 1987
HK537	8.45	8.35	R_{23}	Garnett & Shields, 1987
HII4	8.60	8.38	R_{23}	Stanghellini et al., 2010
HII5	8.89	8.21	R_{23}	Stanghellini et al., 2010
HII31	8.62	8.21	R_{23}	Stanghellini et al., 2010
HII72	8.84	8.40	R_{23}	Stanghellini et al., 2010
HII79	8.27	8.41	R_{23}	Stanghellini et al., 2010
HII81	8.42	8.24	R_{23}	Stanghellini et al., 2010
HII123	8.45	8.31	R_{23}	Stanghellini et al., 2010
HII133	8.69	8.33	R_{23}	Stanghellini et al., 2010
HII201	8.28	8.54	R_{23}	Stanghellini et al., 2010
HII228	8.37	8.26	R_{23}	Stanghellini et al., 2010
HII233	8.52	8.30	R_{23}	Stanghellini et al., 2010
HII325	8.20	8.27	R_{23}	Stanghellini et al., 2010
GS1	5.23	8.49	R_{23}	Bresolin et al., 1999
GS2	4.56	8.47	R_{23}	Bresolin et al., 1999
GS4	8.44	8.32	R_{23}	Bresolin et al., 1999

GS7	8.84	8.35	R_{23}	Bresolin et al., 1999
GS9	6.16	8.54	R_{23}	Bresolin et al., 1999
GS11	5.23	8.58	R_{23}	Bresolin et al., 1999
GS12	4.69	8.36	R_{23}	Bresolin et al., 1999
GS13	4.69	8.68	R_{23}	Bresolin et al., 1999

Table 5.1 (cont'd)

NGC 3184

HII Region	Deproj. radius (arcmin)	Oxygen Abundance (12 + log(O/H))	Method	Source
+111-102	2.51	8.27	R_{23}	van Zee et al., 1998
+5+135	2.34	8.47	R_{23}	van Zee et al., 1998
+59-79	1.65	8.71	R_{23}	van Zee et al., 1998
+74+64	1.74	8.74	R_{23}	van Zee et al., 1998
+79+35	1.53	8.79	R_{23}	van Zee et al., 1998
+85-4	1.46	8.75	R_{23}	van Zee et al., 1998
+92-93	2.18	8.64	R_{23}	van Zee et al., 1998
-101-137	3.03	8.51	R_{23}	van Zee et al., 1998
-110-130	3.03	8.46	R_{23}	van Zee et al., 1998
-113-127	3.03	8.51	R_{23}	van Zee et al., 1998
-119-121	3.02	8.52	R_{23}	van Zee et al., 1998
-17+137	2.36	8.63	R_{23}	van Zee et al., 1998
-2+136	2.34	8.63	R_{23}	van Zee et al., 1998
-58-7	1.02	8.86	R_{23}	van Zee et al., 1998
-64-6	1.12	8.82	R_{23}	van Zee et al., 1998
-80-5	1.39	8.81	R_{23}	van Zee et al., 1998
-95-142	3.03	8.47	R_{23}	van Zee et al., 1998
+106-020	1.85	8.65	R_{23}	Zaritsky et al., 1994
+106-020	1.85	8.56	R_{23}	Zaritsky et al., 1994
+000+068	1.18	8.79	R_{23}	Zaritsky et al., 1994
-008+073	1.26	8.69	R_{23}	Zaritsky et al., 1994
-020-097	1.74	8.62	R_{23}	Zaritsky et al., 1994
-011+078	1.33	8.70	R_{23}	Zaritsky et al., 1994
-012-089	1.55	8.66	R_{23}	Zaritsky et al., 1994
-059-041	1.30	8.79	R_{23}	Zaritsky et al., 1994
-075-087	2.07	8.56	R_{23}	Zaritsky et al., 1994
-172-041	3.11	8.35	R_{23}	Zaritsky et al., 1994
+070+091	1.99	8.58	R_{23}	McCall et al., 1985
+073-147	2.68	8.51	R_{23}	McCall et al., 1985
-020-095	1.67	8.62	R_{23}	McCall et al., 1985
-067-039	1.34	8.74	R_{23}	McCall et al., 1985
-077+093	1.95	8.31	R_{23}	McCall et al., 1985

Table 5.1 (cont'd)

NGC 3198

HII Region	Deproj. radius (arcmin)	Oxygen Abundance (12 + log(O/H))	Method	Source
-66-111	2.22	8.30	R_{23}	Zaritsky et al., 1994
-89-110	2.39	8.41	R_{23}	Zaritsky et al., 1994
-41-45	1.07	8.48	R_{23}	Zaritsky et al., 1994
-40-9	1.45	8.36	R_{23}	Zaritsky et al., 1994
-60-7	2.30	8.29	R_{23}	Zaritsky et al., 1994
+30-30	2.04	8.43	R_{23}	Zaritsky et al., 1994
+71+46	2.04	8.45	R_{23}	Zaritsky et al., 1994
+38+44	1.02	8.61	R_{23}	Zaritsky et al., 1994
+83+150	2.98	8.26	R_{23}	Zaritsky et al., 1994
+93+152	3.02	8.35	R_{23}	Zaritsky et al., 1994
+9+113	3.24	8.21	R_{23}	Zaritsky et al., 1994
+36+131	3.07	8.26	R_{23}	Zaritsky et al., 1994

Table 5.1 (cont'd)

NGC 4258

HII Region	Deproj. radius (arcmin)	Oxygen Abundance (12 + log(O/H))	Method	Source
1	6.52	8.42	R_{23}	Bresolin, 2011
2	6.38	8.44	R_{23}	Bresolin, 2011
3	6.06	8.40	R_{23}	Bresolin, 2011
4	3.62	8.48	R_{23}	Bresolin, 2011
5	3.30	8.49	R_{23}	Bresolin, 2011
6	3.09	8.50	R_{23}	Bresolin, 2011
7	3.64	8.54	R_{23}	Bresolin, 2011
8	3.51	8.48	R_{23}	Bresolin, 2011
9	3.45	8.60	R_{23}	Bresolin, 2011
10	3.35	8.56	R_{23}	Bresolin, 2011
11	3.31	8.55	R_{23}	Bresolin, 2011
12	2.91	8.55	R_{23}	Bresolin, 2011
13	2.59	8.56	R_{23}	Bresolin, 2011
14	1.96	8.51	R_{23}	Bresolin, 2011
15	0.68	8.58	R_{23}	Bresolin, 2011
16	0.71	8.48	R_{23}	Bresolin, 2011
17	1.38	8.53	R_{23}	Bresolin, 2011
18	7.81	8.49	R_{23}	Bresolin, 2011
19	3.79	8.45	R_{23}	Bresolin, 2011
20	3.79	8.32	R_{23}	Bresolin, 2011
21	6.67	8.56	R_{23}	Bresolin, 2011
22	8.49	8.45	R_{23}	Bresolin, 2011
23	6.58	8.21	R_{23}	Bresolin, 2011
24	7.99	8.34	R_{23}	Bresolin, 2011
25	7.90	8.62	R_{23}	Bresolin, 2011
26	8.22	8.30	R_{23}	Bresolin, 2011
27	7.06	8.33	R_{23}	Bresolin, 2011
28	7.30	8.41	R_{23}	Bresolin, 2011
29	7.18	8.33	R_{23}	Bresolin, 2011
30	10.29	8.40	R_{23}	Bresolin, 2011
31	7.78	8.34	R_{23}	Bresolin, 2011

32	7.81	8.43	R_{23}	Bresolin, 2011
33	8.27	8.37	R_{23}	Bresolin, 2011
34	8.41	8.33	R_{23}	Bresolin, 2011
35	9.42	8.35	R_{23}	Bresolin, 2011
36	9.53	8.35	R_{23}	Bresolin, 2011

Table 5.1 (cont'd)

NGC 4559

HII Region	Deproj. radius (arcmin)	Oxygen Abundance (12 + log(O/H))	Method	Source
-8+11	0.27	8.45	R_{23}	Zaritsky et al., 1994
+103-26	2.03	8.35	R_{23}	Zaritsky et al., 1994
+117-43	2.19	8.39	R_{23}	Zaritsky et al., 1994
-94-74	4.27	8.41	R_{23}	Zaritsky et al., 1994
-92+135	3.67	8.27	R_{23}	Zaritsky et al., 1994
-113+129	3.40	8.35	R_{23}	Zaritsky et al., 1994
-112+128	3.40	8.33	R_{23}	Zaritsky et al., 1994
-114+124	3.29	8.24	R_{23}	Zaritsky et al., 1994
-153+102	3.07	8.48	R_{23}	Zaritsky et al., 1994
-193+98	3.62	8.24	R_{23}	Zaritsky et al., 1994
-191+95	3.56	8.27	R_{23}	Zaritsky et al., 1994
-51+62	1.64	8.44	R_{23}	Zaritsky et al., 1994
-74+41	1.42	8.39	R_{23}	Zaritsky et al., 1994
-17-14	0.82	8.42	R_{23}	Zaritsky et al., 1994
+4-16	0.49	8.46	R_{23}	Zaritsky et al., 1994

NGC 5194

HII Region	Deproj. radius (arcmin)	Oxygen Abundance (12 + log(O/H))	Method	Source
N5194-01	0.59	8.86	R_{23}	Bresolin et al., 1999
N5194-02	2.16	8.65	R_{23}	Bresolin et al., 1999
N5194-03	2.27	8.76	R_{23}	Bresolin et al., 1999
N5194-04	1.03	8.87	R_{23}	Bresolin et al., 2004
N5194-05	2.38	8.73	R_{23}	Bresolin et al., 2004
N5194-06	2.75	8.69	R_{23}	Bresolin et al., 2004
N5194-07	2.75	8.79	R_{23}	Bresolin et al., 2004
N5194-08	2.75	8.72	R_{23}	Bresolin et al., 2004
N5194-09	2.75	8.81	R_{23}	Bresolin et al., 2004
N5194-10	3.02	8.73	R_{23}	Bresolin et al., 2004
N5194-11	3.19	8.70	R_{23}	Bresolin et al., 2004
N5194-12	3.89	8.72	R_{23}	Bresolin et al., 2004
N5194-13	5.62	8.67	R_{23}	Bresolin et al., 2004

Table 5.1 (cont'd)

NGC 5236

HII Region	Deproj. radius (arcmin)	Oxygen Abundance (12 + log(O/H))	Method	Source
20	14.49	8.20	Direct (T_e)	Bresolin et al., 2009
29	7.79	8.46	Direct (T_e)	Bresolin et al., 2009
39	8.37	8.07	Direct (T_e)	Bresolin et al., 2009
43	8.05	8.14	Direct (T_e)	Bresolin et al., 2009
8	7.53	8.40	R_{23}	Bresolin et al., 2009
10	6.63	8.34	R_{23}	Bresolin et al., 2009
13	4.89	8.54	R_{23}	Bresolin et al., 2009
14	4.64	8.72	R_{23}	Bresolin et al., 2009
15	10.43	8.20	R_{23}	Bresolin et al., 2009
16	4.83	8.75	R_{23}	Bresolin et al., 2009
17	4.31	8.56	R_{23}	Bresolin et al., 2009
18	5.28	8.56	R_{23}	Bresolin et al., 2009
19	5.35	8.55	R_{23}	Bresolin et al., 2009
21	4.89	8.60	R_{23}	Bresolin et al., 2009
22	4.77	8.60	R_{23}	Bresolin et al., 2009
23	4.12	8.71	R_{23}	Bresolin et al., 2009
24	4.19	8.79	R_{23}	Bresolin et al., 2009
29	7.79	8.45	R_{23}	Bresolin et al., 2009
31	11.14	8.27	R_{23}	Bresolin et al., 2009
33	11.08	8.34	R_{23}	Bresolin et al., 2009
34	4.38	8.55	R_{23}	Bresolin et al., 2009
35	5.73	8.74	R_{23}	Bresolin et al., 2009
38	5.22	8.77	R_{23}	Bresolin et al., 2009
39	8.37	8.41	R_{23}	Bresolin et al., 2009
40	8.82	8.30	R_{23}	Bresolin et al., 2009
41	8.63	8.51	R_{23}	Bresolin et al., 2009
42	5.41	8.58	R_{23}	Bresolin et al., 2009
43	8.05	8.28	R_{23}	Bresolin et al., 2009
44	5.41	8.58	R_{23}	Bresolin et al., 2009
46	4.77	8.75	R_{23}	Bresolin et al., 2009
47	6.96	8.44	R_{23}	Bresolin et al., 2009

49	7.66	8.27	R_{23}	Bresolin et al., 2009
207	3.37	8.63	R_{23}	Bresolin et al., 2005
203	3.31	8.52	R_{23}	Bresolin et al., 2005
163	2.66	8.79	R_{23}	Bresolin et al., 2005
184	3.00	8.81	R_{23}	Bresolin et al., 2005
186	3.03	8.71	R_{23}	Bresolin et al., 2005
166	2.71	8.76	R_{23}	Bresolin et al., 2005
75	1.22	8.82	R_{23}	Bresolin et al., 2005
32	0.52	8.83	R_{23}	Bresolin et al., 2005
115	1.87	8.78	R_{23}	Bresolin et al., 2005
5	0.08	8.85	R_{23}	Bresolin et al., 2005
116	1.89	8.73	R_{23}	Bresolin et al., 2005
119	1.94	8.77	R_{23}	Bresolin et al., 2005
107	1.74	8.79	R_{23}	Bresolin et al., 2005
141	2.30	8.77	R_{23}	Bresolin et al., 2005
141	2.30	8.66	R_{23}	Bresolin et al., 2005
159	2.59	8.69	R_{23}	Bresolin et al., 2005
185	3.02	8.64	R_{23}	Bresolin et al., 2005
221	3.60	8.63	R_{23}	Bresolin et al., 2005

Table 5.1 (cont'd)

NGC 5457

HII Region	Deproj. radius (arcmin)	Oxygen Abundance (12 + log(O/H))	Method	Source
N5457 - 1	4.90	8.44	Direct (T_e)	Kennicutt et al., 2003
N5457 - 2	5.91	8.33	Direct (T_e)	Kennicutt et al., 2003
N5457 - 3	6.06	8.23	Direct (T_e)	Kennicutt et al., 2003
N5457 - 4	6.20	8.28	Direct (T_e)	Kennicutt et al., 2003
N5457 - 5	9.66	8.16	Direct (T_e)	Kennicutt et al., 2003
N5457 - 6	8.08	8.50	Direct (T_e)	Kennicutt et al., 2003
N5457 - 7	7.93	8.13	Direct (T_e)	Kennicutt et al., 2003
N5457 - 8	7.93	8.39	Direct (T_e)	Kennicutt et al., 2003
N5457 - 9	6.92	8.36	Direct (T_e)	Kennicutt et al., 2003
N5457 - 10	8.08	8.13	Direct (T_e)	Kennicutt et al., 2003
N5457 - 11	8.22	8.03	Direct (T_e)	Kennicutt et al., 2003
N5457 - 12	8.22	7.99	Direct (T_e)	Kennicutt et al., 2003
N5457 - 13	11.68	8.07	Direct (T_e)	Kennicutt et al., 2003
N5457 - 14	11.68	7.94	Direct (T_e)	Kennicutt et al., 2003
N5457 - 15	11.68	8.03	Direct (T_e)	Kennicutt et al., 2003
N5457 - 16	11.68	8.05	Direct (T_e)	Kennicutt et al., 2003
N5457 - 17	18.03	7.45	Direct (T_e)	Kennicutt et al., 2003
N5457 - 18	2.74	8.59	R_{23}	Kennicutt et al., 2003
N5457 - 19	4.90	8.49	R_{23}	Kennicutt et al., 2003
N5457 - 20	5.91	8.46	R_{23}	Kennicutt et al., 2003
N5457 - 21	6.06	8.36	R_{23}	Kennicutt et al., 2003
N5457 - 22	6.20	8.49	R_{23}	Kennicutt et al., 2003
N5457 - 23	8.08	8.42	R_{23}	Kennicutt et al., 2003
N5457 - 24	7.93	8.50	R_{23}	Kennicutt et al., 2003
N5457 - 25	7.93	8.45	R_{23}	Kennicutt et al., 2003
N5457 - 26	3.17	8.52	R_{23}	Kennicutt et al., 2003
N5457 - 27	6.92	8.67	R_{23}	Kennicutt et al., 2003
N5457 - 28	8.08	8.77	R_{23}	Kennicutt et al., 2003
N5457 - 29	8.22	8.76	R_{23}	Kennicutt et al., 2003
N5457 - 30	8.22	8.27	R_{23}	Kennicutt et al., 2003
N5457 - 31	2.74	8.77	R_{23}	Kennicutt et al., 2003

N5457 - 32	2.31	8.40	R_{23}	Bresolin, 2007
N5457 - 33	1.44	8.27	R_{23}	Bresolin, 2007
N5457 - 34	2.02	8.24	R_{23}	Bresolin, 2007
N5457 - 35	8.31	8.40	R_{23}	Bresolin, 2007
N5457 - 36	1.91	8.24	R_{23}	van Zee et al., 1998
N5457 - 37	8.34	8.40	R_{23}	van Zee et al., 1998
N5457 - 38	7.76	8.33	R_{23}	van Zee et al., 1998
N5457 - 39	7.90	8.29	R_{23}	van Zee et al., 1998
N5457 - 40	1.41	8.86	R_{23}	van Zee et al., 1998
N5457 - 41	1.15	8.74	R_{23}	van Zee et al., 1998
N5457 - 42	1.46	8.79	R_{23}	Cedrés & Cepa, 2002
N5457 - 43	1.91	8.69	R_{23}	Cedrés & Cepa, 2002
N5457 - 44	1.99	8.68	R_{23}	Cedrés & Cepa, 2002
N5457 - 45	1.85	8.68	R_{23}	Cedrés & Cepa, 2002
N5457 - 46	2.22	8.65	R_{23}	Cedrés & Cepa, 2002
N5457 - 47	0.81	8.79	R_{23}	Cedrés & Cepa, 2002
N5457 - 48	2.22	8.67	R_{23}	Cedrés & Cepa, 2002
N5457 - 49	2.40	8.60	R_{23}	Cedrés & Cepa, 2002
N5457 - 50	1.73	8.74	R_{23}	Cedrés & Cepa, 2002
N5457 - 51	1.56	8.74	R_{23}	Cedrés & Cepa, 2002
N5457 - 52	1.77	8.82	R_{23}	Cedrés & Cepa, 2002
N5457 - 53	1.37	8.67	R_{23}	Cedrés & Cepa, 2002
N5457 - 54	1.26	8.65	R_{23}	Cedrés & Cepa, 2002
N5457 - 55	1.36	8.69	R_{23}	Cedrés & Cepa, 2002
N5457 - 56	1.59	8.77	R_{23}	Cedrés & Cepa, 2002
N5457 - 57	1.78	8.75	R_{23}	Cedrés & Cepa, 2002
N5457 - 58	1.69	8.77	R_{23}	Cedrés & Cepa, 2002
N5457 - 59	3.32	8.52	R_{23}	Cedrés & Cepa, 2002
N5457 - 60	1.42	8.78	R_{23}	Cedrés & Cepa, 2002
N5457 - 61	1.68	8.83	R_{23}	Cedrés & Cepa, 2002
N5457 - 62	2.33	8.59	R_{23}	Cedrés & Cepa, 2002
N5457 - 63	1.37	8.77	R_{23}	Cedrés & Cepa, 2002
N5457 - 64	1.00	8.46	R_{23}	Cedrés & Cepa, 2002
N5457 - 65	1.90	8.74	R_{23}	Cedrés & Cepa, 2002
N5457 - 66	2.32	8.57	R_{23}	Cedrés & Cepa, 2002

N5457 - 67	2.51	8.57	R_{23}	Cedrés & Cepa, 2002
N5457 - 68	3.05	8.55	R_{23}	Cedrés & Cepa, 2002
N5457 - 69	2.45	8.62	R_{23}	Cedrés & Cepa, 2002
N5457 - 70	2.05	8.80	R_{23}	Cedrés & Cepa, 2002
N5457 - 71	1.23	8.67	R_{23}	Cedrés & Cepa, 2002
N5457 - 72	1.54	8.66	R_{23}	Cedrés & Cepa, 2002
N5457 - 73	1.88	8.38	R_{23}	Cedrés & Cepa, 2002
N5457 - 74	1.46	8.79	R_{23}	Cedrés & Cepa, 2002
N5457 - 75	1.99	8.82	R_{23}	Cedrés & Cepa, 2002
N5457 - 76	2.17	8.66	R_{23}	Cedrés & Cepa, 2002
N5457 - 77	1.80	8.77	R_{23}	Cedrés & Cepa, 2002
N5457 - 78	1.78	8.60	R_{23}	Cedrés & Cepa, 2002
N5457 - 79	2.06	8.66	R_{23}	Cedrés & Cepa, 2002
N5457 - 80	1.95	8.67	R_{23}	Cedrés & Cepa, 2002
N5457 - 81	1.91	8.58	R_{23}	Cedrés & Cepa, 2002
N5457 - 82	2.08	8.60	R_{23}	Cedrés & Cepa, 2002
N5457 - 83	3.15	8.60	R_{23}	Cedrés & Cepa, 2002
N5457 - 84	2.09	8.75	R_{23}	Cedrés & Cepa, 2002
N5457 - 85	3.20	8.59	R_{23}	Cedrés & Cepa, 2002
N5457 - 86	3.37	8.62	R_{23}	Cedrés & Cepa, 2002
N5457 - 87	3.37	8.77	R_{23}	Cedrés & Cepa, 2002
N5457 - 88	2.83	8.59	R_{23}	Cedrés & Cepa, 2002
N5457 - 89	4.27	8.48	R_{23}	Cedrés & Cepa, 2002
N5457 - 90	3.60	8.65	R_{23}	Cedrés & Cepa, 2002
N5457 - 91	4.03	8.48	R_{23}	Cedrés & Cepa, 2002
N5457 - 92	3.04	8.61	R_{23}	Cedrés & Cepa, 2002
N5457 - 93	3.30	8.61	R_{23}	Cedrés & Cepa, 2002
N5457 - 94	2.58	8.72	R_{23}	Cedrés & Cepa, 2002
N5457 - 95	2.53	8.72	R_{23}	Cedrés & Cepa, 2002
N5457 - 96	3.54	8.28	R_{23}	Cedrés & Cepa, 2002
N5457 - 97	2.62	8.60	R_{23}	Cedrés & Cepa, 2002
N5457 - 98	2.87	8.70	R_{23}	Cedrés & Cepa, 2002
N5457 - 99	3.61	8.65	R_{23}	Cedrés & Cepa, 2002
N5457 - 100	3.42	8.53	R_{23}	Cedrés & Cepa, 2002
N5457 - 101	3.68	8.58	R_{23}	Cedrés & Cepa, 2002

N5457 - 102	3.35	8.61	R_{23}	Cedrés & Cepa, 2002
N5457 - 103	3.81	8.51	R_{23}	Cedrés & Cepa, 2002
N5457 - 104	3.90	8.45	R_{23}	Cedrés & Cepa, 2002
N5457 - 105	4.60	8.28	R_{23}	Cedrés & Cepa, 2002
N5457 - 106	3.93	8.46	R_{23}	Cedrés & Cepa, 2002
N5457 - 107	3.86	8.49	R_{23}	Cedrés & Cepa, 2002
N5457 - 108	3.15	8.74	R_{23}	Cedrés & Cepa, 2002
N5457 - 109	3.23	8.75	R_{23}	Cedrés & Cepa, 2002
N5457 - 110	3.73	8.48	R_{23}	Cedrés & Cepa, 2002
N5457 - 111	4.40	8.33	R_{23}	Cedrés & Cepa, 2002
N5457 - 112	3.22	8.68	R_{23}	Cedrés & Cepa, 2002
N5457 - 113	3.90	8.51	R_{23}	Cedrés & Cepa, 2002
N5457 - 114	3.97	8.47	R_{23}	Cedrés & Cepa, 2002
N5457 - 115	3.81	8.57	R_{23}	Cedrés & Cepa, 2002
N5457 - 116	4.06	8.31	R_{23}	Cedrés & Cepa, 2002
N5457 - 117	3.85	8.57	R_{23}	Cedrés & Cepa, 2002
N5457 - 118	3.56	8.28	R_{23}	Cedrés & Cepa, 2002
N5457 - 119	3.88	8.69	R_{23}	Cedrés & Cepa, 2002
N5457 - 120	3.72	8.65	R_{23}	Cedrés & Cepa, 2002
N5457 - 121	5.05	8.34	R_{23}	Cedrés & Cepa, 2002
N5457 - 122	3.96	8.42	R_{23}	Cedrés & Cepa, 2002
N5457 - 123	4.09	8.41	R_{23}	Cedrés & Cepa, 2002
N5457 - 124	3.82	8.37	R_{23}	Cedrés & Cepa, 2002
N5457 - 125	4.40	8.36	R_{23}	Cedrés & Cepa, 2002
N5457 - 126	3.90	8.27	R_{23}	Cedrés & Cepa, 2002
N5457 - 127	4.21	8.43	R_{23}	Cedrés & Cepa, 2002
N5457 - 128	4.49	8.53	R_{23}	Cedrés & Cepa, 2002
N5457 - 129	4.53	8.48	R_{23}	Cedrés & Cepa, 2002
N5457 - 130	4.11	8.44	R_{23}	Cedrés & Cepa, 2002
N5457 - 131	4.01	8.42	R_{23}	Cedrés & Cepa, 2002
N5457 - 132	4.22	8.46	R_{23}	Cedrés & Cepa, 2002
N5457 - 133	4.18	8.38	R_{23}	Cedrés & Cepa, 2002
N5457 - 134	4.79	8.32	R_{23}	Cedrés & Cepa, 2002
N5457 - 135	4.18	8.38	R_{23}	Cedrés & Cepa, 2002
N5457 - 136	4.44	8.44	R_{23}	Cedrés & Cepa, 2002

N5457 - 137	4.51	8.26	R_{23}	Cedrés & Cepa, 2002
N5457 - 138	4.58	8.27	R_{23}	Cedrés & Cepa, 2002
N5457 - 139	4.76	8.35	R_{23}	Cedrés & Cepa, 2002
N5457 - 140	4.87	8.40	R_{23}	Cedrés & Cepa, 2002
N5457 - 141	5.06	8.26	R_{23}	Cedrés & Cepa, 2002
N5457 - 142	5.04	8.34	R_{23}	Cedrés & Cepa, 2002
N5457 - 143	4.95	8.32	R_{23}	Cedrés & Cepa, 2002
N5457 - 144	4.70	8.28	R_{23}	Cedrés & Cepa, 2002
N5457 - 145	4.62	8.38	R_{23}	Cedrés & Cepa, 2002
N5457 - 146	4.55	8.40	R_{23}	Cedrés & Cepa, 2002
N5457 - 147	4.31	8.48	R_{23}	Cedrés & Cepa, 2002
N5457 - 148	4.13	8.39	R_{23}	Cedrés & Cepa, 2002
N5457 - 149	4.05	8.55	R_{23}	Cedrés & Cepa, 2002
N5457 - 150	4.31	8.29	R_{23}	Cedrés & Cepa, 2002
N5457 - 151	4.36	8.37	R_{23}	Cedrés & Cepa, 2002
N5457 - 152	4.33	8.34	R_{23}	Cedrés & Cepa, 2002
N5457 - 153	4.29	8.40	R_{23}	Cedrés & Cepa, 2002
N5457 - 154	4.38	8.52	R_{23}	Cedrés & Cepa, 2002
N5457 - 155	3.91	8.53	R_{23}	Cedrés & Cepa, 2002
N5457 - 156	4.65	8.41	R_{23}	Cedrés & Cepa, 2002
N5457 - 157	3.98	8.64	R_{23}	Cedrés & Cepa, 2002
N5457 - 158	3.64	8.71	R_{23}	Cedrés & Cepa, 2002
N5457 - 159	4.77	8.51	R_{23}	Cedrés & Cepa, 2002
N5457 - 160	3.83	8.62	R_{23}	Cedrés & Cepa, 2002
N5457 - 161	3.39	8.45	R_{23}	Cedrés & Cepa, 2002
N5457 - 162	3.50	8.56	R_{23}	Cedrés & Cepa, 2002
N5457 - 163	3.93	8.36	R_{23}	Cedrés & Cepa, 2002
N5457 - 164	4.01	8.45	R_{23}	Cedrés & Cepa, 2002
N5457 - 165	4.53	8.65	R_{23}	Cedrés & Cepa, 2002
N5457 - 166	3.51	8.41	R_{23}	Cedrés & Cepa, 2002
N5457 - 167	3.28	8.56	R_{23}	Cedrés & Cepa, 2002
N5457 - 168	3.32	8.58	R_{23}	Cedrés & Cepa, 2002
N5457 - 169	3.25	8.67	R_{23}	Cedrés & Cepa, 2002
N5457 - 170	3.92	8.27	R_{23}	Cedrés & Cepa, 2002
N5457 - 171	3.65	8.61	R_{23}	Cedrés & Cepa, 2002

N5457 - 172	3.99	8.47	R_{23}	Cedrés & Cepa, 2002
N5457 - 173	3.40	8.42	R_{23}	Cedrés & Cepa, 2002
N5457 - 174	3.36	8.42	R_{23}	Cedrés & Cepa, 2002
N5457 - 175	3.19	8.56	R_{23}	Cedrés & Cepa, 2002
N5457 - 176	3.17	8.59	R_{23}	Cedrés & Cepa, 2002
N5457 - 177	3.29	8.58	R_{23}	Cedrés & Cepa, 2002
N5457 - 178	3.19	8.62	R_{23}	Cedrés & Cepa, 2002
N5457 - 179	3.53	8.39	R_{23}	Cedrés & Cepa, 2002
N5457 - 180	2.79	8.83	R_{23}	Cedrés & Cepa, 2002
N5457 - 181	3.82	8.40	R_{23}	Cedrés & Cepa, 2002
N5457 - 182	2.77	8.77	R_{23}	Cedrés & Cepa, 2002
N5457 - 183	3.25	8.63	R_{23}	Cedrés & Cepa, 2002
N5457 - 184	3.50	8.61	R_{23}	Cedrés & Cepa, 2002
N5457 - 185	2.67	8.68	R_{23}	Cedrés & Cepa, 2002
N5457 - 186	3.64	8.50	R_{23}	Cedrés & Cepa, 2002
N5457 - 187	2.92	8.68	R_{23}	Cedrés & Cepa, 2002
N5457 - 188	3.20	8.65	R_{23}	Cedrés & Cepa, 2002
N5457 - 189	3.76	8.51	R_{23}	Cedrés & Cepa, 2002
N5457 - 190	2.65	8.70	R_{23}	Cedrés & Cepa, 2002
N5457 - 191	2.78	8.72	R_{23}	Cedrés & Cepa, 2002
N5457 - 192	4.22	8.41	R_{23}	Cedrés & Cepa, 2002
N5457 - 193	3.40	8.64	R_{23}	Cedrés & Cepa, 2002
N5457 - 194	3.77	8.53	R_{23}	Cedrés & Cepa, 2002
N5457 - 195	2.96	8.71	R_{23}	Cedrés & Cepa, 2002
N5457 - 196	3.51	8.57	R_{23}	Cedrés & Cepa, 2002
N5457 - 197	3.08	8.52	R_{23}	Cedrés & Cepa, 2002
N5457 - 198	3.94	8.55	R_{23}	Cedrés & Cepa, 2002
N5457 - 199	4.05	8.42	R_{23}	Cedrés & Cepa, 2002
N5457 - 200	3.81	8.20	R_{23}	Cedrés & Cepa, 2002
N5457 - 201	3.05	8.67	R_{23}	Cedrés & Cepa, 2002
N5457 - 202	4.25	8.65	R_{23}	Cedrés & Cepa, 2002
N5457 - 203	4.06	8.46	R_{23}	Cedrés & Cepa, 2002
N5457 - 204	3.38	8.61	R_{23}	Cedrés & Cepa, 2002
N5457 - 205	2.82	8.72	R_{23}	Cedrés & Cepa, 2002
N5457 - 206	4.09	8.40	R_{23}	Cedrés & Cepa, 2002

N5457 - 207	3.23	8.71	R_{23}	Cedrés & Cepa, 2002
N5457 - 208	3.55	8.37	R_{23}	Cedrés & Cepa, 2002
N5457 - 209	3.03	8.58	R_{23}	Cedrés & Cepa, 2002
N5457 - 210	3.13	8.55	R_{23}	Cedrés & Cepa, 2002
N5457 - 211	3.11	8.49	R_{23}	Cedrés & Cepa, 2002
N5457 - 212	2.60	8.58	R_{23}	Cedrés & Cepa, 2002
N5457 - 213	3.11	8.62	R_{23}	Cedrés & Cepa, 2002
N5457 - 214	3.53	8.60	R_{23}	Cedrés & Cepa, 2002
N5457 - 215	2.37	8.73	R_{23}	Cedrés & Cepa, 2002
N5457 - 216	3.64	8.39	R_{23}	Cedrés & Cepa, 2002
N5457 - 217	3.24	8.63	R_{23}	Cedrés & Cepa, 2002
N5457 - 218	3.20	8.60	R_{23}	Cedrés & Cepa, 2002
N5457 - 219	3.34	8.58	R_{23}	Cedrés & Cepa, 2002
N5457 - 220	2.57	8.52	R_{23}	Cedrés & Cepa, 2002
N5457 - 221	3.45	8.50	R_{23}	Cedrés & Cepa, 2002
N5457 - 222	3.62	8.64	R_{23}	Cedrés & Cepa, 2002
N5457 - 223	2.31	8.53	R_{23}	Cedrés & Cepa, 2002
N5457 - 224	3.28	8.45	R_{23}	Cedrés & Cepa, 2002
N5457 - 225	2.62	8.62	R_{23}	Cedrés & Cepa, 2002
N5457 - 226	3.12	8.48	R_{23}	Cedrés & Cepa, 2002
N5457 - 227	3.49	8.55	R_{23}	Cedrés & Cepa, 2002
N5457 - 228	2.66	8.63	R_{23}	Cedrés & Cepa, 2002
N5457 - 229	2.50	8.70	R_{23}	Cedrés & Cepa, 2002
N5457 - 230	2.10	8.39	R_{23}	Cedrés & Cepa, 2002
N5457 - 231	1.55	8.66	R_{23}	Cedrés & Cepa, 2002
N5457 - 232	1.60	8.54	R_{23}	Cedrés & Cepa, 2002
N5457 - 233	2.35	8.43	R_{23}	Cedrés & Cepa, 2002
N5457 - 234	2.95	8.53	R_{23}	Cedrés & Cepa, 2002
N5457 - 235	3.16	8.47	R_{23}	Cedrés & Cepa, 2002
N5457 - 236	2.55	8.60	R_{23}	Cedrés & Cepa, 2002
N5457 - 237	3.45	8.45	R_{23}	Cedrés & Cepa, 2002
N5457 - 238	3.45	8.51	R_{23}	Cedrés & Cepa, 2002
N5457 - 239	1.93	8.63	R_{23}	Cedrés & Cepa, 2002
N5457 - 240	0.37	8.89	R_{23}	Cedrés & Cepa, 2002
N5457 - 241	2.28	8.57	R_{23}	Cedrés & Cepa, 2002

N5457 - 242	1.88	8.64	R_{23}	Cedrés & Cepa, 2002
N5457 - 243	0.78	8.98	R_{23}	Cedrés & Cepa, 2002
N5457 - 244	1.17	8.68	R_{23}	Cedrés & Cepa, 2002
N5457 - 245	2.25	8.88	R_{23}	Cedrés & Cepa, 2002
N5457 - 246	2.31	8.68	R_{23}	Cedrés & Cepa, 2002
N5457 - 247	1.37	8.81	R_{23}	Cedrés & Cepa, 2002
N5457 - 248	1.82	8.68	R_{23}	Cedrés & Cepa, 2002
N5457 - 249	1.48	8.83	R_{23}	Cedrés & Cepa, 2002
N5457 - 250	2.08	8.58	R_{23}	Cedrés & Cepa, 2002
N5457 - 251	1.01	8.82	R_{23}	Cedrés & Cepa, 2002
N5457 - 252	2.27	8.57	R_{23}	Cedrés & Cepa, 2002
N5457 - 253	1.83	8.56	R_{23}	Cedrés & Cepa, 2002

Table 5.1 (cont'd)

NGC 6946

HII Region	Deproj. radius (arcmin)	Oxygen Abundance (12 + log(O/H))	Method	Source
FGW 6946A	0.61	8.46	R_{23}	Ferguson et al., 1998
FGW 6946B	0.65	8.55	R_{23}	Ferguson et al., 1998
FGW 6946C	1.50	8.29	R_{23}	Ferguson et al., 1998
+144-003	0.45	8.59	R_{23}	McCall et al., 1985
-008+066	0.22	8.62	R_{23}	McCall et al., 1985
-034-080	0.61	8.61	R_{23}	McCall et al., 1985
-099-261	0.86	8.39	R_{23}	McCall et al., 1985
-128+146	0.67	8.49	R_{23}	McCall et al., 1985
+182+103	0.61	8.38	R_{23}	McCall et al., 1985
-245+055	0.81	8.52	R_{23}	McCall et al., 1985

NGC 7793

HII Region	Deproj. radius (arcmin)	Oxygen Abundance (12 + log(O/H))	Method	Source
33	1.26	8.45	R_{23}	Webster & Smith, 1983
36	1.45	8.32	R_{23}	Webster & Smith, 1983
25	1.63	8.45	R_{23}	Webster & Smith, 1983
25N	1.63	8.32	R_{23}	Webster & Smith, 1983
20S	1.87	8.45	R_{23}	Webster & Smith, 1983
13	2.38	8.19	R_{23}	Webster & Smith, 1983
13S1	2.38	8.40	R_{23}	Webster & Smith, 1983
13S2	2.38	8.23	R_{23}	Webster & Smith, 1983
10	2.94	8.23	R_{23}	Webster & Smith, 1983
2	3.83	8.19	R_{23}	Webster & Smith, 1983
-010+033	0.84	8.29	R_{23}	McCall et al., 1985
-075-024	1.64	8.46	R_{23}	McCall et al., 1985
-104+035	1.81	8.36	R_{23}	McCall et al., 1985
-173+102	3.44	8.23	R_{23}	McCall et al., 1985
+092+098	3.46	8.32	R_{23}	McCall et al., 1985

Chapter 6

Overall Quantities of Hydrogen and Oxygen

6.1 Motivation

The gradients calculated in §5 enable the computation of "cumulative" oxygen abundances, namely the total number of oxygen atoms divided by the total number of hydrogen atoms within any radius. In order to examine how cumulative abundances vary with radius, it is necessary to track as a function of radius:

1. The total number of hydrogen atoms

2. The oxygen abundance

Together, the total number of oxygen atoms is constrained. Oxygen abundances have already been determined for each galaxy in §5. Therefore, only the hydrogen is left to be found. In order to find the total hydrogen column density, it is necessary to calculate the column densities of all types of hydrogen:

$$N(H) = N(H^0) + 2(H_2) + N(H^+) \tag{6.1}$$

The column density of molecular hydrogen is multiplied by 2 to account for the two hydrogen atoms from which it is made. It can be assumed that $N(H^+)$ is approximately zero, since it is restricted to HII regions or the hot ISM (which has a very small density). As explained in the following subsections, calculating amounts of neutral and molecular hydrogen turns out to be a relatively easy feat.

6.2 Calculating the Quantity of Neutral Hydrogen

Neutral hydrogen is referred to as "HI" by astronomers. The majority of atomic hydrogen within each galaxy is neutral, and most atoms are in the ground state. The associated electrons can have a spin in the same direction as that of the proton or in the opposite direction. The energy of atoms with their electron spinning in an opposite direction to their proton is slightly lower compared to that of atoms whose electron is spinning in the same direction as their proton. An electron spinning in the same direction will therefore spontaneously flip every so often. When the transition happens, radiation in the radio spectrum at a wavelength of 21.1 cm is emitted. Although this transition can take millions of years to occur, there is enough hydrogen making the transition at any given time that the emission is easily detected with radio telescopes. The 21.1 cm line intensities can be used to derive column densities,

expressed as either neutral hydrogen atoms per square centimetre, atoms/cm^2, or else solar masses per square parsec, $M_\odot/pc^2$. To obtain a column density from the 21.1 cm radiation requires adoption of a "spin temperature," T_s. Normally, T_s is adopted to be 100 K, as is done here (Fukui 2007).

Figue 6.1 shows a plot of the neutral hydrogen column density as a function of radius for one of the galaxies in the sample, NGC 1232. The source of data for this plot, along with sources for HI data for all of the other galaxies, are listed in Table 4.1.

6.3 Calculating the Absolute Amounts of Molecular Hydrogen, H_2

Unlike neutral hydrogen, molecular hydrogen, H_2, does not produce any easily observable emission lines. Although it may produce emission lines in the ultraviolet, these lines are attenuated by gas and dust in the interstellar medium by such a degree that they become too difficult to measure.

Fortunately, there exists a direct correlation between the column density of carbon monoxide, CO, and the column density of molecular hydrogen (Lebrun et al. 1983; Strong et al. 1988; Désert et al. 1988; Dame et al. 2001). CO is easily detected via emission lines at 2.6 mm, and less so at 1.3 mm. These emission lines arise because of collisions between H_2 and CO molecules. Thus, the CO emission lines can be used as a tracer of molecular hydrogen.

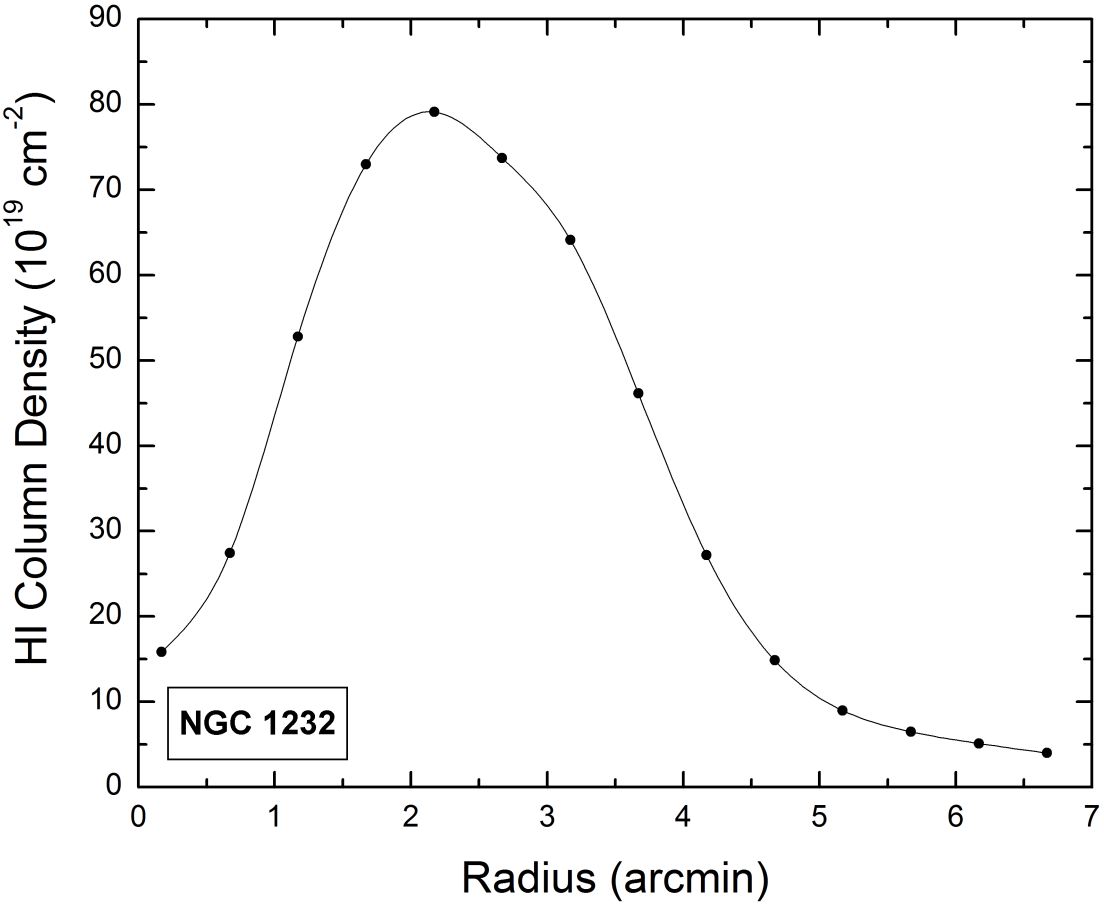

Figure 6.1: **HI column density versus deprojected radius across NGC 1232.**

The relationship between CO and H_2 can be stated as:

$$\mathrm{N(H_2)} = X * \mathrm{I(CO)} \tag{6.2}$$

where $\mathrm{N(H_2)}$ is the column density of H_2, I(CO) is the surface brightness of CO, and X is a conversion factor. The conversion factor, X, has been shown to be strongly related to metallicity (Wilson 1995; Israel 1997). Several different methods have been used to calculate the value of X. Here, one of the more popular of these methods, that developed by Wilson (1995), is used. Wilson determined the CO to H_2 relationship by studying extragalactic giant molecular clouds. The relationship between the X factor and the oxygen abundance is given by:

$$\log\frac{X}{X_0} = 5.95 - 0.67 * [12 + \log(\mathrm{n(O)/n(H)})] \tag{6.3}$$

where $X_0 = 3 * 10^{20}\ \frac{\mathrm{molecules/cm^2}}{\mathrm{K\,km/s}}$.

Since H_2 column densities derived in various published works are calculated using a variety of CO to H_2 calibrations, only original CO data were taken from sources. These data were then converted into H_2 column densities as a function of radius via equation 6.2 using oxygen abundances derived from the gradients determined in §5.

The column density of molecular hydrogen is known to decrease with radius at approximately an exponential rate (Young & Scoville 1982). Thus, graphs of the logarithm of the column density of H_2 molecules versus deprojected radius were plot-

ted and a line was fit by least squares. This fit was used to define the approximate amount of H_2 at every radius.

Data on molecular hydrogen was not available for all galaxies in this study. For those lacking coverage, the cumulative abundance will not be truly "cumulative." However, as will be discussed in §7.3, the implications of removing the contribution of H_2 are minimal.

Figure 6.2 shows a typical comparison of column densities of HI and H_2. The column density scale is logarithmic, and the linear H_2 trend is displayed as a dashed line. Although the column density of H_2 starts at a higher level than that of HI, it quickly diminishes, leaving HI to dominate at large radii.

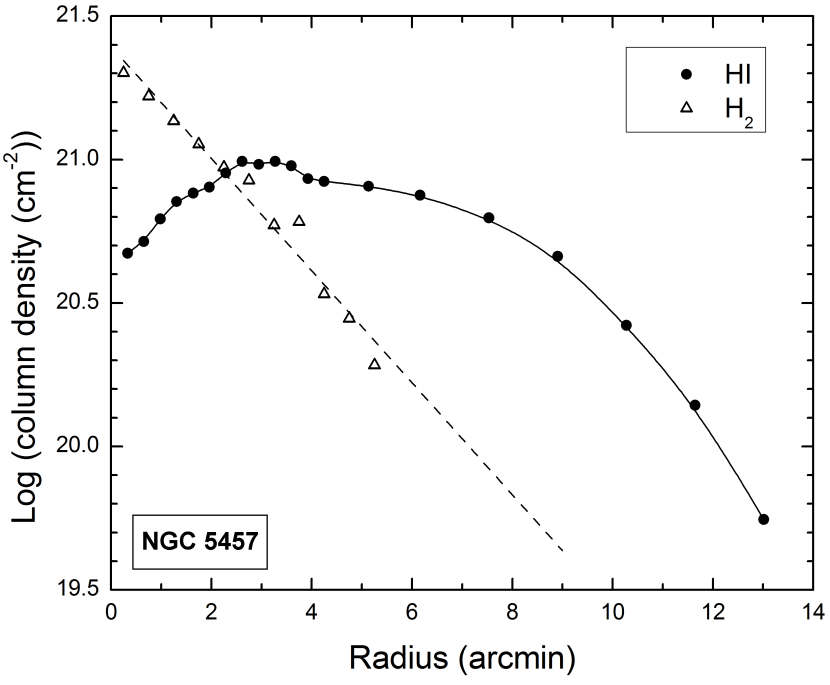

Figure 6.2: **HI and H_2 column densities versus deprojected radius across NGC 5457.**

Chapter 7

Cumulative Oxygen Abundances

7.1 Method of Calculation

The "cumulative" oxygen abundance at a particular radius refers to the *total* number of oxygen atoms divided by the *total* number of hydrogen atoms within a disk of that radius. It is denoted here by $\Sigma(O)/\Sigma(H)$. A plot of cumulative oxygen abundance versus radius differs from the standard abundance plots (e.g., in Figure 5.1) in that standard abundance plots show only the number of oxygen atoms divided by the number of hydrogen atoms within progressively larger "rings" or "annuli" (as judged from n(O)/n(H) in the HII regions. Cumulative oxygen abundances were estimated as follows.

1. Setting of annuli: For each galaxy, deprojected radial intervals were chosen based on available HI data. "Rings" with a width as large as the HI radial

intervals were generated. For example, in the plot of NGC 5236, the disk was divided into 0.1 arcminute intervals (i.e., HI data was given for $r = 0'.1$, $0'.2$, $0'.3$, etc., where "r" is the deprojected radius). For this galaxy, a ring was made with boundaries at $r = 0'.5$ to $r = 1'.5$ and another was made with boundaries at $r = 1'.5$ to $r = 2'.5$, etc. For each of these rings, a total surface area was calculated.

2. n(O)/n(H) in each annulus: At each radial interval (set by the HI column density data), the oxygen abundance is given by the linear fit to the HII region measurements (see Figure 5.1).

3. N(HI) in each annulus: Neutral hydrogen was calculated in each annulus by multiplying the HI column density at the corresponding radius by the surface area of the annulus.

4. N(H_2) in each annulus: For those galaxies for which the molecular hydrogen contribution could be determined, the H_2 column density was found by multiplying the value of H_2 taken from the gradient of the log(N(H_2)) versus radius graph, at each radial interval (set by the HI column density data) by the surface area of each annulus.

5. N(H) in each annulus: For those galaxies for which the H_2 contribution could not be determined (i.e., NGC 300, NGC 1232, NGC 1365, NGC 4559, and NGC 7793), the hydrogen column density was generated using only the atomic

hydrogen density. For galaxies for which H_2 could be determined, the total number of hydrogen atoms ($2N(H_2)$ + N(HI)).

6. N(O) in each annulus: Knowing the total hydrogen column density in each annulus, N(H), as well as the oxygen abundance at every annulus, calculating the column density of oxygen at every annulus is accomplished by multiplying the two together.

7. $\Sigma(O)/\Sigma(H)$ out to radius r: With knowledge of the oxygen and hydrogen column densities at every annulus, the total amounts of hydrogen and oxygen atoms in each successive annulus were then added to those of the annulus preceding it. In this way, a cumulative oxygen abundance out to any radius, r, was calculated.

Plots of the cumulative oxygen abundance as a function of radius are shown in Figure 7.2. All cumulative abundances (vertical axis) are expressed as 12+log(O/H). For easy comparison of trends, ordinates of all graphs span 0.5 dex in O/H (with the exception of NGC 3198). Galaxies for which the H_2 contribution could not be determined are indicated on the plot.

The radius at which the curves start in Figure 7.2 is that at which the HI column density reaches a maximum. For example, the maximum column density of HI in NGC 1232 occurs at $r = 2'.2$ (Figure 6.1). Therefore, in Figure 7.2(g), cumulative abundances are displayed starting at that same radius. At radii before this value, the cumulative oxygen abundance plots do not generally show any sort of overall trend. However, as more and more oxygen and hydrogen atoms are integrated, the trends

become more stable and eventually tend to follow an exponentially decaying curve. In the HI plots of both NGC 598 and NGC 4258 (see Figure 7.1), the peak of the HI curve actually occurs at $r = 0$. In these cases, the secondary peaks, which occur at $r = 8'.5$ and $r = 7'$ respectively, have been used as starting points.

Two of the galaxies, NGC 1365 and NGC 5236, have prominent bars which seem to distort the cumulative oxygen abundance trends at small radii. The presence of the bar within the inner part of each of these galaxies distorts the HI map and, in turn, oxygen abundance values. Therefore, for these two galaxies, the first points in the cumulative abundance plots have been chosen to be at radii at the edges of the bar.

7.2 The Asymptotic Value of O/H

The trends in the cumulative oxygen abundance with radius in Figure 7.2 can be approximated by an exponentially decaying curve. This trend is especially evident in such galaxies as NGC 224, NGC 927, NGC 1232, NGC 2903, and NGC 4258, where the curve reaches an asymptote toward the last few points. This trend is less evident in other galaxies where the curve does not reach its asymptote until well after the last point. This inconsistency can be explained simply by the sampling of HI in each galaxy. The last point of each plot occurs at the radius of the last HI measurement available from the literature. The approach of deriving asymptotes from exponential

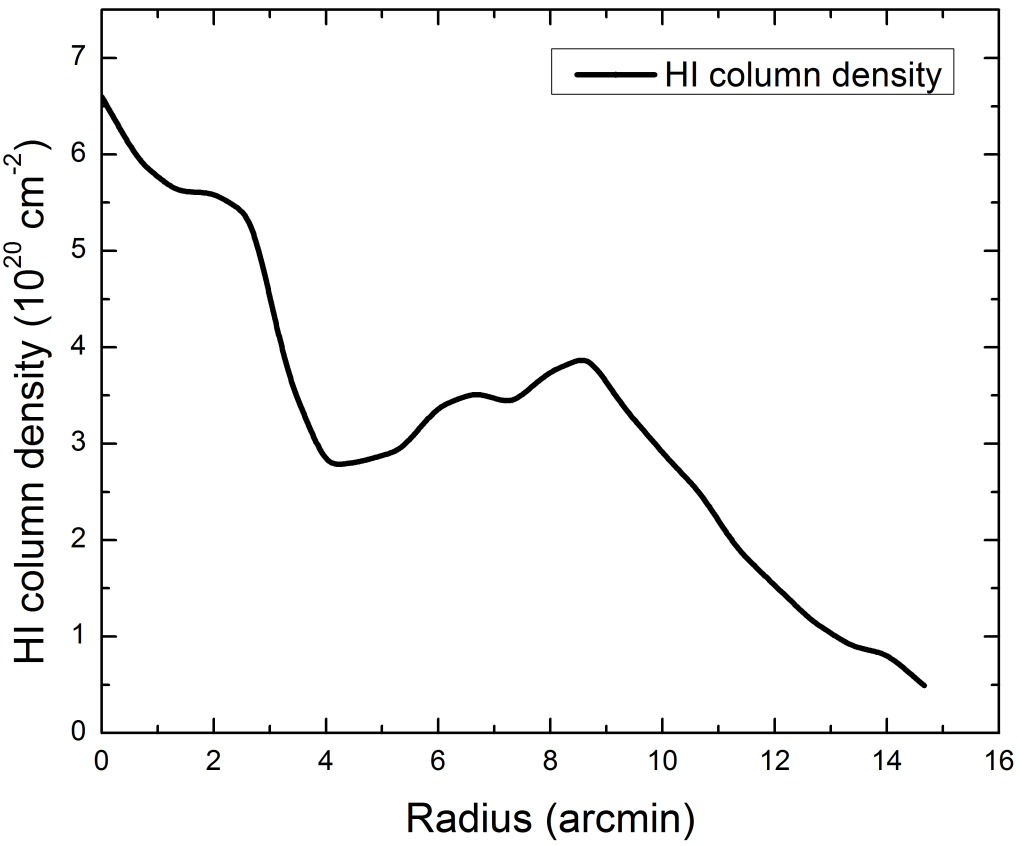

Figure 7.1: **HI column density versus deprojected radius for NGC 4258.**

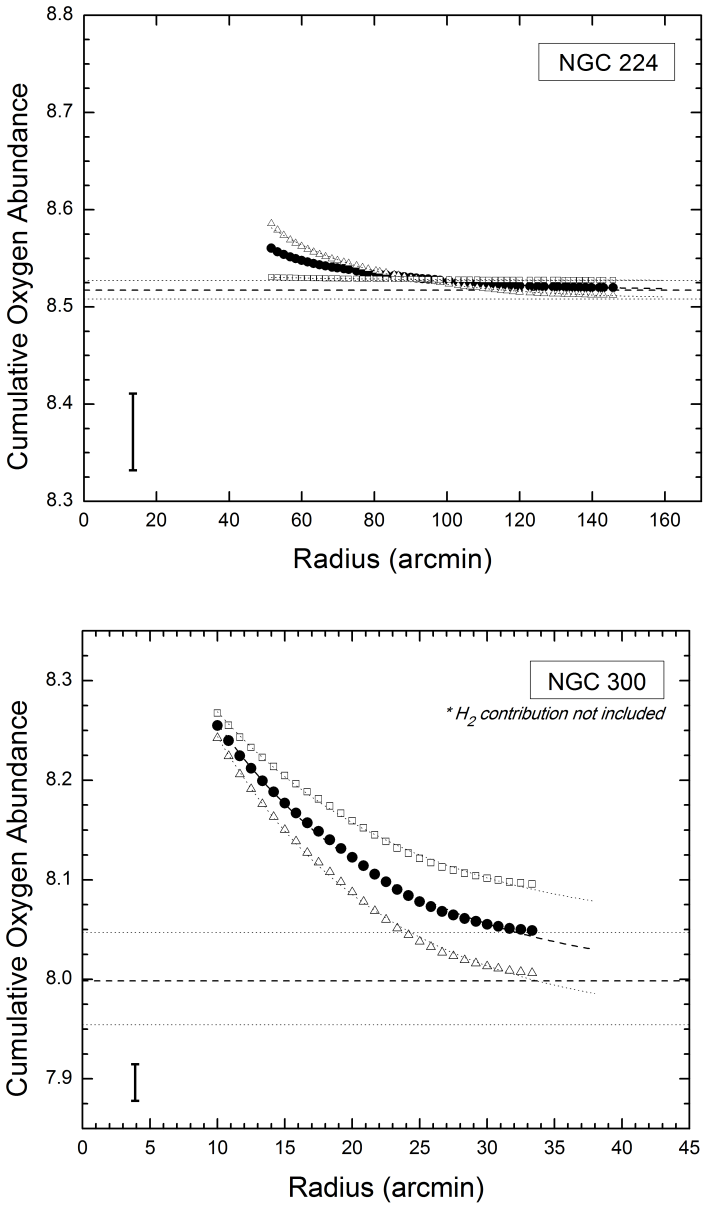

Figure 7.2: **Cumulative oxygen abundance versus deprojected radius for all galaxies in the sample. The dashed line passing through the closed circles represents an exponential fit. The horizontal dashed line is the asymptote to the exponential fit, and it represents the overall oxygen abundance of the galaxy. The vertical error in the fit from the oxygen abundance plots in §5 is shown in the bottom-left corner. The open triangles and open squares represent cumulative abundances using the maximum and minimum gradients allowed for the abundances (Figure 5.1), and the dotted horizontal lines represent their respective asymptotes. The difference between the dashed asymptote and the upper and lower bounds constitutes the error in the overall oxygen abundances.**

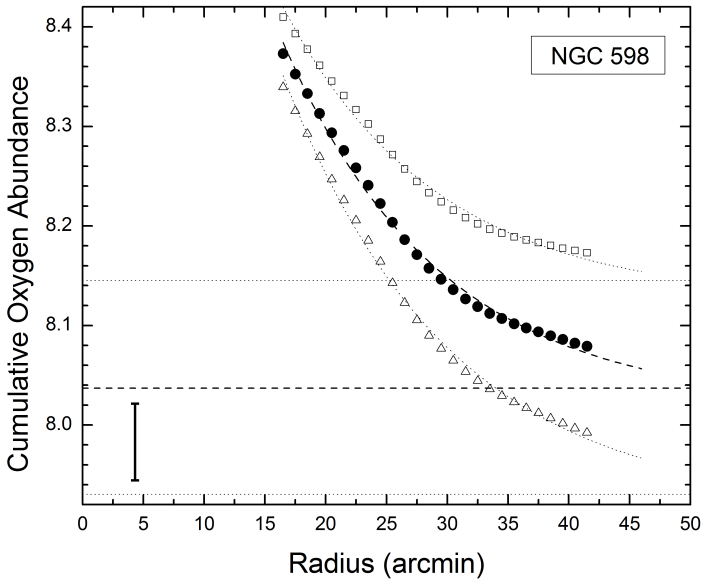

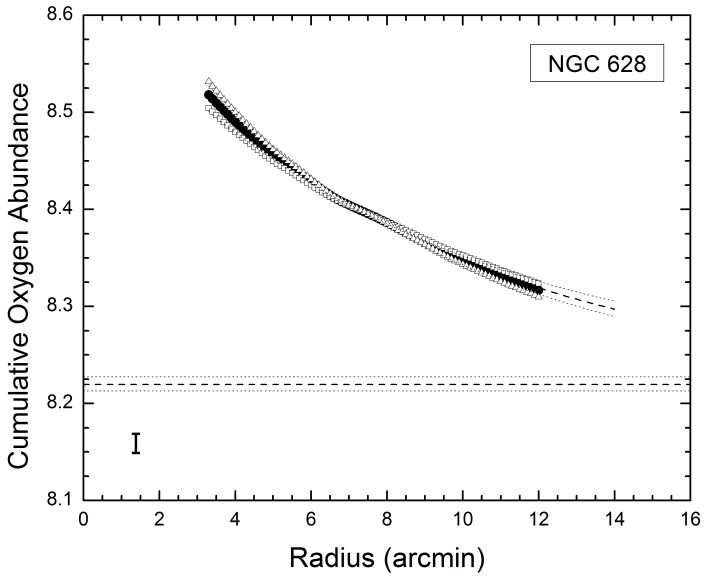

Figure 7.2 (cont'd): **Cumulative oxygen abundance versus deprojected radius for c) NGC 598 and d) NGC 628.**

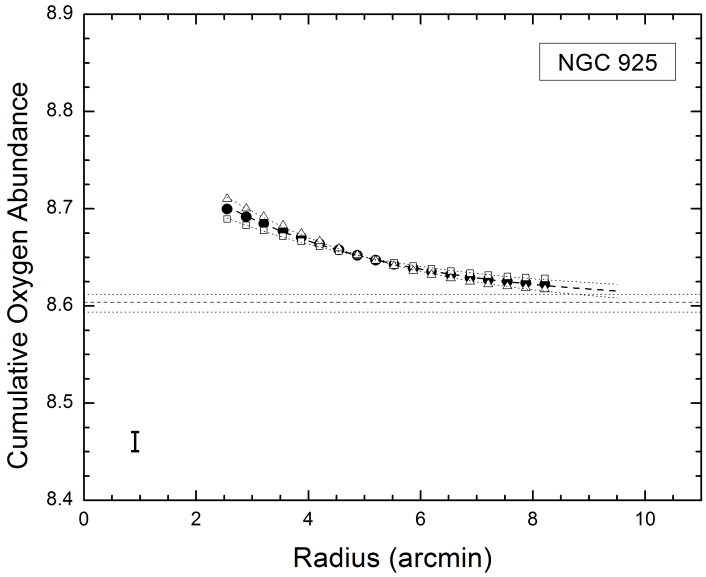

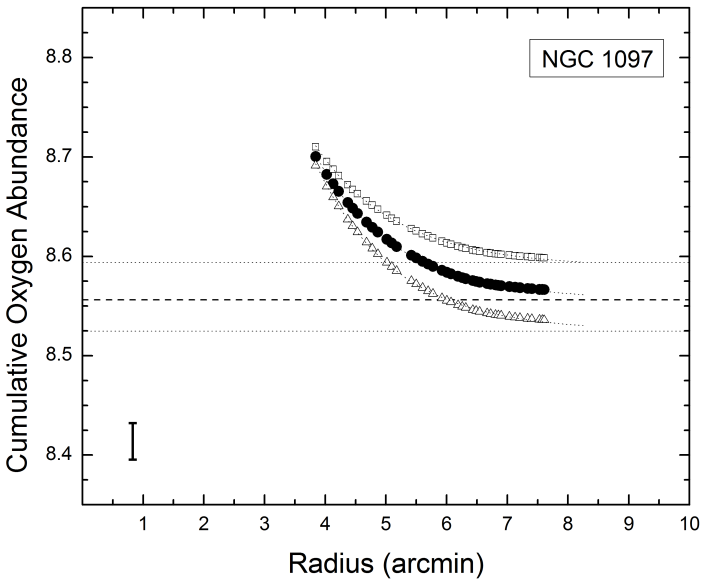

Figure 7.2 (cont'd): **Cumulative oxygen abundance versus deprojected radius for e) NGC 925 and f) NGC 1097**

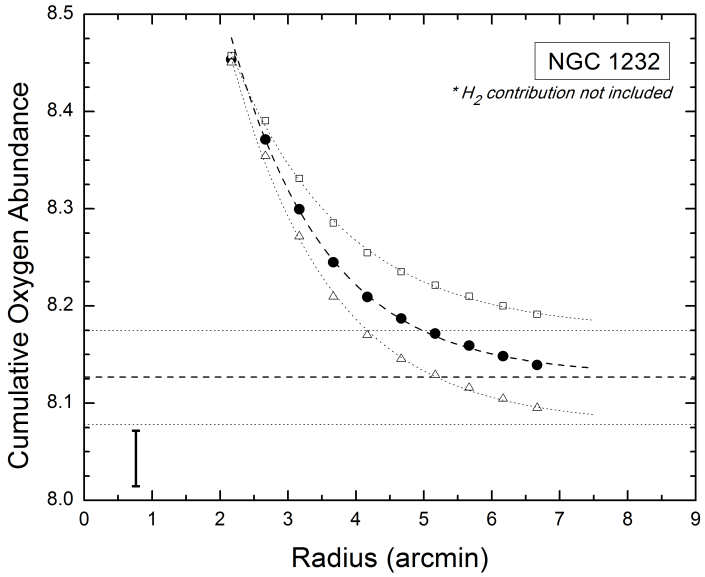

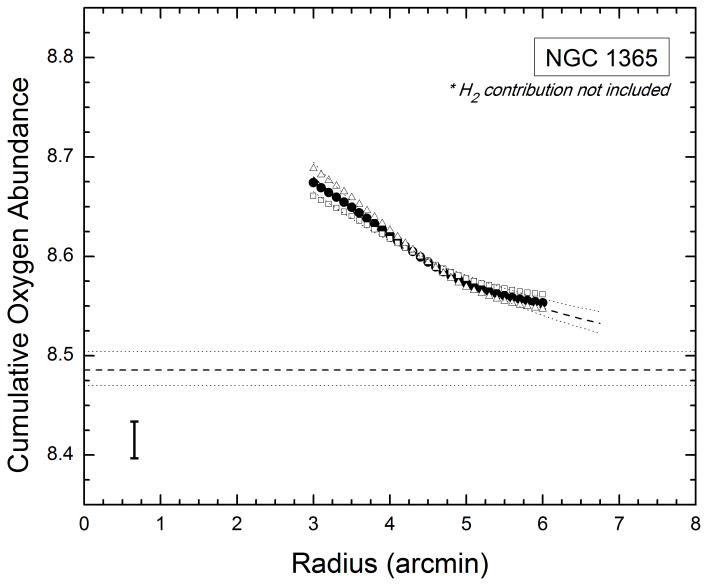

Figure 7.2 (cont'd): **Cumulative oxygen abundance versus deprojected radius for g) NGC NGC 1232 and h) NGC 1365**

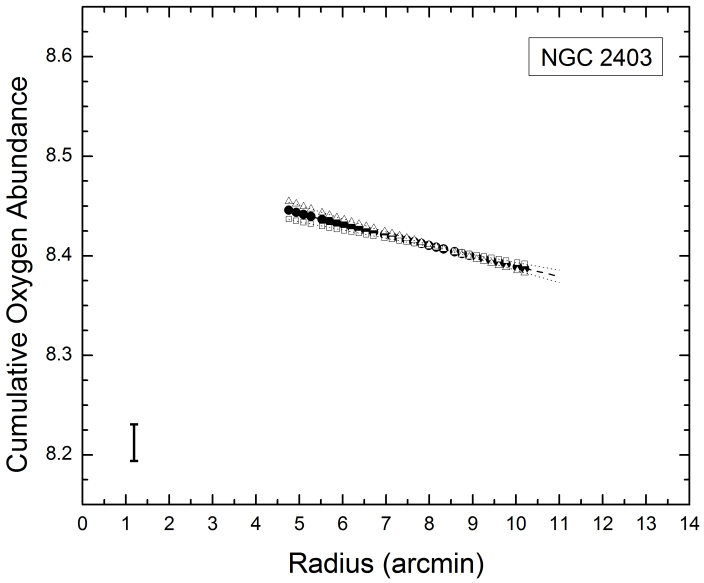

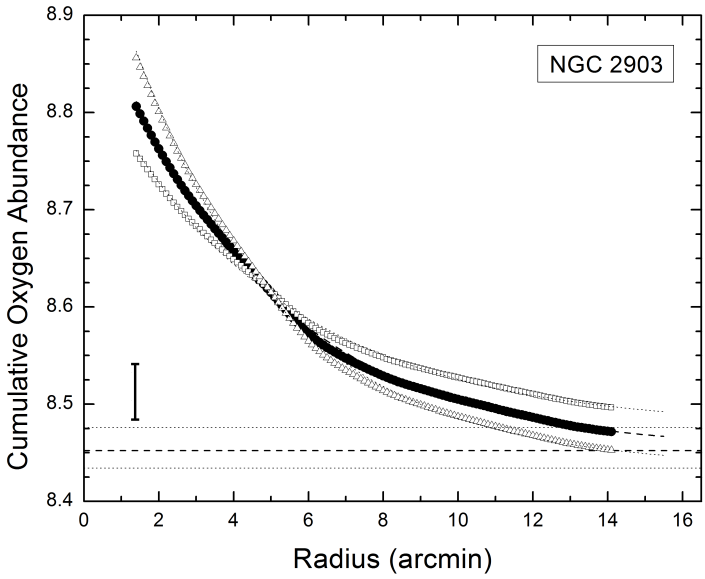

Figure 7.2 (cont'd): **Cumulative oxygen abundance versus deprojected radius for i) NGC 2403 and j) NGC 2903. The data for NGC 2403 do not show any evidence of an approach to an asymptote, so no conclusions about the overall abundance of this galaxy can be made.**

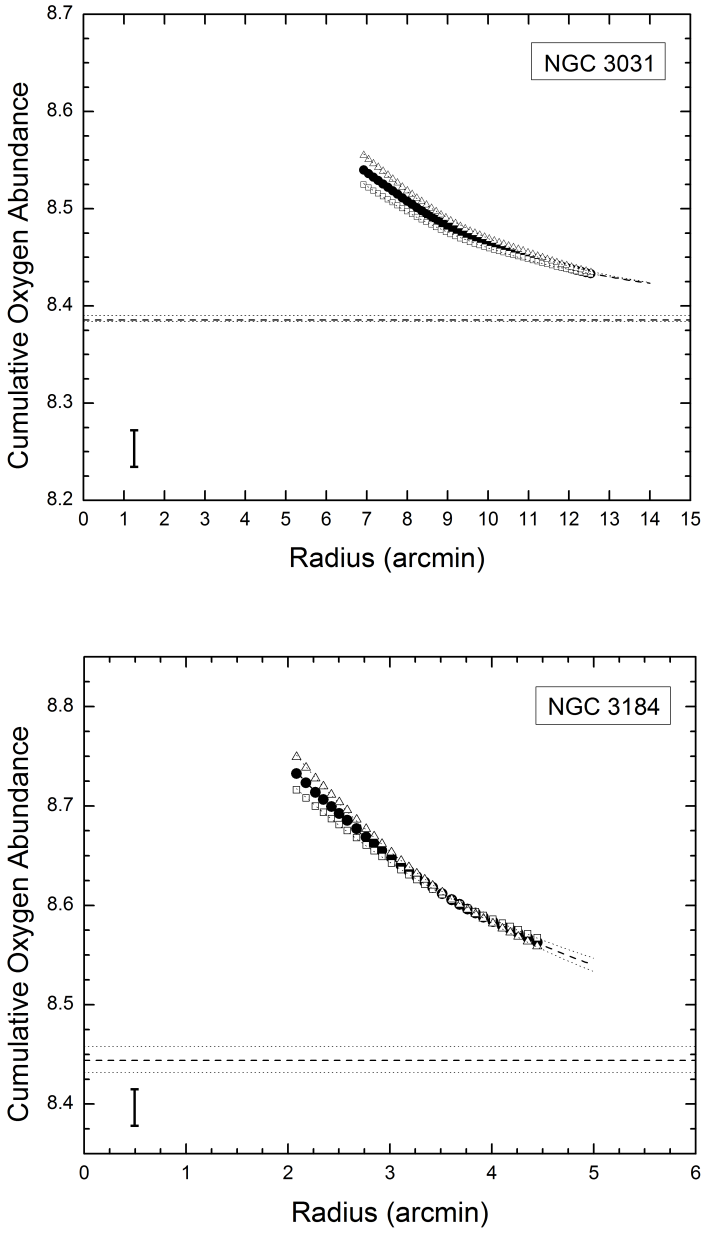

Figure 7.2 (cont'd): **Cumulative oxygen abundance versus deprojected radius for k) NGC 3031 and l) NGC 3184.**

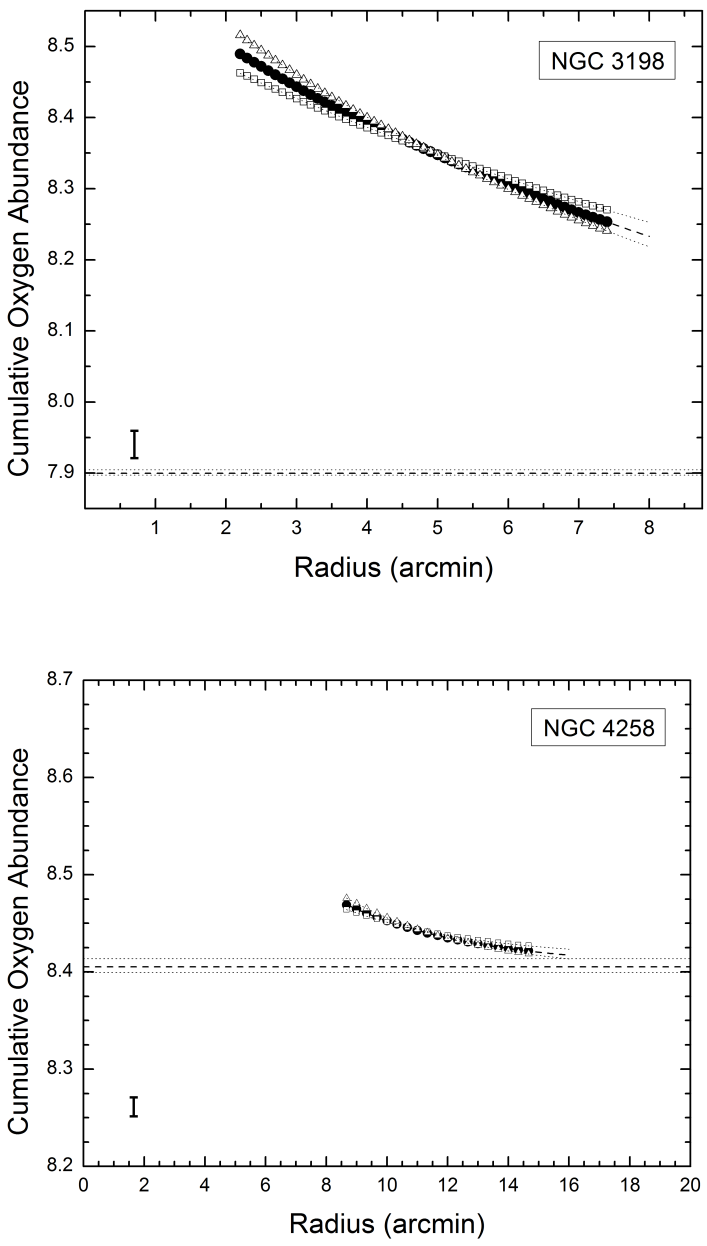

Figure 7.2 (cont'd): **Cumulative oxygen abundance versus deprojected radius for m) NGC 3198 and n) NGC 4258. The range of ordinates for NGC 3198 has been expanded to 0.7 dex in order to show all data points as well as the asymptote.**

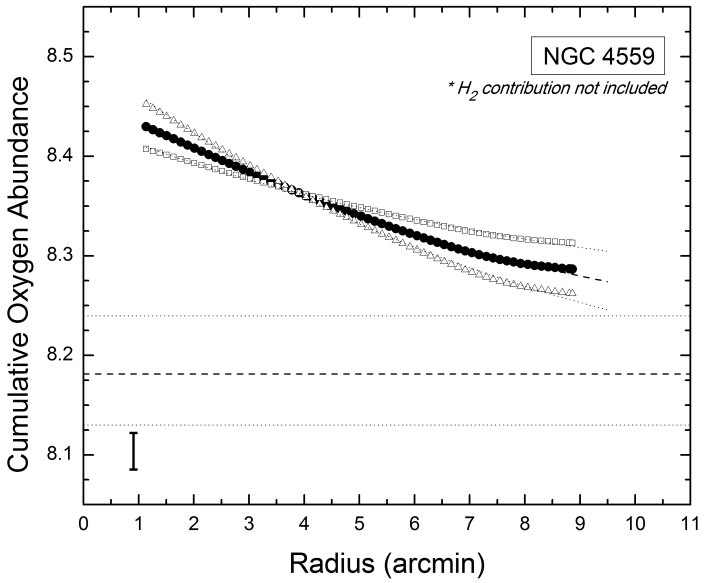

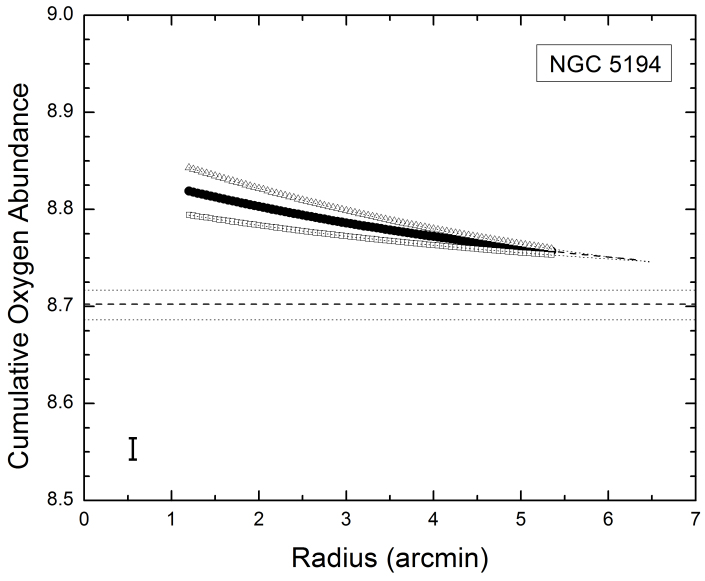

Figure 7.2 (cont'd): **Cumulative oxygen abundance versus deprojected radius for o) NGC 4559 and p) NGC 5194.**

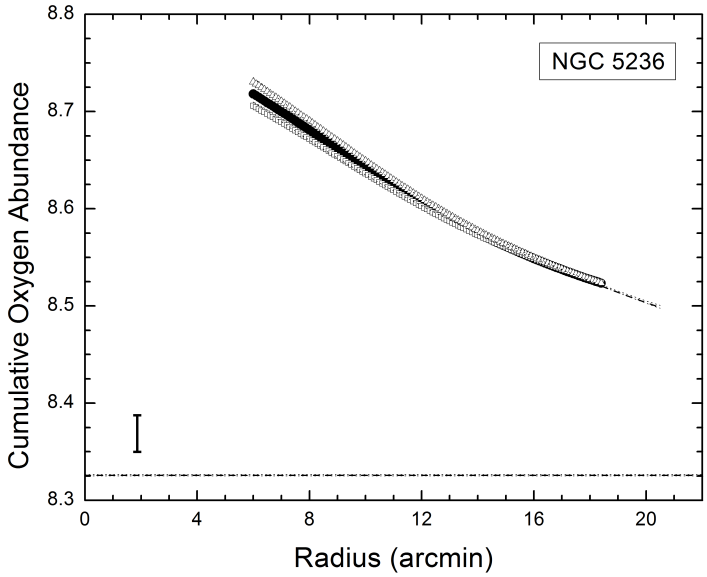

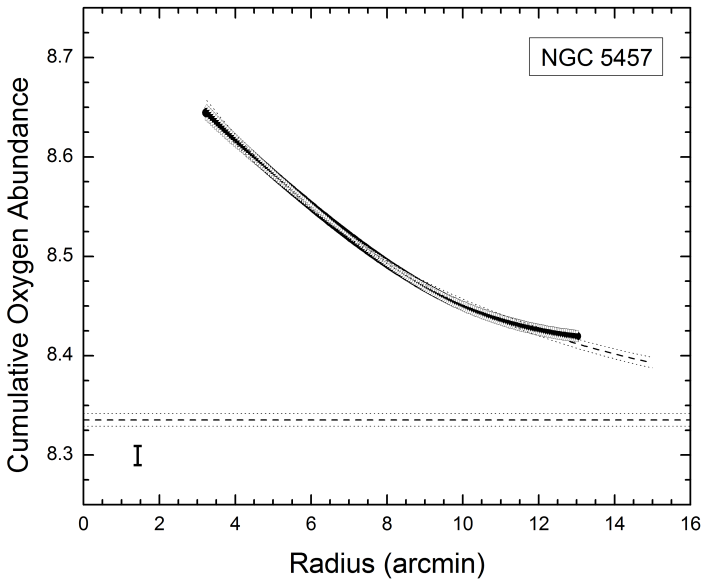

Figure 7.2 (cont'd): **Cumulative oxygen abundance versus deprojected radius for q) NGC 5236 and r) NGC 5457.**

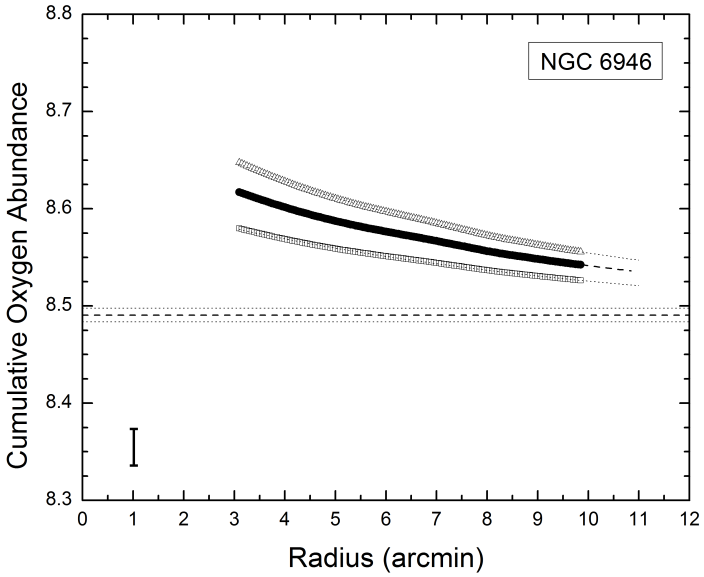

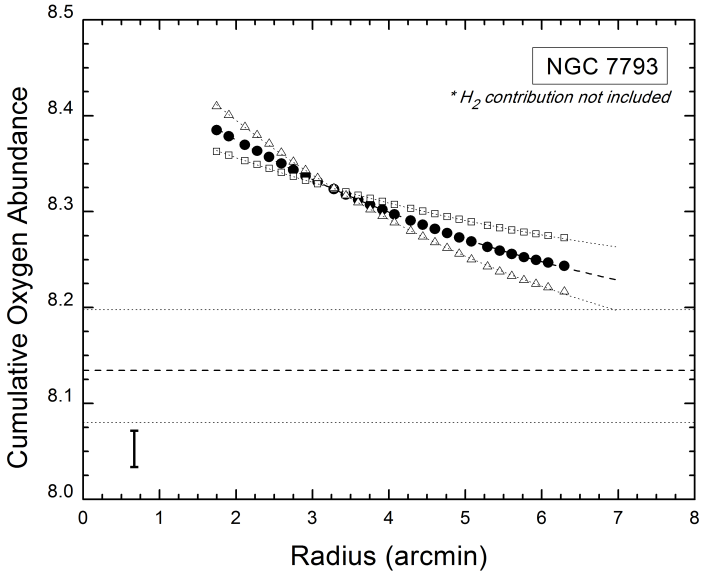

Figure 7.2 (cont'd): **Cumulative oxygen abundance versus deprojected radius for s) NGC 6946 and t) NGC 7793**

fits appears to be valid on the basis of the shape of the cumulative abundance curves for those galaxies for which HI is sampled out the farthest relative to the peak HI column density, although there is at least one notable exception (NGC 2403).

Beyond the peak in HI column density, the trend in the cumulative abundances with radius can be modeled by:

$$12 + \log(\mathrm{O/H}) = Ae^{-\frac{r}{\lambda}} + b \tag{7.1}$$

In equation 7.1, λ is the decay constant, b is the asymptote, and $A + b$ is the nominal abundance at $r = 0$. As r grows, and, hence, increasingly more of the total oxygen and hydrogen is included in the cumulative plot, the value of 12+log(O/H) decays until it reaches the offset, b. Thus, the value of b determines the oxygen abundance of the galaxy as a whole.

The robustness of this method was tested by calculating the asymptote with an exponentially decaying curve beginning at a radius 10% greater than that of the peak of the HI column density. In 15 of the 20 galaxies, no significant variation was calculated. Of all galaxies in the sample, the maximum difference was less than the error associated with each asymptote (i.e., less than 0.01 dex).

7.3 Contribution of Molecular Hydrogen

As shown in Table 4.1, data for molecular hydrogen were available for the galaxies NGC 224, NGC 598, NGC 628, NGC 925, NGC 2403, NGC 2903, NGC 3184, NGC 4258, NGC 5194, NGC 5236, NGC 5457, and NGC 6946. Therefore, for these galaxies it was possible to compare cumulative oxygen abundances including molecular hydrogen to abundances that leave out the contribution from molecular hydrogen.

Figure 7.3 shows the cumulative oxygen abundance versus radius for NGC 628 when molecular hydrogen is included (circles) and when it is not included (squares). In this plot, the upper (solid) horizontal line represents the asymptote obtained when molecular hydrogen is included, while the lower (dashed) horizontal line represents the asymptote when it is not. The respective values for these two asymptotes are 8.22 and 8.13. Likewise, Sadavoy and McCall (2006) found differences for NGC 5457 and NGC 6946 to be 0.07 and 0.12, respectively.

Of the fifteen galaxies for which H_2 data were available, only NGC 2903 showed a difference of greater than 0.09 dex between the asymptotic abundance with H_2 compared to the abundance not taking into account H_2. The difference between the asymptotes for NGC 2903 was 0.17 dex. Of all the galaxies for which H_2 data were available, none of them showed any significant increase in the asymptotic oxygen abundance when molecular hydrogen was factored in. The average difference in asymptotes when H_2 is taken into account versus when it is not, when NGC 2903 is excluded, is 0.046 dex. When NGC 2903 is included, the difference is 0.55 dex. Since

this is a systematic effect, an increase of 0.05 dex should be added to the asymptote of the cumulative abundances for all galaxies lacking H_2 data.

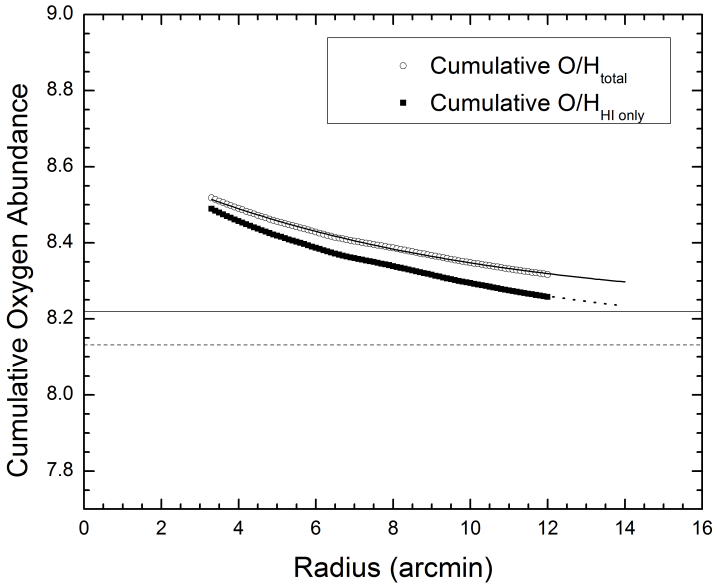

Figure 7.3: **Cumulative oxygen abundance versus deprojected radius for NGC 628, with and without the contribution of H_2. The upper points, exponential fit, and solid horizontal line are equivalent to those in Figure 7.2(d), i.e., they apply to the cumulative abundances including H_2. The lower points are the cumulative abundances of oxygen including atomic hydrogen atoms only. The dotted line running through the curve and the dashed horizontal line represent the exponential fit and the asymptote, respectively.**

7.4 Uncertainties in Asymptotes

Table 7.1 provides a summary of the following abundance parameters for all galaxies in the sample: oxygen abundance gradient, asymptote of the cumulative abundances, the cumulative oxygen abundance at the last point sampled, and the difference in

cumulative abundance between the last point sampled and the asymptote.

It is the contention here that asymptotes obtained from the plots in Figure 7.2 constitute good estimates of the overall oxygen abundances for most of the spiral galaxies in this study. Exponential functions were used to obtain asymptotes (and hence the overall abundances) since they generally fit well most of the cumulative oxygen abundance trends with radius.

Some of the cumulative abundance trends demonstrate slight deviations from exponentials that can lead to the suspicion that the asymptotes obtained are systematically too low. For example, for NGC 300, NGC 4559, and NGC 5457, it can be seen that the cumulative abundances at the largest radii begin to level out faster than the exponential does. For these galaxies, the asymptote of the exponential function may be a lower limit to the true overall cumulative abundance. An upper limit is given by the point at the largest radius. In 17 of the 20 galaxies, the asymptote and the last point are within 1.1 dex of each other. Notable exceptions are NGC 2403, NGC 3198, and NGC 5263.

Several measures could be taken to improve the confidence of the asymptotes. For example, HI maps that extend to larger radii would allow for an extension to the cumulative abundance plots. Since many of the curves only begin to level out toward the outermost points from the HI maps, sampling HI out a farther will likely lead to clearer asymptotic behaviour for the cumulative abundances. The exponential fit to the cumulative abundance plots is directly related to the radius at which fitting begins.

Here, the starting point was chosen to be the radius at which the column density of HI peaks. For many of the galaxies, this choice appears to be valid. However, for others, it appears that another starting point may in fact lead to a better fitting exponential (see Figure 7.2).

7.5 Cumulative Abundance of NGC 2403

Although the radial trend of cumulative oxygen abundances leads to an asymptotic abundance for most spiral galaxies, this is not the case for all of them. Specifically, it can be seen from Figure 7.2 that NGC 2403 does not reach an asymptote. In this case, an exponential function cannot be said to approximate the shape of the cumulative oxygen abundance plot. The reason why the method fails for NGC 2403 is probably due to the fact that it possesses a very shallow abundance gradient. When integrating out to larger and larger radii, the cumulative abundance decreases very slowly with radius. This same shortcoming is observed (though to a much lesser extent) for some of the other shallow-gradient galaxies, such as NGC 925, NGC 4258, and NGC 5194.

For NGC 2403, a better approximation to the overall abundance may be the cumulative abundance at the limiting radius of measurement. This value has to be considered to be an upper limit. For this galaxy, the upper limit has been adopted for the study of chemical evolution in §9.

7.6 Oxygen Abundance at $0.4R_o$

Zaritsky et al. (1994) proposed that overall abundances for spirals be quantified by O/H at $0.4R_o$, where R_o is the "isophotal radius," i.e., the radius at which the surface brightness in B is 25 mag/arcsec^2, corrected for extinction and to face-on. Values of R_o were listed in Table 4.2. Table 7.2 lists the asymptotic cumulative abundances and the abundances at $0.4R_o$ for all galaxies in the sample. In all instances, the abundance at $0.4R_o$ is larger than the asymptotic abundance. The average difference between the two is 0.22 dex. Clearly, the abundance at $0.4R_o$ is an unreliable index of the overall oxygen abundance of a spiral.

Figure 7.4 shows a comparison between the overall oxygen abundances ($\Sigma(O)/\Sigma(H)$) obtained via asymptotes, and oxygen abundances at $0.4R_o$. It is easy to see that there is no correlation from which to gauge $\Sigma(O)/\Sigma(H)$ from $0.4R_o$. For example, NGC 5194 and NGC 5236 have abundances at $0.4R_o$ equal to 8.77 and 8.73, respectively. However, those same galaxies have $\Sigma(O)/\Sigma(H)$ equal to 8.70 and 8.33, respectively. It is clear that no direct relation exists between the two abundance estimates.

The Zartisky method for calculating overall oxygen abundances suffers from several inadequacies. The method necessarily relies on an estimation of metallicity for the whole galaxy based on the oxygen abundance at a radius of a particular surface brightness. It is based on a comparison of the oxygen abundance at $0.4R_o$ versus blue magnitude, circular velocity, and Hubble type. However, no proof has been found to directly relate the oxygen abundance at $0.4R_o$ to any of these parameters. Moreover,

no standard shape to HI column density distributions has been observed. Therefore, absolute amounts of both hydrogen and oxygen at radii larger than $0.4R_o$ can vary unpredictably, leading to an unpredictable cumulative oxygen abundance.

On the other hand, the new method discussed in this study takes into account absolute amounts of both oxygen and hydrogen at all radii. Therefore, this new method calculates the true ratio of oxygen atoms to hydrogen atoms. It is not based on an estimation of oxygen abundance at any specific radius. Thus, it is justified to conclude that the method described in this study gives a more accurate estimation of the overall oxygen abundance.

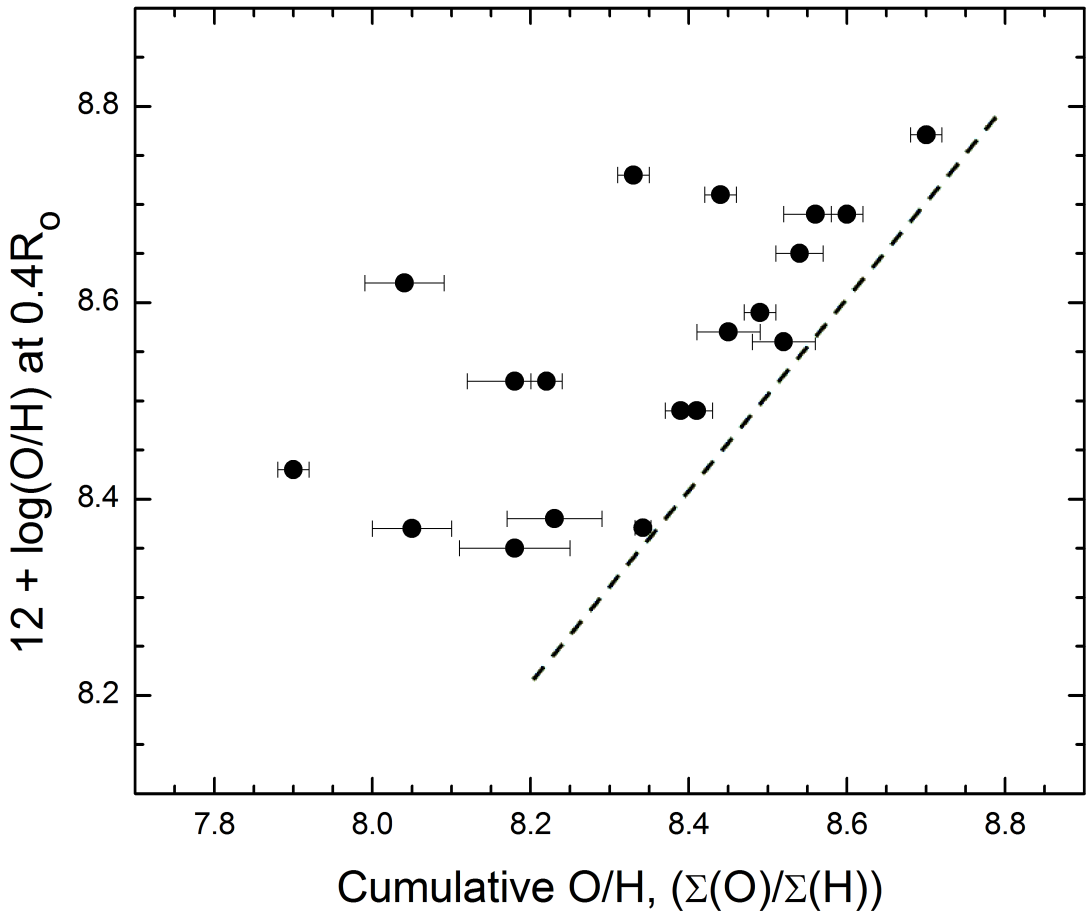

Figure 7.4: **A comparison of the asymptotic cumulative abundances versus abundances at $0.4R_o$.**

Table 7.1: **Parameters of the oxygen abundance plots.**

Galaxy	**O/H gradient** (dex/kpc)	+/-	**Asymptote**	+/-	**Σ(O)/Σ(H) at last point**	+/-	**Difference in O/H**
	(1)		(2)		(3)		(4)
NGC 224	-0.009	0.008	8.52	0.04	8.52	0.04	0.00
NGC 300	-0.072	0.016	8.05 *	0.05	8.10 *	0.05	0.05
NGC 598	-0.150	0.031	8.04	0.11	8.08	0.10	0.04
NGC 628	-0.031	0.004	8.22	0.02	8.32	0.02	0.10
NGC 925	-0.013	0.003	8.60	0.02	8.62	0.02	0.02
NGC 1097	-0.027	0.006	8.56	0.04	8.57	0.04	0.01
NGC 1232	-0.056	0.012	8.15 *	0.06	8.19 *	0.06	0.01
NGC 1365	-0.022	0.004	8.54 *	0.03	8.60 *	0.03	0.07
NGC 2403	-0.024	0.006	-	-	8.39	0.02	-
NGC 2903	-0.057	0.015	8.45	0.04	8.47	0.04	0.02
NGC 3031	-0.050	0.008	8.39	0.02	8.43	0.02	0.05
NGC 3184	-0.056	0.008	8.44	0.02	8.56	0.02	0.12
NGC 3198	-0.031	0.007	7.90	0.02	8.25	0.03	0.35
NGC 4258	-0.010	0.002	8.41	0.02	8.42	0.02	0.02
NGC 4559	-0.016	0.006	8.23 *	0.06	8.34 *	0.03	0.11
NGC 5194	-0.017	0.006	8.70	0.02	8.76	0.02	0.05
NGC 5236	-0.043	0.004	8.33	0.02	8.52	0.02	0.20
NGC 5457	-0.035	0.002	8.34	0.01	8.42	0.01	0.08
NGC 6946	-0.027	0.007	8.49	0.02	8.54	0.03	0.05
NGC 7793	-0.086	0.024	8.18 *	0.07	8.29 *	0.04	0.11

Notes:

* *0.05 dex has been added to these values to account for the systematic effect of missing H_2 data*

(1) Oxygen abundance gradient (see Figure 5.1), in dex/kpc

(2) Asymptote of the cumulative abundance plots (see Figure 7.2)

(3) Cumulative oxygen abundance at the last point in the cumulative abundance plots

(4) Difference between cumulative oxygen abundance at last point and asymptote

Table 7.2: **A comparison of the asymptotic cumulative abundances versus abundances at $0.4R_o$.**

Galaxy	**$0.4*R_o$** (arcmin)	**O/H at $0.4*R_o$**	**O/H cumulative, $\Sigma(O)/\Sigma(H)$**	**Error, $\delta[\Sigma(O)/\Sigma(H)]$**	**Difference: O/H ($0.4R_o$) - $\Sigma(O)/\Sigma(H)$**
NGC 224	38.11	8.56	8.52	0.04	**0.04**
NGC 300	4.38	8.37	8.05 *	0.05	**0.32**
NGC 598	3.72	8.62	8.04	0.11	**0.58**
NGC 628	1.96	8.52	8.22	0.02	**0.30**
NGC 925	2.10	8.69	8.60	0.02	**0.08**
NGC 1097	1.87	8.69	8.56	0.04	**0.13**
NGC 1232	1.48	8.52	8.18 *	0.06	**0.35**
NGC 1365	2.24	8.65	8.54 *	0.03	**0.11**
NGC 2403	4.38	8.41	-	-	-
NGC 2903	2.52	8.57	8.45	0.04	**0.12**
NGC 3031	5.38	8.49	8.39	0.02	**0.10**
NGC 3184	1.48	8.71	8.44	0.02	**0.27**
NGC 3198	1.70	8.43	7.90	0.02	**0.53**
NGC 4258	3.72	8.49	8.41	0.02	**0.08**
NGC 4559	2.14	8.38	8.23 *	0.06	**0.15**
NGC 5194	2.16	8.77	8.70	0.02	**0.06**
NGC 5236	2.58	8.73	8.33	0.02	**0.40**
NGC 5457	5.77	8.36	8.34	0.01	**0.02**
NGC 6946	2.30	8.59	8.49	0.02	**0.09**
NGC 7793	1.87	8.35	8.18 *	0.07	**0.16**

* *0.05 dex has been added to these values to account for the systematic effect of missing H_2 data*

Chapter 8

Gas Fractions

8.1 Background

One of the goals of this study is to be able to compare overall oxygen abundances to gas fractions, and in the process examine chemical evolution. The gas fraction of a galaxy is the ratio of the mass of its gas to the total baryonic mass, which is composed of both gas and stars. In §8.2, the calculation of the total mass of gases will be explored. In §8.3 to §8.5, the mass from stars will be derived. Finally, in §8.6, the gas fraction will be calculated using both the gas mass and stellar mass.

8.2 Gas Masses

The column densities of hydrogen integrated over the area of a disk were calculated in §6. These column densities were then converted into masses by multiplying the total

number of hydrogen atoms by the mass of hydrogen. To account for the presence of helium, the total mass of hydrogen is multiplied by a factor of 1.36 (Oey & Kennicutt 1990). Since the composition of the gas is overwhelmingly dominated by hydrogen and helium, the result can be regarded as the total mass of gas. Then, this overall gas mass was converted into units of solar masses.

The gas masses were calculated with and without the contribution of H_2 for those galaxies for which molecular hydrogen data were available. The difference in gas fractions turns out to be relatively small, and the systematic error introduced by missing H_2 data will be introduced in §8.6.

8.3 Light Profiles

The next task is to calculate the mass of each galaxy contained in the stars. This feat is achieved by finding the integrated brightness of each galactic disk and then converting the luminosity into a mass. To this end, flux distributions were obtained from the *Two Micron All Sky Survey* (2MASS, Skrutskie et al. 2006). This was a joint project of the University of Massachusetts and the Infrared Processing and Analysis Center (IPAC) at the California Institute of Technology (Caltech) to survey the entire sky in three near-infrared bands, J, H, and K_s.

In order to find the stellar mass, it is necessary to examine the light profile of each galaxy. It is necessary to separate the inner bulge of each galaxy from the disk, because it is the evolution of the disk which is under study. As will be seen in §8.4,

the bulge can vary greatly from galaxy to galaxy. The ratio of the flux from the disk to that of the disk and bulge can then be used to find the portion of the overall absolute magnitude of each galaxy contributed by the disk alone.

2MASS does not provide total magnitudes extrapolated to infinity, but rather only to a specified radius, R. Accordingly, a correction to the 2MASS magnitude was necessary, as described in §8.4. At that point, the mass of the disk could be estimated with a suitable choice of a mass-to-light ratio for the stars.

The K_s-band was chosen to give the most meaningful representation of the stars in each galaxy. The K_s-band refers to the part of the near-infrared portion of the electromagnetic spectrum at 2.2 μm $\pm$ 0.3 μm. Young massive stars constitute relatively little mass overall, yet tend to contribute a relatively large amount of light in the "blue" end of the spectrum (shorter wavelengths). Older, less massive stars make up the bulk of the mass, but because they are so much cooler their contribution to light in blue wavelengths can be swamped by that from massive stars. "Redder" (longer) wavelengths more accurately trace mass because low-mass stars contribute proportionally more light. Beyond 2.2 μm, the luminosity tends to be contaminated by emission from dust grains. The K-band allows for the luminosity of young stars to be maximally suppressed while not suffering from dust contamination (Joy & Lester 1988). The K_s-band is the 2MASS rendition of *Johnson K*, which is advantageous because it is less sensitive to variations in ambient temperature (Carpenter 2001).

The annular median surface brightness as a function of radius, corrected for incli-

nation, was taken from the 2MASS database. The units are in magnitudes per square arc second. The profile for NGC 1232 is shown in Figure 8.1. From this graph, it can be seen that a large amount of light is emitted within the nearest 0'.25 from the centre of the galaxy. This light is due to the contribution of the galaxy's bulge. At distances greater than about 0'.25 from the centre, the shape of the profile straightens out into a simple exponential curve. Since the y-axis is in magnitude units (a logarithmic scale), the exponential is seen as a linear trend. The linear portion of the graph represents light from the disk of the galaxy.

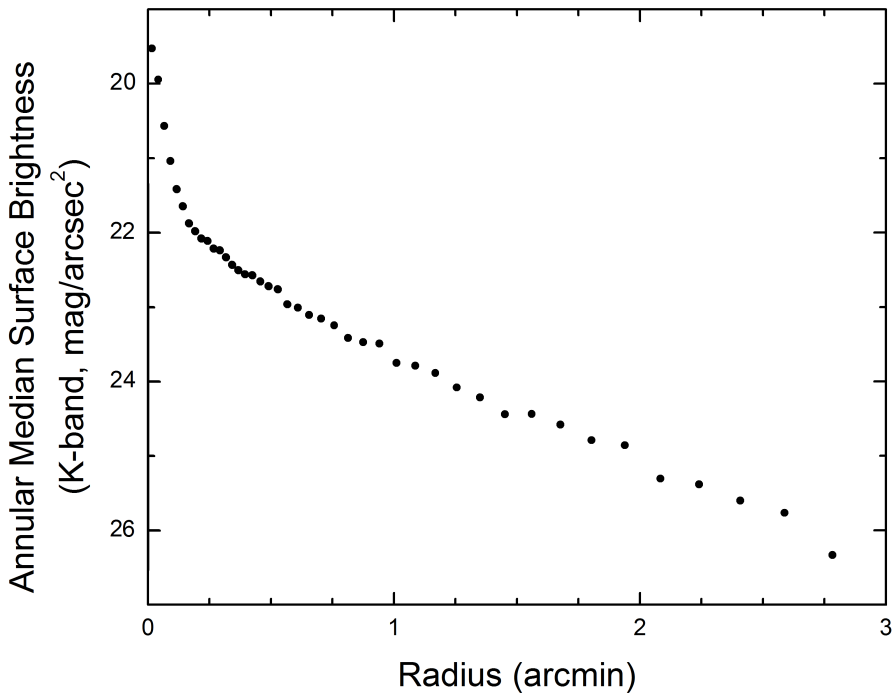

Figure 8.1: **K_s-band light profile of NGC 1232. Both surface brightness and radii have been corrected for projection**

The K_s-band surface brightness profiles were plotted for each galaxy in the study. Then, these profiles were fitted with a formula combining an exponential describing the disk and a de Vaucouleurs profile describing the spheroid. This function takes the following form:

$$I(r) = -2.5\log\left(I_1 e^{-\left(\frac{r}{a}\right)} + I_2 e^{-\left(\frac{r}{b}\right)^{1/4}}\right) \tag{8.1}$$

where r is the deprojected radius. The first term, $I_1 e^{-\left(\frac{r}{a}\right)}$, represents the disk of the galaxy, while the second, $I_2 e^{-\left(\frac{r}{b}\right)^{1/4}}$ (the de Vaucouleurs profile), represents the bulge. The parameters I_1 and a, and I_2 and b are the central surface brightness and scale lengths for the disk and bulge, respectively.

Table 8.1 lists the parameters obtained from fitting each light profile with equation 8.1. Beside each parameter is the error associated with it. $I_{disk} = -2.5\log(I_1)$ is the surface brightness of the disk at $r = 0$, in mag/arcsec^2. The exponential scale length is given by a. $I_{sph} = -2.5\log(I_2)$ is the surface brightness of the bulge at $r = 0$, in mag/arcsec^2. The root mean square error of the fit is given in the rightmost column.

8.4 Calculating Absolute Magnitudes

To calculate the absolute magnitude of the disk, it is necessary first to calculate the flux contributed by the disk of each galaxy in the 2MASS system. Then, the ratio of this flux to the 2MASS flux for the entire galaxy (disk + bulge) is determined. This

Table 8.1: **Parameters for fits to the K_s-band light profile. Parameters are taken from equation 8.1.**

Galaxy	I_{disk}	δI_{disk}	a	δ a	I_{sph}	δI_{sph}	b	δ b	RMSE
	(mag / arcsec^2)		(arcmin)		(mag / arcsec^2)		(arcmin)		
NGC 224	8.41	0.11	9.41	1.82	4.56	0.07	1.0E-01	1.4E-02	0.018
NGC 300	8.34	0.07	3.21	0.23	9.48	0.42	1.8E+02	7.3E+02	0.048
NGC 598	8.72	0.06	4.74	0.66	7.19	0.06	1.13	0.28	0.048
NGC 628	7.72	0.04	2.25	0.07	2.97	0.52	2.6E-04	1.1E-04	0.071
NGC 925	8.81	0.26	4.08	0.51	-1.54	0.47	2.6E-02	4.4E-02	0.065
NGC 1097	8.51	0.39	3.64	0.65	-2.44	0.37	2.2E-02	2.6E-02	0.108
NGC 1232	7.87	0.21	1.94	0.19	-1.08	0.54	1.3E-02	2.6E-02	0.053
NGC 1365	7.94	0.12	2.55	0.19	-3.24	0.36	2.6E-03	1.5E-03	0.169
NGC 2403	8.23	0.03	3.00	0.57	-0.21	0.18	4.01	52.33	0.087
NGC 2903	7.09	0.04	1.60	0.04	-10.94	0.19	1.1E-05	5.9E-05	0.156
NGC 3031	7.73	0.04	5.98	0.10	3.73	0.06	4.5E-03	4.5E-04	0.043
NGC 3184	7.78	0.04	2.08	0.10	-5.98	0.27	6.5E-05	9.7E-05	0.179
NGC 3198	7.85	0.04	1.73	0.05	-5.51	0.24	7.6E-05	1.1E-04	0.138
NGC 4258	7.74	0.10	3.66	0.17	-1.88	0.24	1.3E-02	8.6E-03	0.113
NGC 4559	8.29	0.03	2.34	1.17	-1.33	0.11	2.6E-02	0.73	0.094
NGC 5194	7.19	0.07	2.18	0.09	1.58	0.11	1.8E-04	1.4E-04	0.225
NGC 5236	7.35	0.03	4.14	0.11	0.63	0.53	1.6E-04	4.8E-05	0.062
NGC 5457	7.79	0.02	4.69	0.08	3.88	0.20	5.9E-04	1.1E-04	0.040
NGC 6946	7.50	0.03	3.55	0.10	-3.76	0.42	5.4E-04	2.2E-04	0.089
NGC 7793	7.85	0.08	2.63	0.16	-1.34	0.99	3.2E-03	5.7E-03	0.078

ratio is applied to the best estimate of the total absolute magnitude from McCall (2011) in order to calculate the absolute magnitude of the disk alone.

The general equation for calculating flux is:

$$F = \int_{\Omega} I \, \mathrm{d}\Omega \tag{8.2}$$

where I is the surface brightness, and $\mathrm{d}\Omega$ is the differential angle of the disk. To find

the flux of each galaxy, a substitution is made for $I = I(r)$. In order to integrate over the radius, r, it is necessary to convert the differential solid angle, $\mathrm{d}\Omega$, to a differential radius, $\mathrm{d}r$. Isophotes are elliptical, so $\Omega = \pi r^2 q$, where q is the ratio of the semi-minor to semi-major axes of the isophotes. We then get:

$$\frac{\mathrm{d}\Omega}{\mathrm{d}r} = \frac{\mathrm{d}}{\mathrm{d}r}(\pi r^2 q)$$

$$\mathrm{d}\Omega = 2\pi r q \cdot \mathrm{d}r \tag{8.3}$$

In equation 8.3, the q accounts for the inclination of the galaxy. For face-on galaxies, or for galaxies for which the surface brightness data has already been corrected for inclination, q will equal 1.

Now it is possible to rewrite equation 8.2 using the terms from parameters I_1 and a listed in Table 8.1. The flux from the disk, F_{disk}, within radius R is given by:

$$F_{disk} = \int_0^R I(r) \cdot 2\pi r q \mathrm{d}r$$

$$= \int_0^R I_1 e^{-\left(\frac{r}{a}\right)} \cdot 2\pi r q \mathrm{d}r$$

Thus,

$$F_{disk}(R) = 2\pi a^2 q I_1 \left(1 - e^{-(\frac{R}{a})} \left[\left(\frac{R}{a}\right) + 1\right]\right) \tag{8.4}$$

When integrated to infinity, the flux becomes:

$$F_{disk}(\infty) = 2\pi a^2 q I_1 \tag{8.5}$$

From 2MASS, it is possible to obtain apparent K_s-band magnitudes (and thus fluxes) for all of the galaxies in this study. These magnitudes incorporate the flux from the entire galaxy (disk + bulge) out to a finite radius, R, which will be referred to as $F_{disk+bulge}(R)$. It is necessary to add the missed flux from R out to infinity to get the total flux from starlight. The full ratio of flux from the disk to flux from the entire galaxy, integrated to infinity, is calculated from:

$$\frac{F_{disk}}{F_{disk+bulge}} = \frac{F_{disk}(\infty)}{F_{disk+bulge}(R) + [F_{disk}(\infty) - F_{disk}(R)]} \tag{8.6}$$

The absolute magnitude of the disk then follows from the absolute magnitude of the whole galaxy as given by McCall (2011). All of the apparent magnitudes, m, (equal to -2.5log(F)), ratios of $F_{disk}/F_{disk+bulge}$, and absolute magnitudes, M, can be found in Table 8.2. Uncertainties in disk absolute magnitudes are dominated by errors in the distance moduli. These errors are all less than 0.1, with the exception of NGC 6946 and NGC 7793, whose distance modulus errors are 0.22 and 0.24, respectively.

Fluxes obtained from 2MASS for the galaxy NGC 224 were deemed unreliable. Since the apparent size of this galaxy is so large, 2MASS had to make several passes over thin strips of the galaxy to map out its light. In lieu of the data from 2MASS, a disk-to-total flux ratio of 0.55 has been adopted from optical measurements (Walterbos & Kennicutt 1988). Although they did not specifically calculate the ratio of light from the disk to that of the entire galaxy for the K_s-band, Walterbos and Kennicutt did find it to be 0.55 in both the V-band and the R-band.

8.5 Stellar Masses

With the absolute magnitudes of the disk, the total stellar mass can be calculated. This is possible because of known relations between absolute magnitude and luminosity, and between luminosity and mass. First, to convert absolute magnitude to luminosity in the K_s-band, the following relation is used:

$$M_{disk} - M_{\odot} = -2.5\log\left(\frac{L_{disk}}{L_{\odot}}\right) \tag{8.7}$$

M_{disk} refers to the absolute magnitude of the disk of the galaxy and $L_{disk}/L_{\odot}$ is the luminosity of the disk in units of the solar luminosity. The adopted value for the absolute magnitude of the sun in K_s, $M_{\odot}$, is +3.32 (Bell et al. 2003). The luminosity of each galaxy can be converted into a mass by adopting a suitable mass-to-light ratio, x, for the K_s-band. The mass-to-light ratio used in this study is x=0.88±0.20

$\frac{\mathrm{M}_\odot}{L_\odot}$, estimated by McCall et al. (2011). This adopted value of x is examined further in §9.2. The mass of the disk is computed as follows:

$$\frac{\mathrm{M}_{disk}}{\mathrm{M}_\odot} = x \left(\frac{L_{disk}}{L_\odot} \right) \tag{8.8}$$

Here, $\mathrm{M}_{disk}/\mathrm{M}_\odot$ refers to the total stellar mass of the disk, in units of solar masses.

8.6 Gas Fractions

The gas fraction is the ratio of the mass of the gas to that of baryons (gas + stars) in the disk:

$$\mu = \frac{\mathrm{M}_{gas}}{\mathrm{M}_{disk} + \mathrm{M}_{gas}} \tag{8.9}$$

The values for L_{disk}, M_{disk}, M_{gas} and μ are listed for all galaxies in this study in Table 8.3.

The contribution of H_2 turns out to have a small impact on the overall gas fraction. Of the 15 galaxies for which H_2 was available, the average proportion of gas mass made up by neutral hydrogen was 72%. Therefore, for the 5 galaxies for which H_2 was not available, the neutral hydrogen gas mass was multiplied by a factor of 1.38 to compensate.

Table 8.2: **Apparent magnitudes, flux ratios, and absolute magnitudes for all sample galaxies.**

Galaxy	**R** (arcmin)	$\mathbf{m_{disk+bulge}(R)}$ (dex)	$\mathbf{m_{disk}(R)}$ (dex)	$\mathbf{m_{disk}(\infty)}$ (dex)	$\mathbf{F_{disk}}$ / $\mathbf{F_{disk+bulge}}$	$\boldsymbol{M}_{\mathbf{disk+bulge}}(\infty)$ (dex)	$\boldsymbol{M}_{\mathbf{disk}}(\infty)$ (dex)
(1)	(2)	(3)	(4)	(5)	(6)	(7)	(8)
NGC 224	-	-	-	-	0.55	-24.82	-24.17
NGC 300	7.10	6.379	6.417	6.180	0.97	-21.07	-21.04
NGC 598	17.92	4.102	4.221	4.196	0.90	-21.65	-21.54
NGC 628	4.60	6.845	6.959	6.925	0.90	-23.02	-22.91
NGC 925	4.60	7.873	7.977	7.751	0.92	-22.18	-22.10
NGC 1097	5.43	6.252	7.011	6.952	0.51	-21.81	-21.08
NGC 1232	3.17	7.381	7.581	7.507	0.84	-20.44	-20.25
NGC 1365	4.60	6.373	6.937	6.883	0.61	-25.11	-24.57
NGC 2403	6.28	6.191	6.265	6.244	0.94	-22.14	-22.07
NGC 2903	4.12	6.036	6.260	6.240	0.82	-23.88	-23.66
NGC 3031	12.58	3.831	4.510	4.481	0.54	-24.22	-23.55
NGC 3184	4.60	7.225	7.323	7.290	0.92	-19.82	-19.73
NGC 3198	3.97	7.779	7.860	7.825	0.93	-23.19	-23.12
NGC 4258	7.66	5.464	5.559	5.530	0.92	-24.16	-24.07
NGC 4559	5.25	7.584	7.726	7.710	0.88	-21.97	-21.83
NGC 5194	5.90	5.496	5.734	5.719	0.81	-24.13	-23.89
NGC 5236	8.52	4.619	4.857	4.828	0.81	-23.96	-23.73
NGC 5457	8.76	5.512	5.586	5.533	0.94	-23.93	-23.86
NGC 6946	7.98	5.369	5.496	5.471	0.89	-23.81	-23.68
NGC 7793	5.43	6.855	6.960	6.919	0.91	-21.16	-21.06

Notes:

(1) Name of galaxy
(2) Limiting radius for 2MASS magnitude, in arcmin
(3) Apparent magnitude of the galaxy (disk+bulge) within radius R, taken from 2MASS
(4) Apparent magnitude of just the disk within radius R
(5) Apparent magnitude of just the disk out to infinity
(6) Ratio used to derive the absolute magnitude of the disk alone from the total absolute magnitude. For NGC 224, a ratio of 0.55 has been adopted from Walterbos & Kennicutt (1988)
(7) Total absolute magnitude
(8) Absolute magnitude of the disk alone

Table 8.3: **Luminosities, masses and gas fractions.**

Galaxy	Stars		Gas	Gas Fraction, μ
	log (L_{disk}/ L_{sun})	log (M_{disk} / M_{sun})	log (M_{gas} / M_{sun})	
NGC 224	11.00	10.60	9.88	0.08
NGC 300	9.74	9.35	9.54 *	0.41
NGC 598	9.94	9.54	9.42	0.25
NGC 628	10.49	10.09	10.03	0.28
NGC 925	10.16	9.77	10.36	0.64
NGC 1097	9.76	9.36	10.23	0.18
NGC 1232	9.43	9.03	10.20 *	0.16
NGC 1365	11.15	10.76	10.41 *	0.17
NGC 2403	10.15	9.75	9.57	0.23
NGC 2903	10.79	10.39	9.97	0.15
NGC 3031	10.75	10.35	9.25	0.03
NGC 3184	9.22	8.82	9.81	0.34
NGC 3198	10.57	10.17	10.11	0.28
NGC 4258	10.95	10.55	9.98	0.11
NGC 4559	10.06	9.66	9.73 *	0.39
NGC 5194	10.88	10.48	10.51	0.33
NGC 5236	10.82	10.42	10.18	0.21
NGC 5457	10.87	10.47	10.24	0.21
NGC 6946	10.80	10.40	10.19	0.22
NGC 7793	9.75	9.35	9.22 *	0.25

* *A factor of 1.39 has been multiplied to these original values to account for the systematic effect of missing H_2 data*

Chapter 9

Evolution

9.1 Review of Past Work

The closed-box model can be used to provide a good understanding of the chemical evolution of galaxies (Searle & Sargent 1972; Pagel & Edmunds 1981; Pagel 1997). Lee et al. (2003a) showed that the relationship between metallicity and gas fraction (equation 1.2) can be written as:

$$\mathrm{O/H} = y_o \ln(1/\mu)$$

which then leads to the equation relating 12+log(O/H) to log(log(1/μ):

$$12 + \log(\mathrm{O/H}) = 12 + \log\left(2.303 y_\mathrm{o}\right) + \log(\log(1/\mu))$$

In this equation, y_o refers to the yield of oxygen by number. It is related directly to the yield of oxygen by mass, which is the ratio of the mass of newly formed oxygen to the mass of gas locked permanently in stars. In a plot of 12+log(O/H) against log(log($1/\mu$)), therefore, the closed-box model predicts a slope of unity, and the yield can be derived from the intercept of the plot.

Lee et al. (2003a) explored the relationship between oxygen abundances and gas fractions in dwarf irregular galaxies. In that study, a linear correlation with a slope of unity was found. Vaduvescu et al. (2007) confirmed this correlation by looking at 21 more dwarf irregulars whose stellar masses were derived from sech (hyperbolic secant function) magnitudes in the K_s-band (Vaduvescu et al. 2005).

9.2 Mass-to-Light Ratio

In order to plot oxygen abundances versus gas fractions for spirals alongside those of dwarf irregulars, a self-consistent method for determining gas fractions must be established. A key factor in determining gas fractions is the mass-to-light ratio, defined as $\frac{\mathrm{M/M_\odot}}{L/L_\odot}$ for the entire population of disk stars. One possible option for this ratio would be to adopt that of the Milky Way. This particular value has been estimated by Portinari et al. (2009) and was found to be $x = 0.4$. Vaduvescu et al. (2007) adopted 0.8 based on a survey of the literature devoted to modelling of the Milky Way and galaxy evolution. More recently, a value of $x = 0.88 \pm 0.20$ has been found by McCall et al. (2011) by minimizing residuals in the relationship between the

potential, line width, and surface brightness of star-forming dwarfs.

In Figure 9.1, a comparison of gas fractions and oxygen abundances is shown using both $x = 0.4$ and $x = 0.88$. Points obtained using $x = 0.4$ are systematically shifted to the left with respect to those obtained using $x = 0.88$. The mean difference between pairs of points is 0.20 ± 0.08.

Here, the mass-to-light ratio for all galaxies was adopted to be 0.88. This ratio was chosen above those by Portinari et al. , and Vaduvescu et al. since it leads to the least scatter.

9.3 A Comparison of Oxygen Abundances and Gas Fractions for Spirals

Figure 9.2 plots the cumulative oxygen abundance versus $\log(\log(1/\mu))$ for spirals alongside the data from dwarf irregular galaxies. Oxygen abundances for these dwarf irregulars come from a variety of sources (Hidalgo-Gamez & Olofsson 2002; Lee et al. 2003(a); Lee et al. 2007; Vaduvescu et al. 2007; van Zee & Haynes 2006), and gas fractions were calculated by McCall et al. (2011). On this graph, the gas fraction increases to the left (since the horizontal axis is plotted as $\log(\log(1/\mu))$). The linear fit to the dwarf irregulars with a slope fixed at unity is plotted with a dotted line, while a similar fit for spirals is plotted with a solid line. At $\log(\log(1/\mu))=0$, these two fits have oxygen abundances of 8.44 and 8.46, respectively. These two fits are the same within the errors associated with them. The standard errors for both fits are

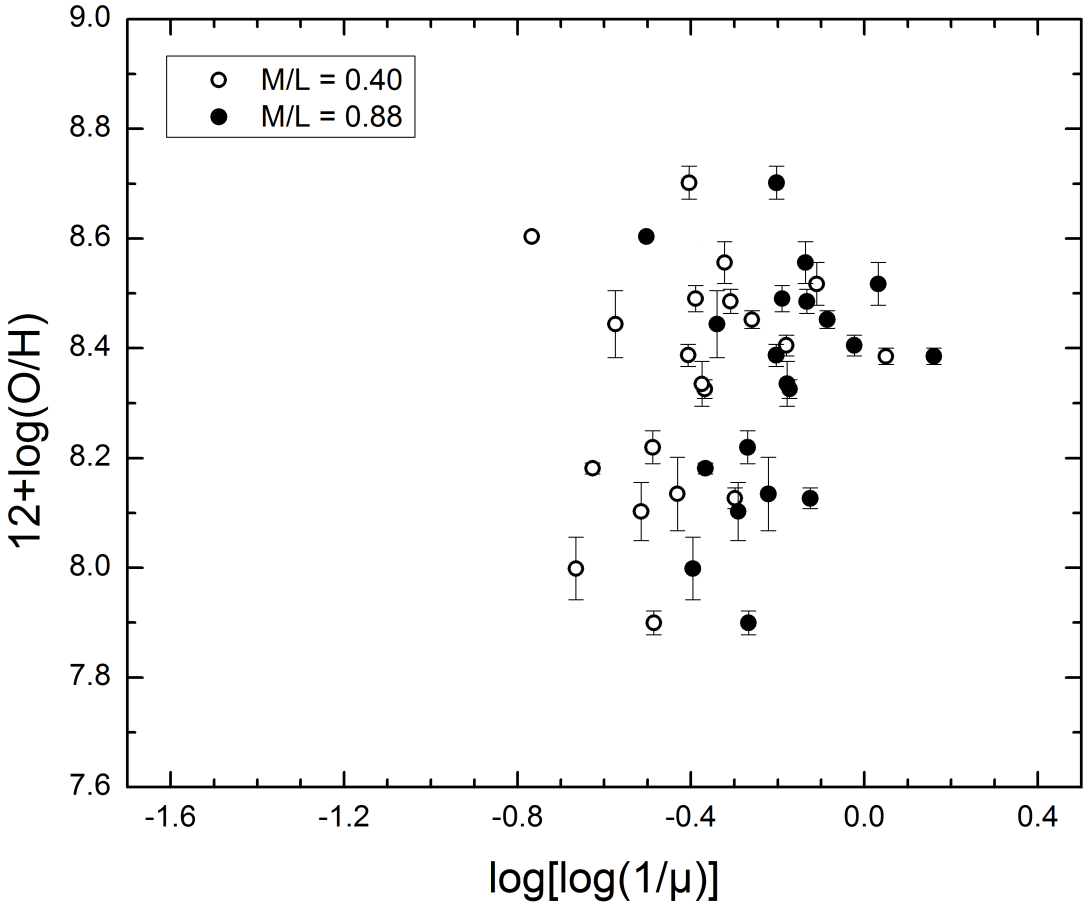

Figure 9.1: **Oxygen abundance versus gas fraction for spirals for two choices of the mass-to-light ratio for disk stars (x=0.4 (Portinari et al. 2009) and x=0.88 (McCall et al. 2011)). Pairs of points are separated horizontally by a value of 0.20±0.08. Some of the error bars are so small that they do not extend beyond the height of the points.**

0.03. As can be seen, 18 of the 20 spirals lie within $\log(\log(1/\mu))=\pm 0.4$ dex in the linear fit for dwarfs. Two of the galaxies, however, show a significant deviation from this trend, as discussed in section 9.4.

9.4 Do Spiral Galaxies Follow the Closed-Box Model?

Dwarf irregular galaxies appear to follow the closed-box model of galactic evolution, and the best fit line fixed at unity in Figure 9.2 conveys the relationship between the oxygen abundance and the gas fraction. It can be seen that spiral galaxies mostly fall along the trend displayed by the dwarf irregulars. Not only do most of the galaxies in the sample appear to follow the closed-box model (i.e., they lie within a short distance of a line with a slope of 1), but they seem to have the same yield of oxygen as dwarf irregulars. The yield relates to the initial mass function (IMF). The conclusion is that the same distribution of heavy and light stars form in spiral galaxies as in dwarf irregulars. In other words, it appears that the galaxy type does not have a bearing on the way stars form or the efficiency with which oxygen is produced and dispersed. Although it has been suspected that the yield depends on metallicity, no such dependence is evident here.

The two main deviants are NGC 925 and NGC 5194. One possible reason for NGC 925 straying from the grouping of other galaxies in Figure 9.2 could be that the oxygen abundance has been over-estimated. NGC 925 has a bar. Within the inner regions

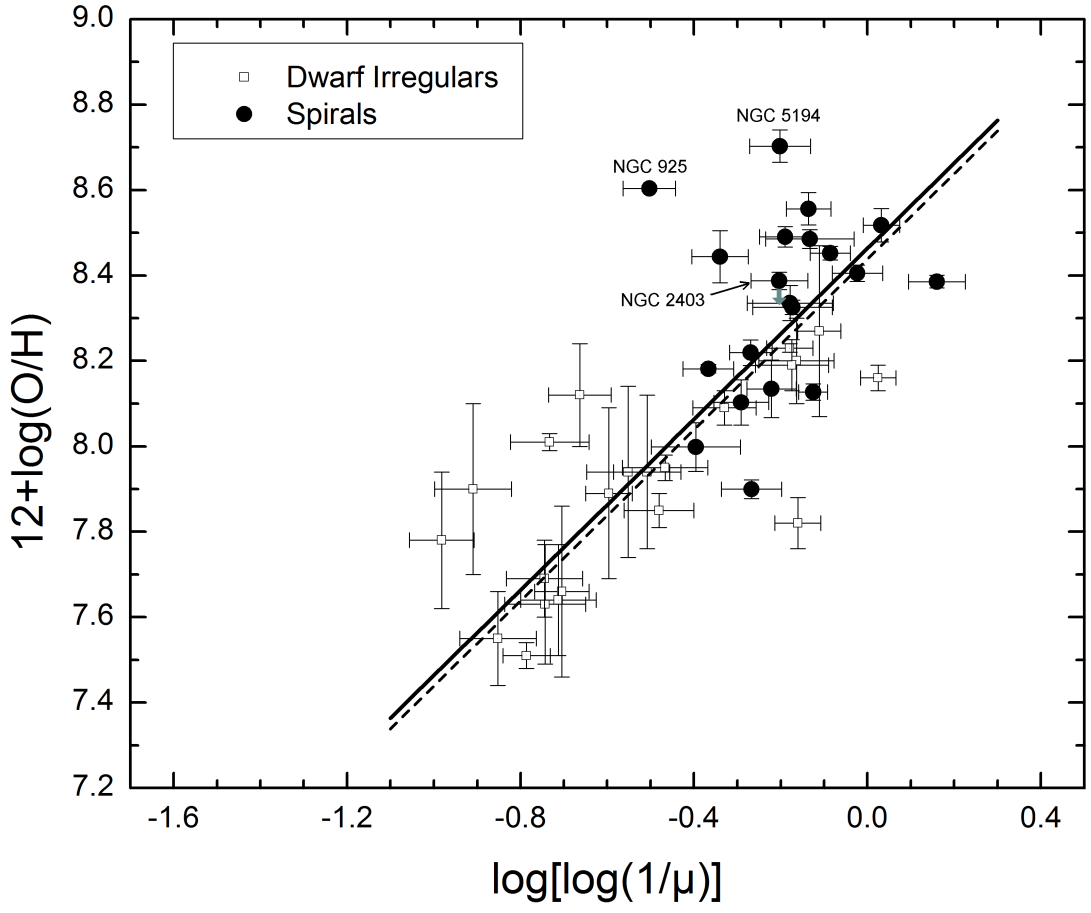

Figure 9.2: **Oxygen abundance vs. gas fraction for 22 dwarf irregular galaxies (open squares) and the 20 spiral galaxies from this study (filled circles). The dashed line shows the linear least squares best fit (fixed to have a slope of 1) to the dwarf irregulars and the solid line shows the linear least squares fit (fixed slope of 1) to the spirals. Error bars along the x-axis (relating to gas fractions) are due to the uncertainty in the mass-to-light ratio used. For the spirals, errors along the y-axis (oxygen abundance) arise from the maximum and minimum asymptotes obtained from the cumulative oxygen abundance plots. A downward-pointing arrow from the point representing NGC 2403 indicates that the cumulative oxygen abundance is an upper limit.**

of NGC 925, there may be an exceptional amount of mixing of enriched gas, even beyond the bar. This fact would account for the relatively shallow gradient amongst the eight HII regions sampled (see Figure 5.1(e)). The cumulative abundance from Figure 7.2(e) is a rather high abundance of 8.60. If more HII regions were sampled at larger radii, a steeper gradient may emerge, which would lower the cumulative abundance.

NGC 5194 may be an outlier due to its interaction with NGC 5195. The interaction between the two galaxies may be causing a disruption in the balance between oxygen abundance and gas fraction in an unpredictable manner.

Chapter 10

Conclusions and Future Directions

10.1 Asymptotic Abundances

Analyzing the metallicity of a galaxy gives insight into its global evolution. Metallicity has been shown to correlate with various properties of galaxies, including mass (Zaritsky 1993), luminosity (Garnett 2002), disk rotation (Spagna et al. 2010), and Hubble type (Zaritsky 1993). The most popular tracer of metallicity is the oxygen abundance, since oxygen is relatively abundant and easily detectable via spectroscopy of HII regions.

In this study, a new method for calculating the total oxygen abundance of spiral galaxies, first introduced by Sadavoy and McCall (2006), has been established and improved. This method involves finding the cumulative amounts of oxygen and hydrogen at increasing radii. The cumulative oxygen abundance approaches an asymptote

at large radii. At radii beyond the peak in the column density of HI, the trend in cumulative oxygen abundances can be approximated by an exponential function, and the asymptote can be used to gauge the overall oxygen abundance of the galaxy.

The bulk of the hydrogen gas within each galaxy is contained in two forms: neutral hydrogen, H, and molecular hydrogen, H_2. Therefore, in order to obtain the true overall oxygen abundance of a galaxy, it is necessary to calculate the absolute amounts of both of these forms of hydrogen. Neutral hydrogen is easily detectable since its signature can be seen via 21.1 cm radiation. The emission can be seen out to great distances, and it has been mapped extensively in many nearby galaxies. Molecular hydrogen, on the other hand, is not as easy to map. It must be inferred by the presence of carbon monoxide, CO. A metallicity-dependent relationship between CO and H_2 exists so that the contribution of molecular hydrogen can be calculated. In 15 of the galaxies in this study, this was possible. From analysis of these 15 galaxies, it was found that molecular hydrogen only contributes a minimal amount to the overall hydrogen in the galaxy. This might be surprising since, especially at relatively small radii, H_2 can dominate over neutral hydrogen. However, when integrating over an entire disk, the relative amount of molecular hydrogen decreases with increasing radius. Of the 15 galaxies with CO data available, the average difference in cumulative oxygen abundance (from when H_2 was taken into account compared to when it was not) was 0.05 dex. Only one showed a difference of more than 0.1 dex in cumulative oxygen abundance when H_2 was factored in. That galaxy, NGC 2903, had its

cumulative oxygen abundance increase by 0.17 dex. Cumulative oxygen abundances for which H_2 data were not available were augmented by 0.05 dex to account for the systematic error. Gas fractions of galaxies for which H_2 data were not available were augmented by 0.05.

The method developed in this thesis is the best technique for finding overall oxygen abundances of galaxies displaying radial gradients in chemical composition, particularly spirals. It is unambiguous in the way it estimates abundances, since it incorporates total absolute amounts of oxygen and hydrogen, and it does not rely on any particular arbitrary choice of radius. Other techniques for estimating the overall oxygen abundance, most notably the estimate of $0.4R_o$ proposed by Zaritsky et al. (1994), are unreliable because they are explicitly tied to radius. While the estimate of $0.4R_o$ may sometimes give a good approximation, it has been shown that a difference between the $0.4R_o$ method and the one presented here can be more than 0.5 dex (see Table 7.2). Each galaxy is unique in its distribution of oxygen and hydrogen, and no clear evidence has been given to show that the overall oxygen abundance can be gauged from a measurement at a single radius.

Despite its success, the new method for calculating oxygen abundances is not without limitations. In this study, NGC 2403 did not demonstrate an exponentially decaying profile when cumulative abundances were calculated out to large radii. This could be explained by its very shallow oxygen abundance gradient, similar to dwarf irregular galaxies. This shallow gradient contributed to an almost flat cumulative

abundance curve. It might even be reasonable to approximate the oxygen abundance of this galaxy to be constant across all radii. In this case, the cumulative abundance curve would also be flat, and the global abundance would be obvious.

One of the main goals of this study was to see if spirals follow the closed-box model of galactic evolution. This model is based on the theory that galaxies begin with a collection of gas that mostly consists of hydrogen and helium. Stars are formed, live out their lives, and die out, leaving behind metal-rich gas which is dispersed in the galaxy. In this manner, the fraction of metals increases as the of gas in the interstellar medium declines.

Dwarf galaxies have been shown to follow the closed-box model fairly well, as shown in Figure 1.1 and 9.2 (Lee et al. 2003a; Lee et al. 2003b; Vaduvescu et al. 2007). Of the 20 spiral galaxies in this study, 18 of them follow a similar trend. These 18 galaxies all lie within ± 0.4 dex in $\log(\log(1/\mu))$ (or ± 0.4 dex in $12+\log(\mathrm{O/H})$ along the y-axis) of the linear least squares fit to the dwarfs (see Figure 9.2). It appears that the same yield persists in both spiral galaxies and dwarf irregulars. This is surprising, since it has been suspected that yield is related to metallicity. This fact may show that the mechanics of star formation and enrichment, especially the ratio of massive-to-small stars, is independent of the type of galaxy.

Two of the spiral galaxies appear to deviate from the closed-box model. These galaxies are NGC 925 and NGC 5194. As discussed in §9.4, the cumulative oxygen abundance of NGC 925 may in fact be an overestimate, and more oxygen abundances

of HII regions at larger radii may lead to a steeper gradient. The deviation in NGC 5194, on the other hand, may be due to the fact that it is highly interacting with NGC 5195 in ways that upset the balance between the abundance and gas fraction.

10.2 Future Directions

The findings from this study naturally lead to several follow-up studies.

More galaxies should be studied to further demonstrate the reliability of the cumulative method for deriving oxygen abundances introduced in this study. Moreover, better spectroscopy of existing HII regions within galaxies in this study should be sought to obtain better abundances for HII regions. With new observations, better oxygen abundance profiles could be obtained for galaxies with limited data. Moreover, better CO observations could help to verify the conclusion that the contribution of molecular hydrogen is insignificant compared to that of neutral hydrogen, and that it is not needed to derive reliable asymptotic abundances.

The correlation between oxygen abundance and the gas fraction for spirals should be looked into further, especially in relation to the closed-box model. Variations to the closed-box model have been derived to account for inflows and outflows with different flow rates (Edmunds 1990; Pagel 1997; Lee et al. 2003(a)). With better constraints on cumulative abundances and gas fractions, it may be possible to gain insights into the global evolution of specific galaxies.

Third, a closer look into NGC 2403 may give a better clue as to why the method

of obtaining cumulative oxygen abundances as described here does not seem to work for this galaxy. One possible explanation could be that the abundance gradient is too shallow, as with some large dwarf galaxies such as the LMC. If this is the case, then the cumulative oxygen abundance derived at the outermost radius should give a fairly good indication of the true overall oxygen abundance. On the other hand, an extension of oxygen abundances to greater distances than those that have already been studied may lead to a steeper gradient, which in turn might lead to as a well-defined cumulative oxygen abundance asymptote.

Fourth, further study into NGC 925 and NGC 5194 might paint a better picture as to why these galaxies do not appear to follow the closed-box model. A more thorough examination of either galaxy might reveal an over-estimation of the oxygen abundance, or an over-estimation of the gas fraction.

Finally, the method of finding cumulative oxygen abundances (or more generally, metallicities), can be used to investigate many different characteristics relevant to the evolution of spiral galaxies. Possible areas of research could include connections between the metallicities of spiral galaxies and age, mass, and dark matter content.

Appendix A:

Glossary of Names and Terms

Glossary of names and terms	Description	Symbol or abbreviation
absolute magnitude	The apparent magnitude of a celestial body if viewed from a distance of 10 parsecs (≈32.6 light years)	M
angstrom	Unit of length used to measure the wavelength of light. 1 Å = 10^{-10} m	Å
apparent magnitude	A measure of brightness as seen by an observer on Earth, normally converted to the brightness that would be observed in the absence of the atmosphere. It is related to flux via: m_1-m_2=-2.5log(f_1/f_2)	m
axis ratio	The ratio of the minor axis of a galaxy to the major axis	q
Balmer series of hydrogen	The portion of the emission spectrum of hydrogen that represents electron transitions from energy levels n > 2 to n = 2	
bulge	A spheroidal distribution of stars that is centered on the nucleus of a galaxy	
chemical	Any element	
closed box model of galactic evolution	A model for the evolution of a galaxy in which all gas is initially unenriched. Gas neither enters nor leaves the galaxy, and metals are built up over time as a result of the death of massive stars alone.	
CO 2.6 mm radiation	Emission line from the rotational transition J=1-0 of the ^{12}CO isotope of carbon monoxide. The emission from this molecule is a tracer of molecular hydrogen (H_2)	

CO-to-H2 conversion factor	The metallicity-dependent ratio of the column density of molecular hydrogren, $N(H_2)$, in units of cm^{-2}, to the intensity of carbon monoxide emission, I(CO), in units of $K*km*s^{-1}$	X
cumulative oxygen abundance	The total number of oxygen atoms divided by the total number of hydrogen atoms within a specified radius of a galaxy	$\Sigma(O) / \Sigma(H)$
deprojected galactocentric distance	The apparent distance on the sky from the centre of a galaxy to a constituent object, deprojected onto the plane of the galaxy	r
disk galaxy	A gravitationally-bound stellar system which contains a disk component, possibly containing spiral arms	
dust	Solid particles occurring throughout interstellar space	
dwarf irregular galaxy	Small, faint disk galaxy which tends to contain a lot of gas and usually shows strong signs of ongoing star formation	
effective radius	Radius containing half of the total luminosity of a galaxy	R_{eff}
elliptical galaxy	Gravitationally-bound stellar system on triaxial geometry, with an oblate spheroidal, no disk, little or no gas, and no star formation	
equivalent width	A spectral measure of the total absorption of radiant energy by an absorption line or absorption band. It is the bandwidth of a hypothetical perfect absorber that would absorb the same amount of energy as the absorption line or absorption band	W
exponential scale length	The radius at which the surface brightness of the galaxy has fallen off by a factor of e (≈2.718) from the centre	a
flux	Observed energy per unit area per unit time from a radiating body	F
forbidden line	A spectral line arising from a transition which violates electric dipole selection rules, i.e. a magnetic dipole or electric quadrupole transition	
gas fraction	The ratio of a galaxy's mass of gas to the mass of the stars plus gas (all baryons)	μ
HI 21.1 cm emission line	Emission line from neutral hydrogren (HI) due to a spin flip of an electron in the ground state	
HII region	A nebula of ionized hydrogen in interstellar space, arising from the ultraviolet radiation of newborn O- and B-type stars within it	
Hα emission line	Emission line at 6563 Å produced from the transition of an electron in a hydrogen atom from the third energy state (n=3) to the second (n=2)	Hα
Hβ emission line	Emission line at 4861 Å produced from the transition of an electron in a hydrogen atom from the fouth energy state (n=4) to the second (n=2)	Hβ
inclination	Angle between the normal to the disk galaxy and the line of sight. A face-on galaxy has i=0° and an edge-on galaxy has i=90°	i

intensity	The amount of light that passes through or is emitted from a particular projected area, falling within a given solid angle in a specified direction	I
ionization	The process of removing electrons from, or the adding electrons to, atoms or molecules	
iron abundance	The ratio of the number density of iron relative to that of hydrogen	Fe/H
isophotal radius	Radius at which the average surface brightness is 25 mag/arcsec^2 in B	R_{25}
K-band	The infrared region within ± 0.3 μm of 2.2 μm	
linear least squares	A method of determining the line that best describes the relationship between two variables by minimizing the sums of the squares of deviation between observed and expected values	
luminosity	The rate at which an astronomical object emits energy, usually in the form of electromagnetic radiation	L
Magellanic Clouds	Two small dwarf irregular galaxies, the Large Magellanic Cloud (Nubecula Major) and the Small Magellanic Cloud (Nubecula Minor), lying near the south celestial pole	LMC, SMC
metallicity	Proportion of an object's matter made up of chemical elements other than hydrogen and helium	
metals	All elements heavier than hydrogen or helium	
nebula	A visible, thinly spread cloud of interstellar gas and dust	
[OII]λ3727 nebular line	Forbidden emission lines found in the spectra of diffuse nebulae. This line is located in the near ultraviolet part of the spectrum, and is actually a doublet of the lines [OII] λ3726 and [OII] λ3729	
[OIII]λ4363 auroral line	A violet line in the spectrum of the aurora (and nebulae) at a wavelength of 4363 Å, resulting from a certain forbidden transition of doubly-ionized oxygen	
[OIII]λλ4959,5007 nebular lines	Forbidden emission lines found in the spectra of diffuse nebulae. These lines are located in the green part of the spectrum, and they are produced by doubly ionized oxygen at a wavelength of 4959 Å and 5007 Å.	
optical depth	The dimensionless path length of a photon through an attenuating medium. It is given by the integral of the linear absorption coefficient over distance.	τ_λ
oxygen abundance	The ratio of the number density of oxygen relative to that of hydrogen, most often expressed as 12 plus the logarithm, 12+log(O/H)	12+log(O/H)
parsec	A unit of length equal to approximately 3.26 light years	pc

planetary nebulae	A nebula consisting of a slowly expanding shell of glowing gas, ejected from a red giant before its evolution into a white dwarf	
R_{23} index	The ratio of the [OII] λ3727 and [OIII] λλ4959,5007 nebular emission lines to the Hβ emission line, used in calculating oxygen abundances when the [OIII] λ4363 auroral line is not available	R_{23}
reddening	The differential extinction between two wavelengths from emissions suppressed by dust between the source and the observer	$E(\lambda_1-\lambda_2)$
reddening law	A curve describing how the opitcal depth of dust varies with wavelength	
semi-major axis	The distance from the centre of an ellipse to the farthest point on its circumference	a
semi-minor axis	The distance from the centre of an ellipse to the nearest point on its circumference	b
spiral galaxy	A gravitationally-bound stellar system composed of a central spheroidal bulge surrounded by a disk containing spiral arms	
spontaneous emission coefficients	Physical constants governing the rate at which atoms pass spontaneously from an upper energy state to a lower one by emission of radiation	A_{ij}
Spreadsheet Nebular Analysis Package	Add-in to Microsoft Excel that was developed by astronomers at York University in order to analyze nebular spectra	SNAP
surface brightness	Flux arriving from a unit solid angle of an extended source. It is equivalent to the intensity in the absence of an obscuring medium. Normally it is expressed in magnitude units, i.e. as -2.5log(I)	
Two Micron All Sky Survey	An imaging survey of the entire sky in three near-infrared bands, J, H, and K_s	2MASS
type II supernovae	Explosive death of a star with a mass greater than eight solar masses, in which the massive highly evolved stellar core collapses and then explodes, ejecting the overlying layers and leaving a neutron star hehind.	

References

Alves, D. R., 2004, arXiv:astro-ph/0408336

Andersson, A., 2002, ASPC, 275, 213

Barbieri, C. V., Fraternali, F., Oosterloo, T., Bertin, G., Boomsma, R., Sancisi, R., 2005, A&A, 439, 947

Barnes, J., 1989, Nature, 338, 123

Barnes, J. E., Hernquist, L. E, 1991, ApJL, 370, L65

Begeman, K. G., 1989, A&A, 223, 47

Bell, E. F., McIntosh, D. H., Katz, N., Weinberg, M. D, 2003, ApJS, 149, 289

Bica, E., Geisler, D., Dottori, H., Clariá, J. J., Piatti, A. E., Santos, J.F. C., Jr., 1998, AJ, 116, 723

Blair, W. P., Kirshner, R. P., Chevalier, R. A., 1982, ApJ, 254, 50

Bournaud, F., Combes, F., 2002, A&A, 392, 83

Bresolin, F., Kennicutt, R. C., Jr., Garnett, D. R., 1999, ApJ, 510, 104

Bresolin, F., Garnett, D. R., Kennicutt, R. C., Jr., 2004, ApJ, 615, 228

Bresolin, F., Schaerer, D., González Delgado, R., Stasińska, G., 2005, A&A, 441, 981

Bresolin, F, 2007, ApJ, 656, 186

(a) Bresolin, F., Ryan-Weber, E., Kennicutt, R. C., Goddard, Q., 2009, ApJ, 695, 580

(b) Bresolin, F., Gieren, W., Kudritzki, R.-P., Pietrzyński, G., Urbaneja, M. A., Carraro, G., 2009, ApJ, 700, 309

Bresolin, F., 2011, ApJ, 729, 56

Carpenter, J. M., 2001, AJ, 121, 2851

Cedrés, B., Cepa, J., 2002, A&A, 391, 809

Chemin, L., Carignan, C., Foster, T., 2009, ApJ, 705, 1395

Chiosi, C. 1980, A&A, 83, 206

Cioni, M.-R. L., 2009, A&A, 506, 1137

Copetti, M.V., Pastoriza, M.G., Dottori, H.A., 1986, A&A, 156, 111

Corbelli, E., Salucci, P., 2000, MNRAS, 311, 441

Corbelli, E., 2003, MNRAS, 342, 199

Crosthwaite, L. P., 2002, PASP, 114, 929

Dahlem, M., Weaver, K. A., Heckman, T. M., 1998, ApJS, 118, 401

Dame, T. M., Hartmann, D., Thaddeus, P., 2001, ApJ, 547, 792

de Vaucouleurs, G., Page, J., 1962, ApJ, 136, 107

de Vaucouleurs, G., de Vaucouleurs, A., Corwin, H. G., Jr., Buta, R. J., Paturel, G., Fouqué, P., 1991, *Third Reference Catalogue of Bright Galaxies* (RC3), New York: Springer-Verlag

Deharveng, L., Peña, M., Caplan, J., Costero, R., 2000, MNRAS, 311, 329

Désert, F. X., Bazell, D., Boulanger, F., 1988, ApJ, 334, 815

Dickman, R. L., 1978, ApJS, 37, 407

Dopita, M. A., Evans, I. N., 1986, ApJ 307, 431

Dors, O. L., Jr., Copetti, M. V. F., 2005, A&A, 437, 837

Edmunds, M. G., Pagel, B. E. J., 1984, MNRAS, 211, 507

Edmunds, M. G., 1990, MNRAS, 246, 678

Fischer, C. F., & Tachiev, G., MCHF/MCDHF Collection, v.2, National Institute of Standards and Technology [Online]. Retrieved November 2010 from http://physics.nist.gov/mchf

Ferguson, A. M. N., Gallagher, J. S., Wyse, R. F. G., 1998, 116, 673

Fich, M., Blitz, L., 1984, ApJ, 279, 125

Fitzpatrick, E. L., 1999, PASP, 111, 63

Fukui, Y., 2007, IAUS, 237, 31

Garnett, D. R., Shields, G. A., 1987, ApJ, 317, 82

Garnett, D. R., 1992, AJ, 103, 1330

Garnett, D. R., 2002, ApJ, 581, 1019

Garnett, D. R., Shields, G. A., Skillman, E. D., Sagan, S. P., Dufour, R. J., 1997, ApJ, 489, 63

Gerin, M., Combes, F., Nakai, N., 1988, A&A, 203, 44

Gratier, P., Braine, J., Rodriguez-Fernandez, N. J., Schuster, K. F., Kramer, C., Xilouris, E. M., Tabatabaei, F. S., Henkel, C., Corbelli, E., Israel, F., van der Werf, P. P., Calzetti, D., Garcia-Burillo, S., Sievers, A., Combes, F., Wiklind, T., Brouillet, N., Herpin, F., Bontemps, S., Aalto, S., Koribalski, B., van der Tak, F., Wiedner, M. C., Röllig, M., Mookerjea, B., 2010, A&A, 522, A3

Güsten, R., Mezger, P.G., 1982, Vistas in Astronomy, 26, 159

Helmboldt, J. F., Walterbos, R. A. M., Bothun, G. D., O'Neil, K., de Blok, W. J. G., 2004ApJ, 613, 914

Hidalgo-Gámez, A. M., & Olofsson, K., 2002, A&A, 389, 836

Holwerda, B. W., González, R. A., Allen, R. J., van der Kruit, P. C., 2005, A&A, 444, 101

Israel, F. P., 1997, A&A, 328, 471

Izotov, Y. I., Thuan, T. X., Lipovetsky, V. A., 1997, ApJS, 108, 1

Joy, M., Lester, D. F., 1988, ApJ, 331, 145

Kaler, J. B., 1978, ApJ, 220, 887

Kenney, J. D. P., Scoville, N. Z., Wilson, C. D., 1991, ApJ, 366, 432

Kennicutt, R. C., Jr., Bresolin, F., Garnett, D. R., 2003, ApJ, 591, 801

Kobulnicky, H. A., Skillman, E. D., 1997, ApJ, 489, 636

Lacey, C. G., Fall S. M., 1985, ApJ, 290, 154

Lebrun, F., Bennett, K., Bignami, G. F., Caraveo, P. A., Bloemen, J. B. G. M., Hermsen, W., Buccheri, R., Gottwald, M., Kanbach, G., Mayer-Hasselwander, H. A., 1983, ApJ, 274, 231

(a) Lee, H., McCall, M. L., Kingsburgh, R. L., Ross, R., Stevenson, C., 2003, AJ, 125, 146

(b) Lee, H., McCall, M. L., Richer, M. G., 2003, AJ, 125, 2975

Lee, H., Zucker, D. B., Grebel, E., K., 2007, MNRAS, 376, 820

Leroy, Adam K., Walter, F., Brinks, E., Bigiel, F., de Blok, W. J. G., Madore, B., Thornley, M. D., 2008, AJ, 136, 2782

Leroy, A. K., Walter, F., Bigiel, F., Usero, A., Weiss, A., Brinks, E., de Blok, W. J. G., Kennicutt, R. C., Schuster, K.-F., Kramer, C., Wiesemeyer, H. W., Roussel, H., 2009, AJ, 137, 4670

Mazzali, P. A., Röpke, F. K., Benetti, S., Hillebrandt, W., 2007, Sci, 315, 825

McCall, M. L., Rybski, P. M., & Shields, G. A., 1985, ApJS, 57, 1

McCall, M. L., Armour, M.-H.,2000, ASPC, 218, 1

McCall, M. L., Richer, M. G., 2003, IAUS, 209, 583

McCall, M. L., 2011, personal communication

McCall, M. L., Vaduvescu, O., Fingerhut, R., Pozo Nunez, F., Barr Dominguez, A., Unda-Sanzana, E., Li, B., 2011, *in progress*

McGaugh, S. S., 1991, ApJ, 380, 140

Mo, H., van den Bosch, F., White, S., 2010, *Galaxy Formation and Evolution*, Cambridge: Cambridge University Press

Newton, K., 1980, MNRAS, 190, 689

Nieten, Ch., Neininger, N., Guélin, M., Ungerechts, H., Lucas, R., Berkhuijsen, E. M., Beck, R., Wielebinski, R., 2006, A&A, 453, 459

Oey, M. S., Kennicutt, R. C., Jr., 1990, NASCP, 3084, 309

Olszewski, E. W., Schommer, R. A., Suntzeff, N. B., Harris, H. C., 1991, AJ, 101, 515

Ondrechen, M. P., van der Hulst, J. M., Hummel, E., 1989, ApJ, 342, 39

Pagel, B. E. J., Edmunds, M. G., Blackwell, D. E., Chun, M. S., Smith G., 1979, MNRAS 189, 95

Pagel, B. E. J., Edmunds, M. G., Smith, G., 1980, MNRAS, 193, 219

Pagel, B. E. J., Simonson, E. A., Terlevich, R. J., Edmunds, M. G., 1992, MNRAS, 255, 325

Pagel, B. E. J., 1997, *Nucleosynthesis and the Chemical Evolution of Galaxies*, Cambridge: Cambridge Univ. Press

Parisi, M. C., Grocholski, A. J., Geisler, D., Sarajedini, A., Clariá, J. J., 2009, AJ, 138, 517

Pettini, M., Steidel, C. C., Adelberger, K. L., Dickinson, M., Giavalisco, M., 2000, ApJ, 528, 96

Phillipps S., Edmunds M. G., 1991, 251, 84

Pilyugin, L. S., 2000, A&A, 362, 325

Pilyugin, L. S., 2001, A&A, 369, 594

Pilyugin, L. S., 2002, A&A, 397, 109

Pilyugin, L. S., Thuan, T. X., 2005, ApJ, 631, 231

Pisano, D. J., Wilcots, E. M., Elmegreen, B. G., 1998,AJ, 115, 975

Portinari, L., Flynn, C., Holmberg, J., Fuchs, B., Jahreiss, H., 2009, IAUS, 254P, 53

Richer, M. G., McCall, M., L., Arimoto, N., 1997, 122, 215

Rogstad, D. H., Lockhart, I. A., Wright, M. C. H., 1974, ApJ, 193, 309

Sadavoy, S. I., McCall, M. L., 2006, CUPJ, 5, 7

Sage, L. J., Westpfahl, D. J., 1991, A&A, 242, 371

Schoenmakers, R.H.M., 1996, arXiv:astro-ph/9610053

Schuster, K. F., Kramer, C., Hitschfeld, M., Garcia-Burillo, S., Mookerjea, B., 2007, A&A, 461, 143

Searle, L., 1971, ApJ, 168, 327

Searle, L., Sargent, W. L. W., 1972, ApJ, 173, 25

Shields, G. A., 1974, ApJ, 193, 335

Shields, G. A., Searle, L., 1978, ApJ, 222, 821

Skillman, E. D., Kennicutt, R. C., Hodge, P. W., 1989, ApJ, 347, 875

Skrutskie, M. F., Cutri, R. M., Stiening, R., Weinberg, M. D., Schneider, S., Carpenter, J. M., Beichman, C., Capps, R., Chester, T., Elias, J., Huchra, J., Liebert, J., Lonsdale, C., Monet, D. G., Price, S., Seitzer, P., Jarrett, T., Kirkpatrick, J. D., Gizis, J. E., Howard, E., Evans, T., Fowler, J., Fullmer, L., Hurt, R., Light, R., Kopan, E. L., Marsh, K. A., McCallon, H. L., Tam, R., Van Dyk, S., Wheelock, S., 2006, AJ, 131, 1163

Smith, H. E., 1975, ApJ, 199, 591

Spagna, A., Bucciarelli, B., Lattanzi, M. G., Re Fiorentin, P., Smart, R., 2010, MSAIS, 14, 67

Stanghellini, L., Magrini, L., Villaver, E., Galli, D., 2010, A&A, 521, 3

Stewart, K. R., Bullock, J. S., Wechsler, R. H., Maller, A. H., Zentner, A. R., 2008, ApJ, 683, 597

Storchi-Bergmann, T., Wilson, A. S., Baldwin, J. A., 1996, ApJ, 460, 252

Strong, A. W., Bloemen, J. B. G. M., Dame, T. M., Grenier, I. A., Hermsen, W., Lebrun, F., Nyman, L.-A., Pollock, A. M. T., Thaddeus, P., 1988, A&A, 207, 1

Tacconi, L. J., Young, J. S., 1986, ApJ, 308, 600

Thornley, M. D., Wilson, C. D., 1995, ApJ, 447, 616

Torres-Peimbert, S., Peimbert, M., Fierro, J., 1989, ApJ, 345, 186

Tsujimoto, T., Yoshii, Y., Nomoto, K., Shigeyama, T. 1995, A&A, 302, 704

Tully, R. B., 1974, ApJS, 27, 437

Vaduvescu, O., McCall, M. L., Richer, M. G., Fingerhut, R. L., 2005, AJ, 130, 1593

Vaduvescu, O., McCall, M. L., Richer, M. G., 2007, AJ, 134, 604

van de Ven, G., Fathi, K., 2010, ApJ, 723, 767

van Zee, L., Salzer, J. J., Haynes, M. P., O'ADonoghue, A. A., Balonek, T. J., 1998, AJ, 116, 2805

van Zee, L., Bryant, J., 1999, AJ, 118, 2172

van Zee, L., Haynes, M. P., 2006, ApJ, 636, 214

Vila-Costas, M. B., Edmunds, M. G., 1992, MNRAS, 259, 121

Vílchez, J. M., Pagel, B. E. J., 1988, MNRAS, 231, 257

Walterbos, R. A. M., Kennicutt, R. C., Jr., 1987, A&AS, 69, 311

Walterbos, R. A. M., Kennicutt, R. C., Jr., 1988, A&A, 198, 61

Webster, B. L., Smith, M. G., 1983, MNRAS, 204, 743

Westmeier, T., Braun, R., Koribalski, B. S., 2011, MNRAS, 410, 2217

Wevers, B. M. H. R., 1984, *A Study of Spiral Galaxies Using HI Synthesis Observations and Photographic Surface Photometry*, Groningen: Rijksuniversiteit

Wilson, C. D., 1995, ApJ, 448, 97

Wyse, R. F. G., Silk, J., 1989, ApJ, 339, 700

Young, J. S., Scoville, N., 1982, ApJ, 258, 467

Young, J. S., Xie, S., Tacconi, L., Knezek, P., Viscuso, P., Tacconi-Garman, L., Scoville, N., Schneider, S., Schloerb, F. P., Lord, S., Lesser, A., Kenney, J., Huang, Y.-L., Devereux, N., Claussen, M., Case, J., Carpenter, J., Berry, M., Allen, L., 1995, ApJS, 98, 219

Zaritsky, D., 1992, ApJ, 390, L73

Zaritsky, D., 1993, PASP, 105, 1006

Zaritsky, D., Kennicutt, R. C., Jr., & Huchra, J. P., 1994, ApJ, 420, 87